DIPLOMA WORK

DISCRETE ELEMENT ANALYSIS OF SINGLE SPAN SKEW STONE MASONRY ARCHES

TAMÁS FORGÁCS – KMEA2K

SUPERVISORS:
DR. KATALIN BAGI, FULL PROFESSOR - DEPARTMENT OF STRUCTURAL MECHANICS
DR. VASILIS SARHOSIS - CARDIFF UNIVERSITY

BUDAPEST, 2015

Acknowledgements

The author wishes to acknowledge the support given to the below diploma work through the Educational Partnership by ITASCA Consulting Group.

The author is also grateful for the many discussions and valuable feedback from the PhD students of Department of Structural Mechanics, namely Gábor Lengyel and Ferenc Szakály.

Finally, the author would also like to show his gratitude to Vasilis Sarhosis and Katalin Bagi for sharing their pearls of wisdom with him during the course of this work.

Abstract

Masonry arch bridges are inherent elements of Europe's transportation system. Many of these bridges have spans with a varying amount of skew. Most of them are well over 100 years old and are supporting traffic loads many times above those originally designed, but the increasing traffic loads may endanger their structural integrity so the need arises to understand the mechanical behaviour in order to inform repair and strengthening options.

There are three main construction methods mostly used in such bridges. The differences in geometry lead to differences in strength and stiffness.

The diploma work to be presented investigates the mechanical behaviour of single span masonry arches. The analysed construction methods were the so-called false skew arch, the helicoidal and the logarithmic method. The three-dimensional computational software 3DEC based on the discrete element method was used: this software allows for the simulation of frictional sliding and separation of neighbouring stone blocks.

The behaviour of the structures was simulated under gravity and under an external full width vertical line load. Types of failure modes, stress levels at the joints will be compared and discussed in the diploma work.

The minimum necessary thickness which can resist the self-weight of the skew arch was also determined.

The investigated parameters of the skew arches were:

- method of construction,
- angle of skew,
- width of the arch,
- element shape and size,
- angle of friction.

KEYWORDS: skew arch, stereotomy, 3DEC

Összefoglaló

A falazott szerkezetű ívhidak Európa közlekedési rendszerének szerves részét képezik. Ezen hidak közül viszonylag sok rendelkezik kisebb-nagyobb mértékű ferdeséggel. A falazott ívek kora jellemzően meghaladja a 100 évet, míg a rájuk ható forgalmi terhek az idők során jelentős mértékben megnövekedtek, így veszélyeztetve a szerkezetek integritását. Ezért egyre nagyobb az igény a falazott ívek mechanikai viselkedésének megértésére azon célból, hogy a felújításokat és megerősítéseket mind hatékonyabb módon tudjuk elvégezni.

Ferde ívek építésére három különböző módszer alakult ki a XIX. század elején. A geometriai kialakítások közti különbségek hatással vannak a szerkezetek teherbírására és merevségére egyaránt.

A bemutatott diplomamunka egynyílású, kőből készült, falazott szerkezetű ferde ívek mechanikai viselkedését vizsgálja. A vizsgált építési módszerek: a hamis ferde ív, a helikális módszer és a logaritmikus módszer.

A munka során egy háromdimenziós, diszkrét elemek módszerén alapuló szoftver (3DEC) került alkalmazásra, mely lehetővé teszi a súrlódásos megcsúszások szimulálását, továbbá figyelembe veszi a szomszédos elemek szétnyílásának lehetőségét is.

A szerkezetek viselkedését gravitációs teher és teljes szélességű, egyenletesen megoszló vonal menti teher hatására vizsgáltam. Az egyes módszerekhez tartozó tönkremeneteli módok, kontakt felületeken létrejövő normál- és nyírófeszültség-eloszlások összehasonlításra kerültek.

Emellett meghatározásra került az ívek azon minimális falvastagsága, amely az önsúly egyensúlyozásához szükséges.

A ferde ívek vizsgált paraméterei:

- eltérő építési módszerek,
- ferdeség szögének hatása,
- ív szélességének hatása,
- elemméret hatása, illetve elemek oldalarányainak hatása,
- súrlódási szög hatása.

KULCSSZAVAK: ferde ív, falazott szerkezetek, diszkrét elemek módszere, 3DEC

Content

1. Introduction

1.1 Background to the research

Masonry arch bridges have enjoyed a long and respected history in both Western and Eastern society. Most of these structures are well over 100 years old and they carry traffic loads many times above those originally designed for. These surviving ancient masonry arch bridges not only prove that a well-constructed masonry arch structure has a long life span, but also that they provide a positive contribution to the landscape. Many arch bridges are listed architectural heritage structures so that replacement schemes are not an option.

In Europe, masonry arch bridges still contribute a major part to the infrastructure of the transportation network.

- There are about 200 000 masonry arch railway bridge in Europe (inclusive the arch bridges whose span is less than 2m), which are the 60% of the total bridge stock. [1] (In Hungary, 655 masonry arch bridge can be found on the railway network. This is 7% of the Hungarian railway bridges.)
- The arch bridges usually have small span. 60% of the total number has smaller span than 2m, while only 8.5% has a larger span than 10m [1]
- 85% of masonry arch bridges have single span.
- 70% of masonry bridges are 100-150 years old, while 12% of them are older than 150 years.

A regular arch bridge was used where the crossing could be perpendicular to the obstacle. In contrast, a skewed arch (also known as oblique arch) was built wherever the obstacle and over-road intersected at any angle other than 90°. This results in the faces of the arch not being perpendicular to its abutments and its plan view being a parallelogram, rather than the rectangle that is the plan view of a regular or “square” arch.

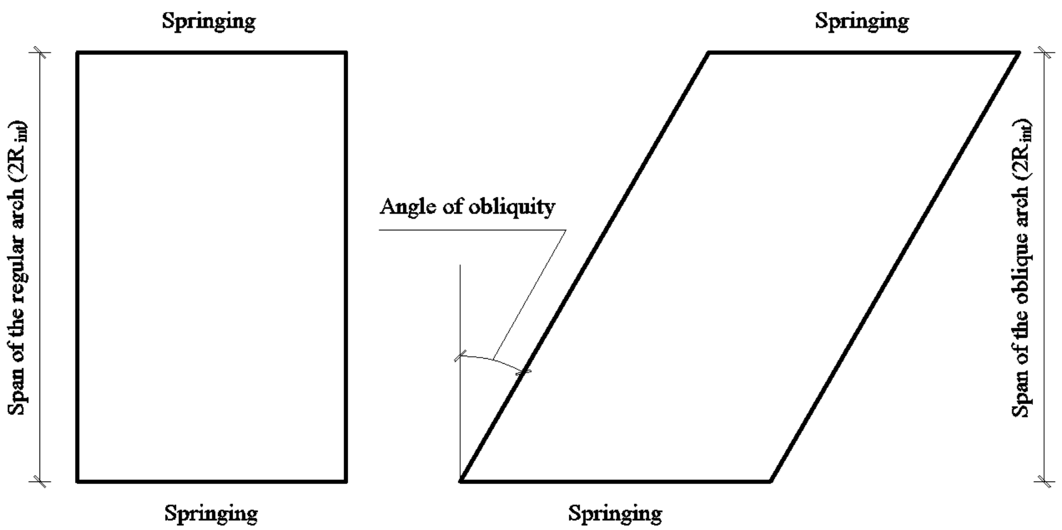

***Figure 1** – Plan view of a regular and a skew arch*

The number of skew bridges started to increase when railways have been introduced, in which it is highly important to preserve the line as direct and straight as possible. Wherever a canal is thus crossed at an angle, there are several ways to span the obstacle:

- The canal can be diverted, so as to bring it at right angles to the railway.
- A usual square bridge of sufficient span can be built over the canal (green in Figure 2).
- A skew arch can be built (red in Figure 2).

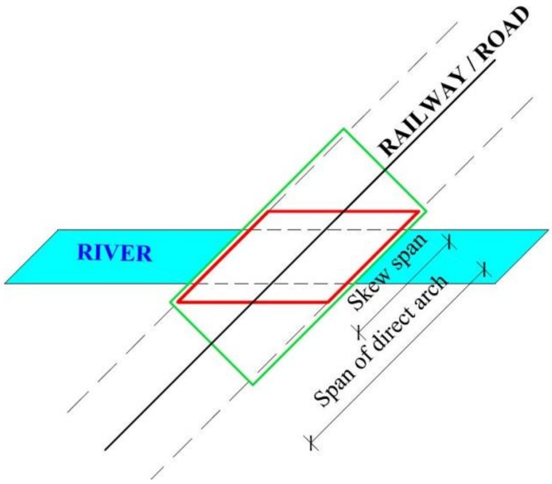

Figure 2 *- Crossing a river with a regular (green) and with an oblique arch (red)*

The amount of traffic and the weight of some of that traffic have increased significantly since most masonry arch bridges were built, and are well in excess of those envisaged by their designers. So there is an increasing demand for a better understanding of the mechanical behaviour in order to inform maintenance and repair.

When considering the balance of forces within a regular arch (assuming that the load is self-weight and/or full width line load) any variation in loading along the length of the barrel can be ignored. The regular arch can be analysed in 2D. In an oblique arch the axis of the barrel is deliberately not perpendicular to the faces, the deviation from perpendicularity being known as the obliquity of the arch. This obliquity of the geometry introduces an obliquity into the internal force system. For this reason a skew arch needs to be thought of as a three-dimensional object.

Although a great deal of work has been carried out to assess the strength of regular arches using 2D methods of analysis, comparatively little work has been undertaken to understand the 3D mechanical behaviour of oblique arches [2] [3]. Today, in many countries, skew arches are routinely assessed as a direct arch whose span is equal to the skew span of the oblique arch. However, experiences clearly show that depending on the methods of construction and geometry, the stiffness and the strength of skew arches might be quite different from those of the direct arch [4].

1.2 Research aims and objectives

In this diploma work skewed masonry arches were analysed. In the 19th century the masonry arch bridges were the most popular solution to span rivers, canals, or any other obstacle. As it was mentioned earlier, lot of these bridges have a varying amount of skew. At that time without the knowledge of the complex mechanical behaviour different methods of constructions developed based on empirical considerations. Up to the present day the differences in mechanical behaviour caused by the construction methods have not been analysed in detail.

Nowadays, the widespread assessment methods are applicable only to the analysis of regular (i.e. straight) arches.

The principal aim of this work is to develop a reliable and accurate computational tool that can be used to improve our understanding of the in-service and near collapse behaviour of skew masonry arches when subjected to gravity and external vertical in-plane static load. In the framework of this study there were no attempts to analyse the effect of backfill, spandrel walls or any other construction detail of a masonry arch bridge.

The objectives of this study are summarized as:

- Review the current literature to gain an up-to-date understanding of the construction methods and structural behaviour of skew masonry arches.
- Review and evaluate the numerical and computational methods that to predict realistically the mechanical behaviour of masonry arches under static load.
- To develop a computational tool that can be used to represent both quantitatively and qualitatively the serviceability and ultimate limit state behaviour of masonry skew arches. The developed discrete element models should be able to predict the failure mode and the ultimate load of the skew arches.
- With the help of the developed models the critical barrel thickness[1] of skewed masonry arches were determined. The effect of a vertical, full-width static external load was also analysed and discussed. The obtained characteristics were compared with those of a direct arch, and the differences caused by the applied construction techniques were found.

It is hoped that this tool will be used by practising engineers and asset managers to compare and evaluate different skew arches in their case.

1.3 Layout of the work

The structure of this diploma work is the following. Chapter 1 presents the background of the work and outlines the main objectives of this research.

In Chapter 2 a short summary follows on the history of the three main methods of construction. The construction details were understood and presented with the help of books and journal papers from the 19th century.

In Chapter 3 the widespread assessment methods for masonry arch bridges are discussed with special regard to the discrete element method, which I used during the analysis.

In Chapter 4 my numerical model is introduced, detailing the construction of geometry, material parameters, loading and verification. The main achievement of the project is the determination of the critical barrel thickness belonging to the different methods of construction of oblique arches. Hitherto, there is no any article in the literature in this topic. A different loading situation was also analysed where a vertical full width line load acting on the arch. Conclusions and further plans were made in Chapter 6 of the work.

The non-specialist reader can found the description of fundamental terms in the appendix.

[1] Critical barrel thickness means the minimal barrel thickness which can resist the self-weight of the structure.

2 Methods of construction

The problem of building skew arches was addressed by a number of civil engineers and mathematicians in the end of the 18th century, including William Chapman, Benjamin Outram, Peter Nicholson, George Stephenson, Edward Sang, Charles Fox, George W. Buck and William Froude. The principles of the construction of oblique arches were fully understood in the early 19th century, so it became considerably easier and cheaper to build skew arches.

Fortunately, the articles from the beginning of the 19th century are available in the libraries of famous universities. In this chapter the main types of methods of construction are introduced on the basis of these old papers.

The investigation was restricted to semi-circular arches, where three main types of construction evolved. These are:

- **False skew arch**, where the coursing joints are parallel to the springing
- **Helicoidal or English method**: where the coursing joints follow helix spirals.
- **Logarithmic or French method**: where the coursing joint are perpendicular to the face of the arch at all elevations.

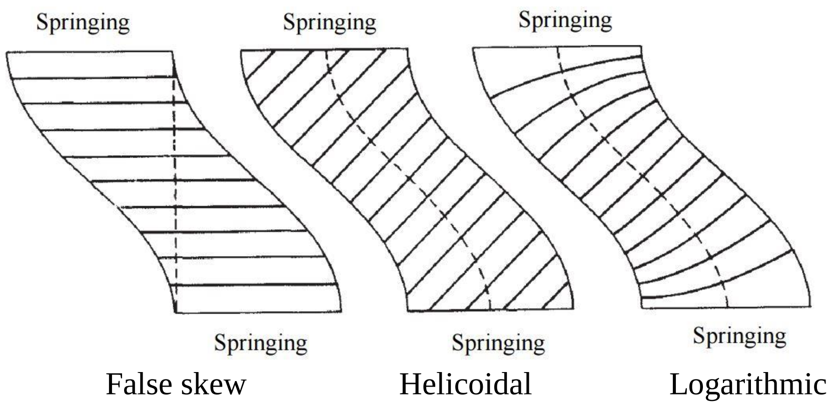

Figure 3 – Developments[2] of the different methods of construction [5]

2.1 The false skew arch

The strength of a regular arch comes from the fact that the mass of the structure causes lines of force that are carried by the stones into the ground and abutments without producing any tendency for the stones to slide with respect to one another. This is due to the fact that the courses of stone are laid parallel to the abutments, which in a regular arch causes them also to lie perpendicular to its faces. For only slightly oblique bridges, where the angle of skew is less than approximately 20°, it is possible to use the same construction method, laying the stones in courses parallel to the abutments. Benjamin Outram could build several arch bridges of up to 20° skew with "unskewed" masonry.

In a skewed arch that was constructed with unskewed masonry, each acute angled haunch is effectively unsupported. The integrity of these regions is dependent upon the ability of the arch to disperse its load in the transverse direction. The analysis of the forces within it shows that in each corner where the face forms an acute angle with an abutment there are resultant forces that

[2] The meaning of the developed surface can be found at the appendix.

are not perpendicular to the planes of the stone courses whose tendency is to push the stones out of face, the only resistance to this being provided by friction and adhesion of the mortar between the stones.

Figure 4 - *„False" skew arch bridge* - *Colorado Street Bridge Saint Paul, Minnesota Span: 21,5m, Width: 18m.Designer: Andreas W. Munster (1888). Today only pedestrian traffic is allowed. [6]*

The fact that these inherently weak structures are still standing today is attributed to their light loading. Most of them serve as pedestrian bridges today.

2.2 Helicoidal method

A characteristic of the regular arch is that the courses of stones run parallel to the abutments and perpendicular to the faces. In an oblique arch these two conditions cannot both be met because the faces and the abutments are not perpendicular. Since skew angles greater than ~20° are required for many applications, mathematicians and engineers, such as Chapman, abandoned the idea of laying the courses of stones parallel to the abutments and considered the alternative of laying the courses perpendicular to the faces of the arch, and accepting the fact that they would no longer run parallel to the abutments. The details of this technique were published in 1828 in a form that was useful to other engineers and stonemasons.

Figure 5*– Askew Bridge in Reading, Pennsylvania – Two track railway bridge – built: 1856, Designer: Richard Osborne, Span: 12m [6]*

2.2.1 Peter Nicholson's helicoidal method in stone

In his book "A Popular and Practical Treatise on Masonry and Stone-cutting" (1828), Scottish architect, mathematician and engineer Peter Nicholson first set out in clear and understandable terms a workable method for determining the shape and position of the stones required for the construction of a strong skew arch that enabled them to be prepared in advance of the actual process. Nicholson approached the problem by constructing a development of the intrados of the arch from the plan and elevation drawings, effectively unrolling and flattening the surface, adding the header joints perpendicular to the courses, then finally rolling up the development diagram by projecting the detail of the intrados back on the plan and elevation drawings, a technique also used by others who would later offer alternative solutions to the problem. This method resulted in the courses of stone voussoirs making up the barrel of the skew arch following parallel helical paths between the abutments, giving the view along the barrel and attractive rifled appearance. Although these courses meet the arch faces at right angles at the crown of the arch, the nearer they are to the springing line the greater their deviation from perpendicularity. Thus Nicholson's method is not the perfect solution, but it is a workable one that has one great advantage over more purist alternatives, namely that since the helical courses run parallel to each other, all the voussoir stones can be cut to the same pattern, the only exceptions being the ring stones, or quoins, where the barrel meets the faces of the arch, each of which is unique but has an identical copy in the other face.

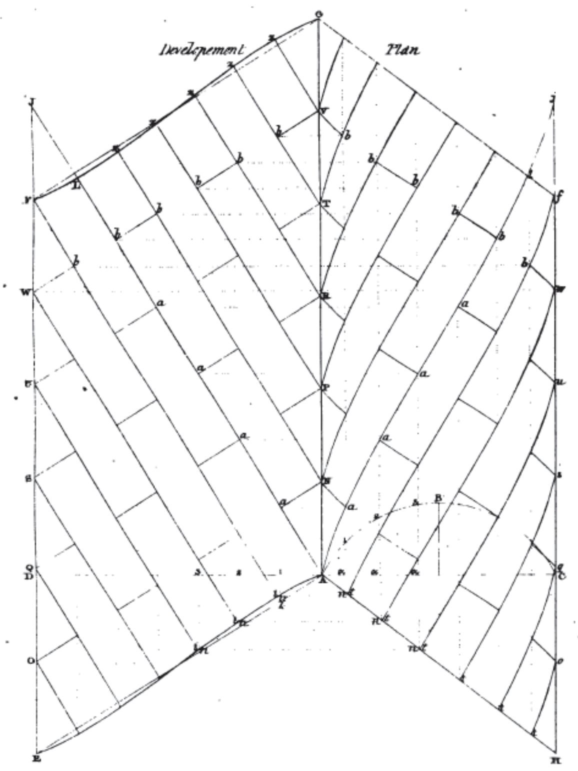

Figure 6 *– Creating the intradosal development according to Nicholson [7]*

Nicholson never pretended to have invented the skew arch but in his later work [7], he does claim to have invented the method for producing the templates that enabled the accurate cutting of the voussoir stones used in all skew bridges built between the years 1828 and 1836, citing testimonials from the builders of major works, such as the Croft Viaduct at Croft-on-Tees near Darlington. However, by 1836 a young engineer called Charles Fox had improved on Nicholson's helicoidal method and other writers were proposing alternative approaches to the problem.

2.2.2 Charles Fox's English method in brick

In performing his calculations **Nicholson considered the arch barrel to be made from one ring of stones and of negligible thickness and therefore he developed only the intrados**. The idea was expanded in Charles Fox's 1836 publication On the Construction of Skew Arches [8], in which he considered the intrados of the barrel and the extrados as separate surfaces mapped onto concentric cylinders by drawing a separate development for each. This approach had two advantages. Firstly, he was able to develop a theoretical third, intermediate surface mid-way between the intrados and the extrados, which allowed him to align the centre of each voussoir, rather than its inner surface, along the desired line, thereby better approximating the ideal placement than Nicholson was able to achieve. Secondly, it enabled him to develop an arbitrary number of concentric intermediate surfaces so as to plan the courses in multi-ring skew arch barrels, allowing them for the first time to be constructed in brick, and therefore much more economically than was previously possible.

In order to explain how he visualized the courses of voussoirs in a stone skew arch, Fox wrote, "The principle which I have adopted is, to work the stones in the form of a spiral quadrilateral solid, wrapped round a cylinder, or, in plainer language, the principle of a square threaded screw: hence it becomes quite evident, that the transverse sections of all these spiral stones are the same throughout the whole arch. It will be obvious, that the beds of the stones should be worked into true spiral (helicoidal) planes." So, a stone skew arch built to Fox's plan would have its voussoirs cut with a slight twist, in order to follow the shape of a square threaded screw.

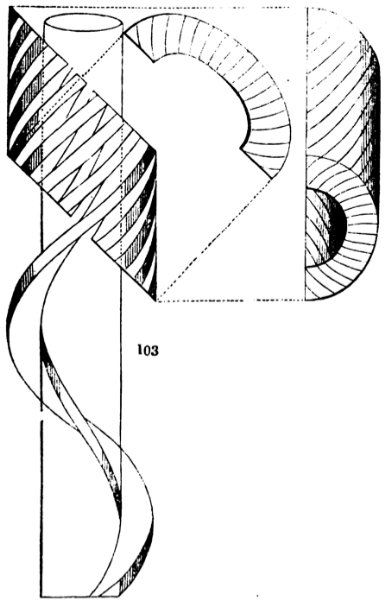

Figure 7 *– Plate from Fox's article [8]*

While claiming a superior method, Fox openly acknowledged Nicholson's contribution but in 1837 he felt the need to reply to a published letter written in support of Nicholson by fellow engineer Henry Welch, the County Bridge Surveyor for Northumberland. Unfortunately the three men became involved in a paper war that, following a number of earlier altercations in which the originality of his writings was questioned, left the 71-year old Nicholson feeling bitter and unappreciated. The following year Fox, still aged only 28 and employed by Robert Stephenson as an engineer on the London and Birmingham Railway, presented his paper encapsulating these principles to the Royal Institution and from this was born the English or helicoidal method of constructing brick skew arches. Using this method many thousands of skew bridges were built either entirely of brick or of brick with stone quoins by railway companies in the United Kingdom, a substantial number of which survive and are still in use today.

Charles Fox prepared a drawing type design method to construct the developed surfaces. The idea behind the design method is that the spiral lines (helices) are appearing as straight lines on the development.

The design method can be understood with the help of **Figure 8**. Let “a” represent the semi-circular curve of the intrados, “c” the extrados, “b” being a line midway between “a” and “c”. Draw a line from “g” with the angle of skew. From points i, j, k draw three line perpendicular to the axis, and of such a lengths that i-l shall be equal length to the semicircle a, and j-m equal to b, and k-m equal to c. From the point o draw the straight line o-l, and also from p to m and h-n: it will be seen that these lines are the approximate lines of the developed soffit. Add q, r, s, which are the centre lines of the three developments. The length of these lines are equal with the width of the arch. Through any point of p-m draw a straight line (v) at right angles with p-m, which straight line shall extend to the axis of the cylinder. The coursing joints on the mid-surface will be parallel to line v. It is important that on the extradosal and intradosal surface the coursing joints are not parallel with the coursing joints of the mid-surface.

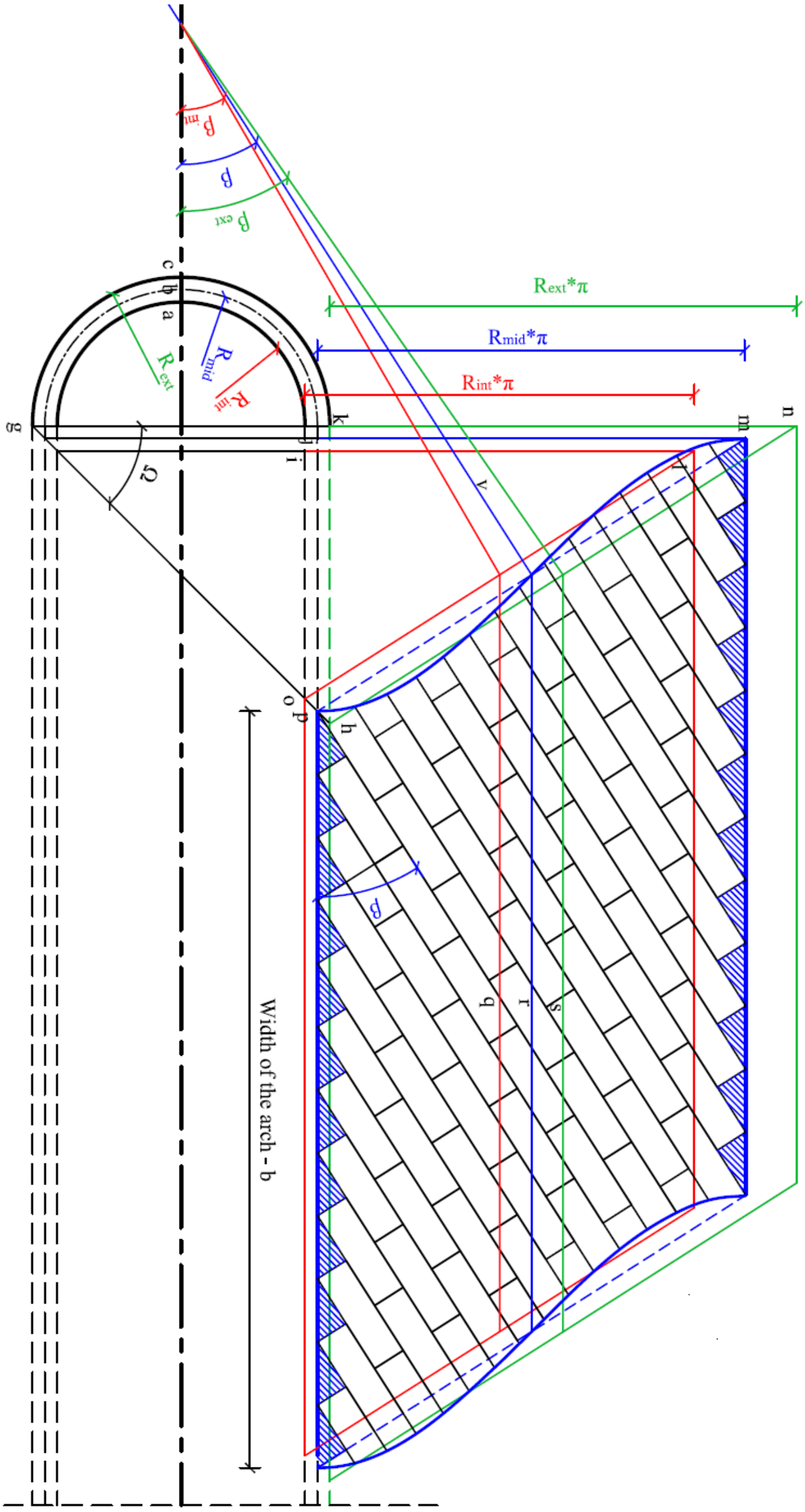

Figure 8 *– Constructing the mid-surface in case of helicoidal method according to Fox*

2.3 Logarithmic method

The helicoidal method of laying down the stone or brick courses championed by Nicholson, Fox and Buck is only an approximation to the ideal. Since the courses are only perpendicular to the faces of the arch at the crown and deviate more from perpendicularity the closer they are to the springing line, thereby over-correcting the deficiencies of the false skew arch and weakening the obtuse angle, the mathematical purists recommend that helicoidal construction be restricted to segmental arches[3] and not be used in full-centred (semi-circular) designs. Despite this there were many full-centred skew bridges built to the helicoidal pattern and many still stand, Kielder Viaduct and Neidpath Viaduct being just two examples.

The search for a technically pure orthogonal method of constructing a skew arch led to the proposal of the logarithmic method by Edward Sang, a mathematician living in Edinburgh, in his presentation in three parts to the Society for the Encouragement of the Useful Arts between 18 November 1835 and 27 January 1836, during which time he was elected vice-president of the Society, though his work was not published until 1840. The logarithmic method is based on the principle of laying the voussoirs in "equilibrated" courses in which they follow lines that run truly perpendicular to the arch faces at all elevations, while the header joints between the stones within each course are truly parallel with the arch face [9].

While a helix is produced by projecting a straight line onto the surface of a cylinder, Sang's method [10] requires that a series of logarithmic curves be projected onto a cylindrical surface, hence its name.

In the following I will derive the equation of coursing joint (Y=f(X) curve) which is perpendicular to the face of the arch at all elevations. The following calculations are made on the developed surface. The equation of the face is known (see in Appendix):

$$Y_{face} = R \cdot \tan(\Omega) \cdot \sin\left(\frac{X}{R}\right)$$

Because of the perpendicularity condition:

$$\frac{dx}{dy} = -\frac{dY}{dX}$$

The first derivative of the equation of the face respect to x:

$$\cos\left(\frac{X}{R}\right) \cdot \tan(\Omega) = -\frac{dX}{dY}$$

Let's integrate the above equation:

$$Y_{coursing\_joint} = -\int \frac{1}{\cos\left(\frac{X}{R}\right) \cdot \tan(\Omega)} dX$$

$$= -\frac{R}{\tan(\Omega)} \cdot \ln\left(sec\left(\frac{X}{R}\right) + \tan\left(\frac{X}{R}\right)\right)$$

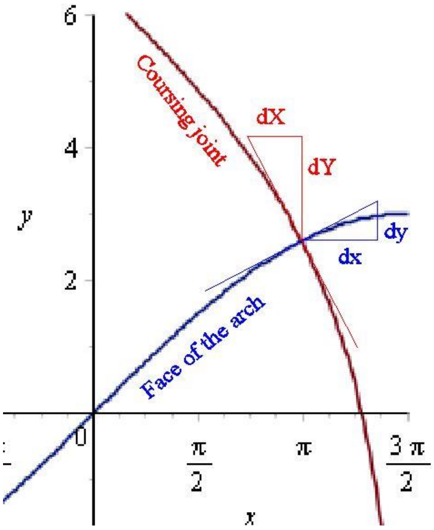

***Figure 9** - Perpendicularity condition between the coursing joint equation and face of the arch*

[3] Segmental arch: An arch in which the curve is a less than semi-circular segment of a circle.

In terms of strength and stability, a skew bridge built to the logarithmic pattern has advantages over one built to the helicoidal pattern, especially so in the case of full-centred designs [11]. However, the courses are not parallel, being thinner towards the most acutely angled quoin, requiring specially cut stones, no two of which in a given course being the same, which precludes the use of mass-produced bricks. Nevertheless, two courses beginning at opposite ends of the barrel at the same height above the springing line are exactly alike, halving the number of templates required.

In 1838, Alexander James Adie, son of the famous optical instrument manufacturer of the same name, as resident engineer on the Bolton and Preston Railway was the first to put the theory into practice, building several skew bridges to the logarithmic pattern on that route, including the semi-elliptical Grade II listed bridge number 74A that carries the line over the Leeds and Liverpool Canal, which was formerly known as the southern section of the Lancaster Canal with the intention of connecting it to the northern section, though this was never achieved as the necessary aqueduct over the River Ribble proved too expensive to build. He presented a paper on the subject to the Institution of Civil Engineers the following year and in 1841, academic William Whewell of Trinity College, Cambridge published his book The Mechanics of Engineering in which he expounded the virtues of building skew bridges with equilibrated courses, but due to the poor complexity to benefit ratio, there have been few other adopters.

Figure 10 *– LLC-74A oblique masonry bridge, constructed with logarithmic method [6]*

2.4 Comparison on the three methods

Construction

The false skew arch and the helicoidal method has a great advantage over against the logarithmic method: all of the voussoirs have exactly the same shape, except the quoin stones. While in case of logarithmic method nearly every stone has a different shape, which requires a lot of templets. More exactly, the two halves of the arch on each side of the keystone are alike, so that any stone cut for one side will fit also in the corresponding place on the other side. The fact that the voussoirs are alike in the helicoidal method, of course lessens the labour of preparing the drawings, and of making the necessary measurements. As regards the difficulty of cuttiny the stone, however, this method does not seem to have any serious advantage over the logarithmic method, while if the coursing and heading joint faces were cut with exactness, as helicoids, the difficulty would be fully equal to if not greater than that by the other methods [11].

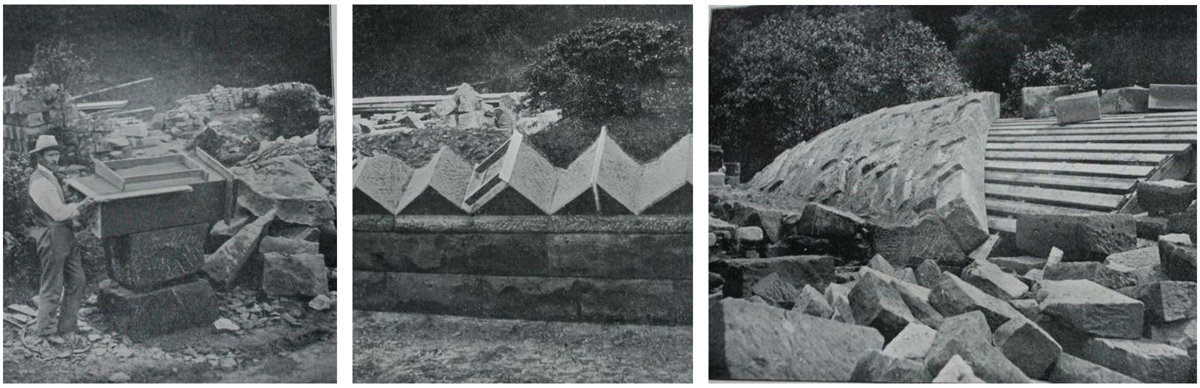

Figure 11 *- Building of Sickergill Skew Bridge in 1898. (Helicoidal method) [6]*

Appearance

It may be considered an advantage as regards appearance that the quoin-stones should be all alike, or rather those faces of the quoin-stones which coincide with the faces of the arch. This, of course, is the case with the false skew arch and the helicoidal method.

Safety

At this part only those considerations are introduced, which were made by civil engineers in the 19th century.

In England, early attempts to construct skewed masonry bridges were largely unsuccessful. According to Hyde [11], the logarithmic method excel by far the helicoidal and the method of false skew arch. It was shown by him that in the case of semi-circular arch there is always a tendency to sliding on the coursing joints, both above and below a certain point; that is, the assumed direction of pressure is nowhere normal to the coursing joints except at a certain height above the springing plane, while in the logarithmic method along each coursing joints curve this tendency is zero. The logarithmic method, therefore, seems to approximate to theoretical perfection as regards security, is followed by the helicoidal method and at a great distance by the false skew arch. They thought that if the main aspect to be considered is security, the logarithmic method must stand first.

3 Assessment of masonry arch bridges

Masonry arches are **statically indeterminate compression structures** which resist external applied loads primarily as a result of the thickness of the masonry and their inherent self-weight. They tend to be resilient to small support movements, with these typically transforming a structure into a statically determinate form. Cracks which might accompany support movements are therefore not formally of great concern, making the notion of crack widths or other conventional serviceability criteria not applicable. Consequently engineers are generally primarily interested in guarding against the ultimate limit state (i.e. structural collapse condition. This typically occurs when sufficient number of hinges or sliding planes are present between blocks to create a collapse mechanism.

In this chapter different techniques are introduced which are - to a certain extent - suitable for the assessment of masonry arch bridges. This section presents a review of these methods, while problems associated with each method are also outlined. The following methods will be introduced:

- The MEXE method (empirical)
- Limit state analysis
- Finite element methods
- Discrete element methods.

Details of the discrete element method will be introduced in detail, because this technique was used during my investigations. As the reader will see, in many respects this method is the most appropriate to the analysis of skewed masonry arches.

3.1 The MEXE method

This method was derived by the Military Engineering Experimental Establishment based on the work done by Pippard et al. [12]. The method is empirical and based on some classic elastic theories and a series of experimental studies [13]. Various assumptions are made in the MEXE method [14]:

- The arch is parabolic,
- It has a span to rise ratio of four
- Both abutments are pinned
- The masonry has a specified unit weight (~22 kN/m^3)
- The arch is loaded at the crown with a transverse line load.

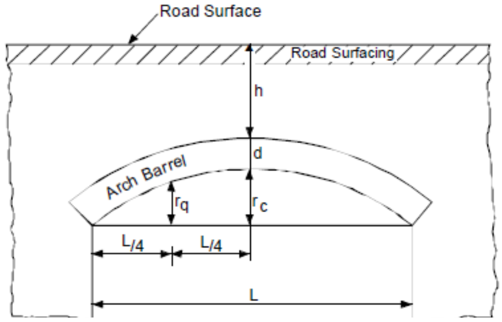

***Figure 12** – Geometrical input data for MEXE method [14]*

The MEXE method involves the evaluation of the provisional axle load (PAL) which is then adjusted by a series of modification factors to account for the geometry, material, and condition of the arch bridge. The expression for the modified axle load is given in the following:

$$Modified\ axle\ load = \frac{740(d+h)^2}{L^{1.3}} \cdot F_{sr} \cdot F_p \cdot F_m \cdot F_j \cdot F_c$$

where	d	the thickness of arch barrel
	h	average depth of the fill at the quarter points
	L	the span
	F_{sr}	span/rise modification factor
	F_p	profile factor
	F_m	material factor
	F_j	joint factor
	F_{cm}	condition based factor, it should be determined on site.

Advantages:

The method was most predominantly used in World War II as a way to quickly classify the load bearing capacity of older masonry arch bridges.

Disadvantages:

The PAL depends equally on the arch and backfill thickness, although the ring thickness has a significantly greater influence on the arch behaviour than the backfill.

The modification factors are introduced without taking into account the arch geometry; the backfill depth, ring thickness.

The application of condition factor is subjective and a wide range of arch capacity could be legitimately assessed.

3.2 Limit state analysis

From 1960's Jaques Heyman authored several books and articles on the topic of masonry analysis [15] [16] [17]. Being inspired by Kooharian [18], his methodologies revolved around plastic analysis techniques. Heyman, who had also previously researched the development of plastic hinges in steel structures, expanded and refined the ideas of Pippard to masonry arches. He applied the idea of hinge formation in unreinforced masonry structures. As part of his studies and analysis, he outlined the following simplifying assumptions:

- Masonry units have an infinite compression strength
- Masonry units behaves as rigid body, i.e. it has infinite stiffness
- Joints transmit no tension
- Masonry units do not slide at the joints

Heyman applied the static and the kinematic theorems of plasticity to determine the ultimate load of a masonry arch. In Chapter 3.2.1 I will introduce a commercial software which is based on the fundamental theory of Heyman.

We should mention that Heyman didn't give a precise proof that the limit state theorems work in case of pure self-weight where a load multiplier has no sense. (Indeed, elementary examples can easily be constructed which point out that the limit state theorems can be violated.) There is no proof either that neglecting the deformability of the elements is a conservative assumption. Another disadvantage of the method is that sliding, and combined (sliding + hinging) type failure modes cannot be analysed.

3.2.1 LimitState:RING

RING is commercial software developed by LimitState Ltd, UK. It ensures rapid analysis for regular masonry arch bridges. The software is primarily designed to analyse the ultimate load bearing capacity of masonry arch bridges. **Unfortunately this software is only capable to analyse regular arches, with 2D method of analysis.**

LimitState:RING idealizes a masonry arch as a series of blocks separated by contacts (where sliding / hinging can occur). The program uses computational limit analysis methods (also known as "plastic" or "mechanism" methods to analyse the ultimate limit state, determining the amount of live load that can be applied before structural collapse.

In addition to basic **equilibrium considerations**, in the context of masonry gravity structures, the following conditions may be used to test for ultimate collapse (assuming both hinging and sliding failures at masonry joints are considered possible):

- The **yield condition**, which may be deemed to be satisfied providing the line of thrust both lies entirely within the masonry and does not cross any joint at a subtended angle (ϑ) less than arctan (μ), where μ is the coefficient of friction.
- The **mechanism condition**, which may be deemed to satisfied providing the line of thrust either touches exterior faces of the masonry blocks and/or crosses sufficient joints at an angle (ϑ) of arctan (μ), to create the releases to transform the structure into a mechanism.

Thus, if a line of thrust satisfies **the equilibrium and yield conditions**, then the true plastic collapse load cannot be less than the applied load. It is **a lower bound**.

Similarly, if a line of thrust **satisfies the equilibrium and mechanism conditions**, then the plastic collapse load cannot be higher than the applied load. It is an **upper bound**.

In **Figure 13** the multiplicator factor of the live load, which causes failure can be seen on the vertical axis, while the statically possible internal forces and the kinematically admissible mechanisms are symbolically shown on the horizontal axis.

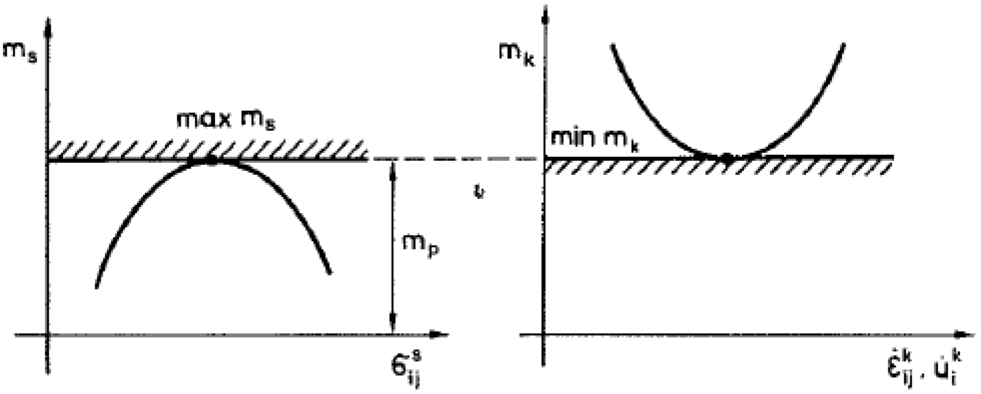

Figure 13 *– Static and kinematic theorem of plasticity [19]*

The joint equilibrium formulation of LimitState:RING works in the following way. Assuming there are b blocks and c contact surfaces, the problem may be stated as we would like to maximise the load factor λ which corresponds to the given live load arrangement in a way that it fulfils the equilibrium and yield conditions both.

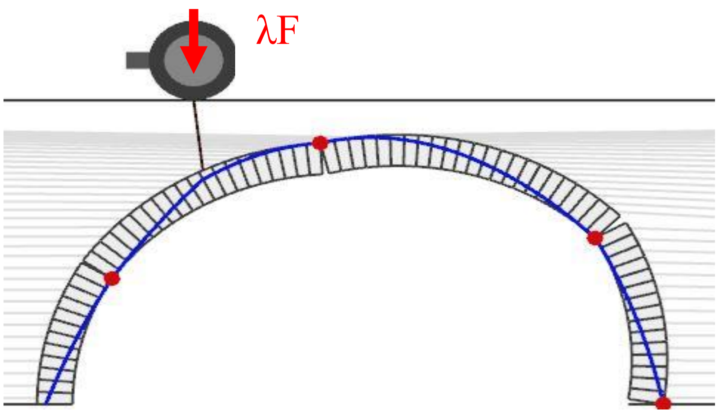

Figure 14 *– Investigated problem*

The equilibrium equations can be written in the following form:

$$\boldsymbol{Bq} - \lambda \cdot \boldsymbol{f}_L = \boldsymbol{f}_D$$

where **B** is a suitable equilibrium matrix (3b × 3c) containing the direction cosines. **q** and **f** are respectively vectors of contact forces and block loads. $\boldsymbol{f} = \boldsymbol{f}_D + \lambda \boldsymbol{f}_L$, where $\boldsymbol{f}_D$ and $\boldsymbol{f}_L$ are respectively vectors of dead and live loads. Contact and block forces, dimensions and frictional properties are shown in **Figure 15**.

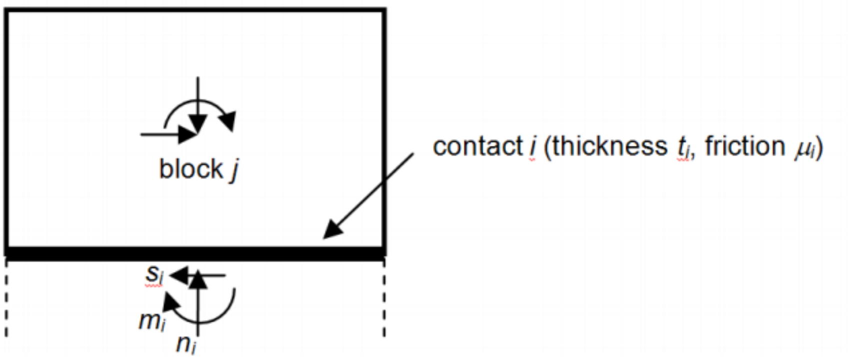

***Figure 15** – Block and contact forces [20]*

The no-tension yield-constraints are the following:

$$for\ each\ contact, i = 1..c \begin{cases} m_i \leq 0.5 n_i t_i \\ m_i \geq -0.5 n_i t_i \end{cases}$$

And the sliding yield constraints:

$$for\ each\ contact, i = 1..c \begin{cases} s_i \leq \mu_i t_i \\ s_i \geq -\mu_i t_i \end{cases}$$

Whilst this formulation produces a large number of constraints and variables, the total number of non-zero elements will generally be relatively small, which means that it can be solved very efficiently using modern interior point Linear Programming algorithms. The program identifies the following failure mode in case of single span, regular masonry arches:

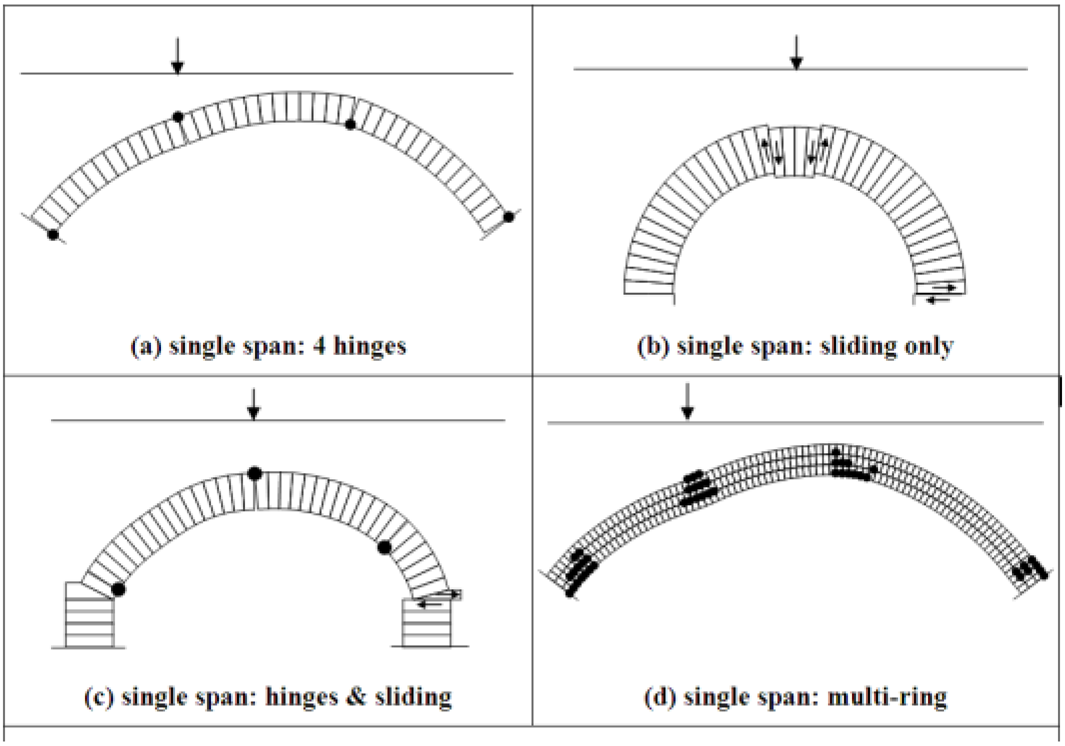

***Figure 16** – Failure modes of regular, single span masonry arches. [20]*

3.3 Finite Element Models

In recent years sophisticated methods of analysis, like finite element method have been applied in the analysis of masonry structures. The main advantage of the finite element method comparing to the above methods is that arbitrary geometries can be constructed, so theoretically all parts of a masonry arch bridge, including spandrel walls, backfill, abutments, or any other construction detail, can be modelled together.

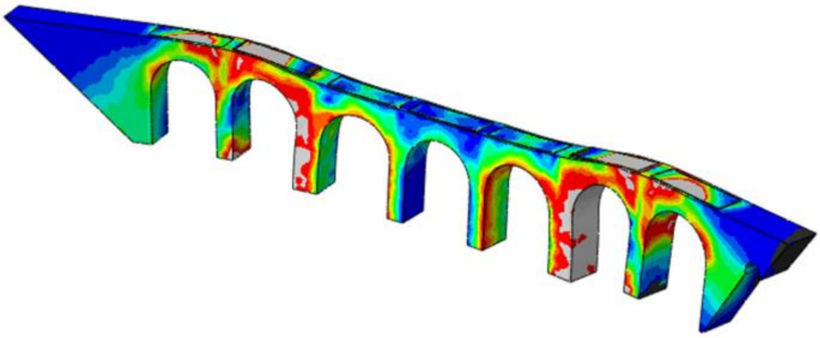

***Figure 17** – Stress-type results from Finite element model of Martinez [21]*

But difficulties arise when trying to model the discontinuities between the elements. If we use linearly elastic material model, the result will be only proper if tensile stresses do not develop during the analysis (or, at least, they do not exceed the tension resistance of the joints). In the case when tensile stresses arise, FEM can approximate the location of cracks, but the real stress distribution, load bearing capacity and failure mode can be totally different from what is predicted by the FEM calculations.

Another way to handle discontinuities to build contact elements into the model. In this case an assemblage of several bodies is created corresponding to the voussoirs, and they are connected with contact elements. These contact elements can handle frictional resistance and sliding, or even finite tensile resistance, too. Unfortunately those surfaces which are in contact have to be defined in advance and manually. In addition to the inconvenience, this type of modelling is computationally very time consuming.

An example for finite element analysis of skewed multi-ring masonry arch bridges constructed with helicoidal method can be found in the PhD thesis of Hodgson [3]. The author used contact elements between the rings and “concrete” material model in his numerical model.

3.4 The Discrete Element code - 3DEC

Structures like masonry arches are mechanical systems whose behaviour is fundamentally determined by the fact that they have a characteristic discrete internal structure which changes as a response to the external effects. In the failure of a masonry arch the separation and/or sliding of neighbouring voussoirs usually plays a basic role.

As we saw in the finite element method the description of discontinuity is limited, as FEM tends to focus on the continuity of the material. In the discrete element method, on the other hand, the discrete nature of the system is incorporated.

A numerical technique is said to be a discrete element model [22]if:

- it consists of separate, finite-sized bodies, so-called discrete elements, each of them being able to displace independently from each other, so the elements have independent degrees of freedom;
- the displacements of the elements can be large;
- the elements can come into contact with each other and loose contact, and these changes of topology are automatically detected during the calculations.

Any discrete element model consists of two basic components: the elements, and the contacts between them.

In the forthcoming part I will introduce the steps of the discrete element method with the help of the commercial software 3DEC, developed by ITASCA [23]. 3DEC was the software I used in my calculations.

3.4.1 Elements

In 3DEC the shape of the elements is polyhedra. Polyhedron means a 3D solid with flat polygonal faces, straight edges, and sharp corners. The blocks may be convex or concave, may contain holes, and may be multiple connected. However, there are so many advantages to convex blocks that within the program concave blocks are decomposed into two or more convex blocks: one is termed as “master block”; the others are “slave blocks”. In contact detection and contact analysis the slave blocks are treated in exactly the same way as master blocks, in order to take advantage of convexity. However, in mechanical calculations, the whole block (master and slaves) is treated as one unit: a common centre of gravity, a common mass, etc. are determined.

The elements can behave in a perfectly rigid way or as deformable blocks. In case of rigid blocks the elements have six degrees of freedom (three translational and three rotational). In case of deformable elements, the blocks are subdivided into tetrahedra that have three translational degrees of freedom at each vertex.

3.4.2 Identification of neighbours

Before the relative geometry of a pair of blocks can be investigated by the computer program, candidate pairs must be identified. It is prohibitive, in computer time, to check all possible pairs, as the search time increases quadratically with the number of the blocks.

3DEC use the method of Cell Mapping and Searching – The space containing the system of blocks is divided into rectangular 3D cells. Each block is mapped into the cell or cells that its “envelope space” occupies. A block’s envelope space is defined as the smallest three-dimensional box with sides parallel to the coordinate axes that can contain the block. Each cell stores, in linked-list form, the addresses of all blocks that map into it. **Figure 18** illustrates the mapping logic for a two-dimensional space (as it is difficult to illustrate the concept in 3D). Once all blocks have been mapped into the cell space, it is an easy matter to identify the candidate neighbours to a given block: the cells that correspond to its envelope space contain entries for all blocks that are near. Normally, this “search space” is increased in all directions by a tolerance, so that all blocks within the given tolerance are found. Note that the computer time necessary to perform the map and search functions for each block depends on the size and shape of the block, but not on the number of blocks in the system. The overall computer time for neighbour detection is consequently directly proportional to the number of blocks, provided that cell volume is proportional to average block volume.

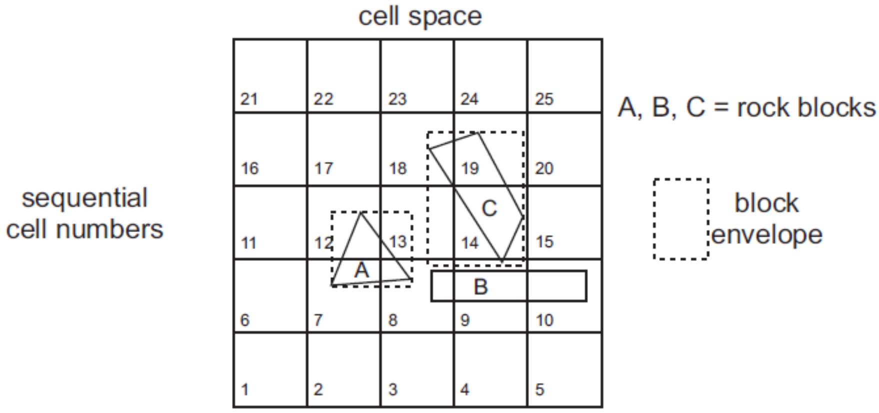

Figure 18 *– Block mapping to cell space: illustration in 2D. [23]*

3.4.3 Contacts

After two blocks have been recognized as neighbours, then they are tested for contact. If they are not in contact, the maximum gap between them must be determined so that block-pairs separated by more than a certain tolerance may be ignored. For block-pairs separated by less than this tolerance, but not touching, a “contact” is still formed. Though such a “contact” carries no load, it is tracked at every step in the mechanical calculation, to ensure that interaction forces start to act as soon as the blocks touch. The contact detection logic must also provide a unit normal vector, which defined the plane along which sliding can occur. This unit normal should change direction in a continuous fashion as the two blocks move relative to one another. The logic should be able to handle, in a reasonable way, certain extreme cases, such as that illustrated in **Figure 19**:

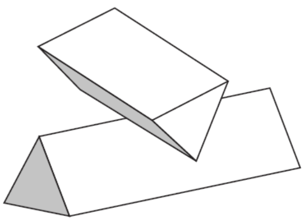

Figure 19 *– Extreme case: the determination of contact normal is difficult [23]*

Finally, the contact-detection logic must classify the type of the contact rapidly – e.g. face to edge or vertex to face. This information is needed in order to select the most appropriate physical law to apply at each contact. In summary, the contact-detection logic must supply, with as little delay as possible, the contact type (if touching), the gap (if not touching), and the unit normal vector.

The simplest approach is to test all possibilities for interaction. In 3D, there are many ways for blocks to touch one another (each vertex of the first block may be tested for contact with each vertex, edge, face of the second block. In case of two cubic blocks it would mean 676 contact possibilities. In response to these difficulties 3DEC uses another scheme.

3DEC applies a scheme based on a **common plane between the two blocks**. The contact detection analysis consists of the following two parts:

- Determining a “common-plane” that, in some sense, bisects the space between the two blocks.
- Testing both blocks separately for contact with the common-plane.

The common-plane is analogous to a metal plate that is held loosely between the two blocks (**Figure 20**). If the blocks are held tightly and brought together slowly, the plate will be deflected by the blocks and will become trapped at some particular angle when the blocks finally come into contact. Whatever the shape and orientation of the blocks, the plate will take up a position that defines the sliding plane for the two blocks even when they do not touch. As the blocks are brought together, the plate will take up a position midway between them, at a maximum distance from both. Then we can easily find the gap between the blocks, simply by adding the block-to-plate distances.

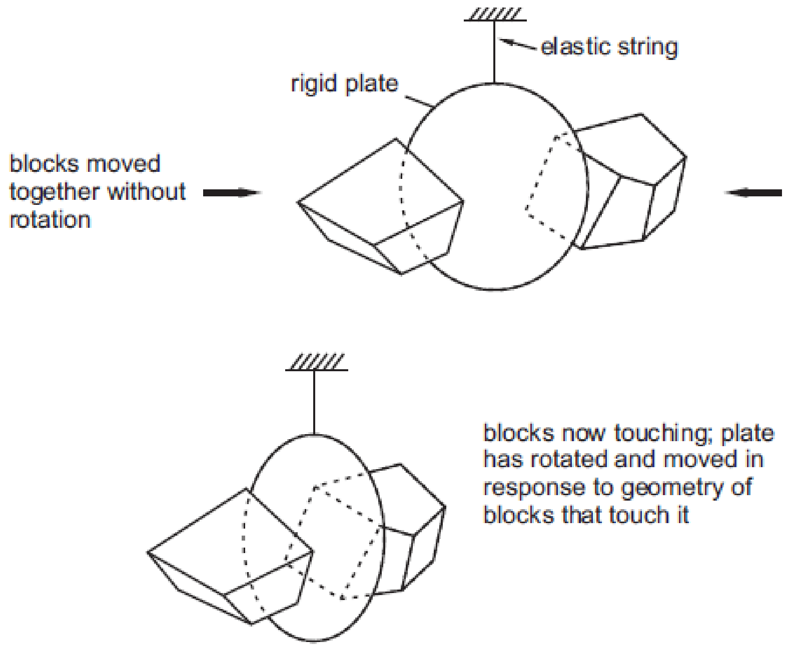

Figure 20 *– Visualization for positioning of common-plane [23]*

The algorithm for locating and moving the common plane is based on geometry alone, and is applied at every timestep, in parallel with the mechanical calculations. The algorithm is stated as "**Maximize the gap between the common plane and the closest vertex**". For overlapping blocks, the same algorithm applies, but the words "gap" and "closest" must be used in their mathematical sense for the case of negative signs—i.e., gap means "negative overlap" and closest means "most deeply buried." To improve readability, the algorithm may be restated for the case of overlapping blocks: "**Minimize the overlap between the common-plane and the vertex with the greatest overlap**". The algorithm then applies a translation and a rotation to the common plane in order to maximize the gap (or minimize the overlap).

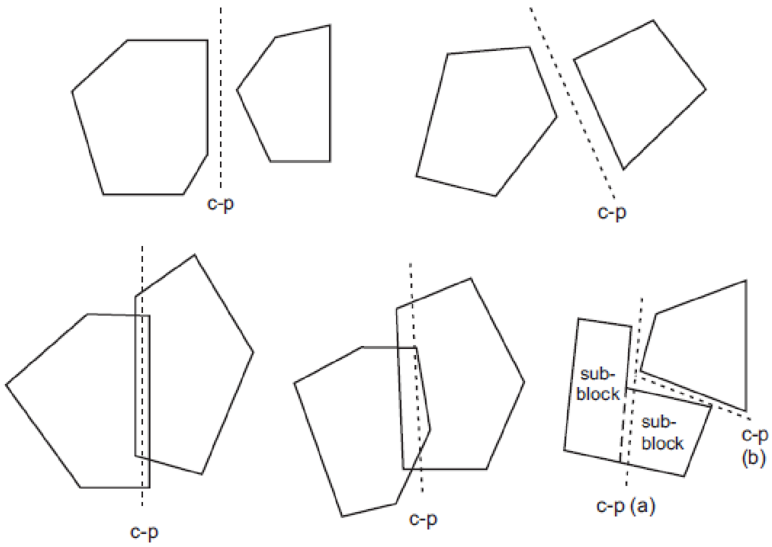

Figure 21 *– Examples of the common-plane between two blocks [23]*

Contact interaction exists if the overlap is positive, or equivalently, if the gap is negative between the two blocks. The normal vector of the common plane is the contact normal; and the contact characteristics can easily be determined from simple geometrical considerations.

If a block face is in contact with the common plane, then it is automatically discretized into sub-contacts. (For rigid blocks, faces are triangulated to create the sub-contacts.) These sub-contacts are generally created with the help of the nodes being located on the block face. For deformable blocks, the triangular faces of tetrahedral zones at the block surface contain surface nodes, each of which has three independent degrees of freedom. In this case, a sub-contact is created for each node on the face (see below the details). Independently of this, the other block being in contact with the common plane is also analysed in a similar manner and another collection of sub-contacts is generated, now from the other side of the contact. Two types of sub-contact are defined in 3DEC: vertex-to-face and edge-to-edge.

- In order to simulate the interior of face-to-face contact between the two blocks, "vertex-to-face"-sub-contacts are applied. Each sub-contact is assigned an area allowing standard joint constitutive relations, formulated in terms of stresses and displacements, to be applied.
- "Edge-to-edge" sub-contacts are used at modelling both edge-to-edge contact between blocks, and face-to-face and face-to-edge contacts at the points of intersection of edges on the common-plane. Details of edge-to-edge sub-contacts are not introduced here.

The area “owned” by each sub-contact is, in general, equal to one-third of the area of the surrounding triangles (this calculation must be adjusted when the sub-contact is close to one or more edges on the opposing block). If the other side of the interface is also a face, then identical conditions apply: sub-contacts are created, and relative displacements, and hence forces, are calculated.

The relative velocity in a sub-contact belonging to one of the two contacting blocks is calculated as the velocity of the analysed node minus the velocity of the coincident point of the opposing face on the other block. This latter velocity can be calculated with the help of a linear interpolation of the three nodes on the surface of the other block, surrounding that opposing coincident point. Then the relative translation vector belonging to the sub-contact is calculated from the relative velocity and from the length of the time step. This relative translation is the basis for the calculation of the uniform distributed normal and shear forces belonging to the sub-contact. The resultant along the sub-contact area is assigned to the analysed node; and the opposite of the resultant is shared among the three nodes surrounding the coincident point on the opposite face. The same is done for all nodes on the analysed face of the first block. Then the other block is analysed in a similar manner: nodes along its contacting face are considered, and another set of sub-contacts is produced where the sub-contact forces are calculated from the corresponding relative displacements.

Consequently, when two blocks come together, the contact logic described above is equivalent to two sets of contact springs in parallel, each carrying sub-contact forces. The sub-contact forces received in the two steps are summed and halved then, in order to receive the overall interface behaviour as the average of that of both sets.

3.4.4 Constitutive models for contacts

The basic joint constitutive model incorporated in 3DEC is the generalization of the Coulomb friction law. Both shear and tensile failure are considered, and joint dilatation can also be included.

In the elastic range, the behaviour is governed by the joint normal and shear stiffnesses (k_n and k_s):

$$\Delta F^n = -k_n \cdot \Delta U^n \cdot A_c$$
$$\Delta F^s = -k_s \cdot \Delta U^s \cdot A_c$$

where	$\Delta F^n, \Delta F^s$	the normal and the shear force increment
	k_n, k_s	the joint normal and the joint shear stiffness
	$\Delta U^n, \Delta U^s$	the normal and the shear displacement increments
	A_c	the sub-contact area

For an intact joint (without previous slip or separation), the tensile normal force is limited to:

$$T_{max} = -T \cdot A_c$$

where T the joint tensile strength

The maximum shear force allowed is given by

$$F^s_{max} = c \cdot A_c + F^n \cdot \tan(\varphi)$$

where c the cohesion

φ the angle of friction

Once the onset of failure is identified at the sub-contact, in either tension or shear, the tensile strength and cohesion are taken as zero:

$$T_{max} = 0 \quad and\ F^s_{max} = F^n \cdot \tan(\varphi)$$

3.4.5 Rigid block motion

During my analysis I used rigid elements to model the mechanical behaviour of oblique arches. The following part contains the corresponding equations of motion:

The equations of translational motion for a single block can be expressed as

$$\ddot{x}_i + \alpha\dot{x}_i = \frac{F_i}{m} + g_i$$

where $\ddot{x}_i$ the acceleration of the centroid of the block

$\dot{x}_i$ the velocity of the centroid of the block

α the viscous (mass-proportional) damping constant

F_i sum of forces acting on the block (contact + applied external forces, except gravitational forces)

m the mass of the block

g_i the gravity acceleration vector.

The rotational motion of an undamped rigid body is described by Euler's equations, in which the motion is referred to the principal axes of inertia of the body. Rigid block models are computationally much more efficient for quasi-static analyses, and in these cases the rotational equations of motion can be simplified. Because velocities are small the nonlinear term in the preceding equations can be dropped, uncoupling the equations. Also, because the inertial forces are small compared with the total forces applied to the blocks, and accurate representation of the inertia tensor is not essential. In 3DEC therefore only an approximate moment of inertia is calculated, based upon the average distance from the centroid of vertices of the block. This allows the preceding equations to be referred to the global axes.

$$\dot{\omega}_i + \alpha\omega_i = \frac{M_i}{I}$$

where $\dot{\omega}_i$ the angular acceleration about the principal axes

ω_i the angular velocity about the principal axes

α the viscous (mass-proportional) damping constant

M_i total torque

I approximate moment of inertia

A central finite-difference procedure is used to integrate the equations of motion explicitly. The velocities and angular velocities are calculated as follows:

$$\dot{x}_i\left(t+\frac{\Delta t}{2}\right) = \left[\left(1-\alpha\frac{\Delta t}{2}\right)\cdot \dot{x}_i\left(t-\frac{\Delta t}{2}\right) + \left(\frac{F_i(t)}{m} + g_i\right)\cdot \Delta t\right]\cdot \frac{1}{1+\alpha\frac{\Delta t}{2}}$$

$$\omega_i\left(t+\frac{\Delta t}{2}\right) = \left[\left(1-\alpha\frac{\Delta t}{2}\right)\cdot \omega_i\left(t-\frac{\Delta t}{2}\right) + \left(\frac{M_i(t)}{I} + g_i\right)\cdot \Delta t\right]\cdot \frac{1}{1+\alpha\frac{\Delta t}{2}}$$

The increments of translation and rotation are given by

$$\Delta x_i = \dot{x}_i\left(t+\frac{\Delta t}{2}\right)\cdot \Delta t$$

$$\Delta \theta_i = \omega_i\left(t+\frac{\Delta t}{2}\right)\cdot \Delta t$$

The position of the block centroid is updated as:

$$x_i(t+\Delta t) = x_i(t) + \Delta x_i$$

The location of the vertices is calculated with the help of the displacement of the centroid plus the rotation calculated earlier.

3.4.6 Mechanical damping

Mechanical damping is used in the discrete element method to solve static (non-inertial) problems. The approach is conceptually similar to dynamic relaxation, proposed by Otter et al. The equations of motion are damped to reach a force equilibrium state as quickly as possible under the applied initial and boundary conditions. Damping is velocity proportional (i.e., the magnitude of the damping force is proportional to the velocity of the blocks). The use of velocity proportional damping in standard dynamic relaxation involves three main difficulties:

- The damping introduces body forces, which are erroneous in “flowing” regions and may influence the mode of failure in some cases.
- The optimum proportionality constant depends on the eigenvalues of the matrix, which are unknown unless a complete modal analysis is done. In a nonlinear problem, eigenvalues may be undefined.
- In its standard form, velocity-proportional damping is applied equally to all nodes. In many cases, a variety of behaviour may be observed in different parts of the model. For example, one region may be failing while another is stable. For these problems, different amounts of damping are appropriate for different regions.

In an effort to overcome these difficulties, alternative forms of damping are applied instead. Two alternative forms of velocity-proportional damping are provided in 3DEC. The first is a numerical servo-mechanism, termed **adaptive global damping**, which is used to adjust the damping constant automatically. Viscous damping forces are used, but the viscosity constant is continuously adjusted in such a way that the power absorbed by damping is a constant proportion of the rate of change of kinetic energy in the system. The adjustment to the viscosity constant is made by a numerical servo-mechanism that seeks to keep the following ratio:

$$R = \frac{\sum P}{\sum \dot{E}_k}$$

where P is the damping power for a node,

$\dot{E}_k$ is the rate of change of nodal kinetic energy.

Another form of damping, in which the damping force on a node is proportional to the magnitude of the unbalanced force. For this scheme, referred to as **local damping**, the direction of the damping force is such that energy is always dissipated.

During my static analysis, both adaptive global damping (auto damping) and local damping were tested. In case of the local damping, the convergence of the solution was much slower compared to the adaptive global damping. Hence adaptive global damping was used in case of the further analysis. The default ratio of the damping power and the rate of change of nodal kinetic energy is 0.5. With this ratio the convergence of the solution is very slow near to the collapse: the structure already wants to collapse under the given loads, but the damping does not allow the development of the failure. That is why is set the R ratio to 0.1.

3.4.7 Numerical stability

The applied central difference method is conditionally stable. A limiting timestep that satisfies the stability criterion for both the calculation of internal block deformation and block-to-block relative displacement is approximated by the software repeatedly throughout the whole simulation process. The timestep required for the stability of block deformation computations is estimated as

$$\Delta t_n = 2 \cdot \min\left(\frac{m_i}{k_i}\right)^{0.5}$$

where m_i the mass associated with block node i.

k_i is the measure of stiffness of the elements surrounding the node.

For calculations of block-to-block relative displacement, the limiting timestep is calculated, by analogy to a simple degree-of-freedom system, as

$$\Delta t_b = frac \cdot 2 \cdot \left(\frac{M_{min}}{K_{max}}\right)^{0.5}$$

where M_{min} is the mass of the smallest block in the system.

K_{max} is the maximum contact stiffness

$frac$ is a user-supplied value that accounts for the fact that a single block may be in contact with several blocks simultaneously. A typical value for frac is 0.1.

The controlling timestep for a discrete element analysis is $\Delta t = \min(\Delta t_n, \Delta t_b)$.

4 Development of the computational model

The analysis was made with the help of 3DEC v.5.00.171, which was achieved in the framework of ITASCA Educational Partnership.

It is important to emphasize that there were no attempt to model backfill, spandrel walls, abutments or any other construction detail. I intended to get an insight into the mechanical behaviour of the skew arch, then in the future the complex behaviour of a full bridge can be analysed too.

4.1 Model geometry

The arch geometries corresponding to three different methods of construction were prepared with the help of MAPLE 17. During this process the following data were handled as a parameter, so it is very easy to modify and create new geometries.

- Method of construction
- Radius of the arch - R
- Thickness of the arch - t
- Width of the arch - b
- Obliquity of the arch - Ω
- Size of the elements:
    - Number of coursing joints
    - Number of heading joints

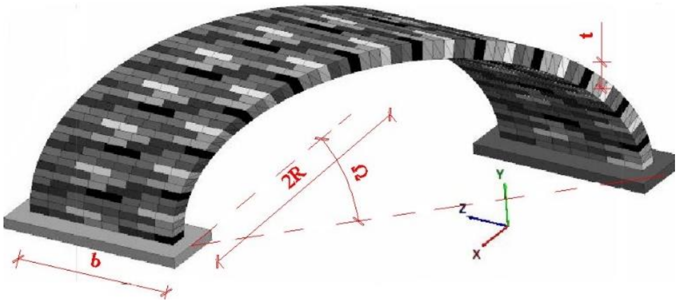

Figure 22 *– Basic parameters of the skew arch*

All of the investigated arches were semi-circular arch. So the span/rise ratio was kept 2:1 in all cases.

4.1.1 False skew arch

Concerning the geometry, the construction method of false skew arch is the simplest. The nodes of the elements can be calculated on the cylindrical surface directly. In 3DEC polyhedrons can be defined with the following command:

$$\boldsymbol{polyhedron\ prism\ a}\ x_{a1}\ y_{a1}\ z_{a1} \dots x_{a4}\ y_{a4}\ z_{a4}\ \boldsymbol{b}\ x_{b1}\ y_{b1}\ z_{b1} \dots x_{b4}\ y_{b4}\ z_{b4}$$

In the first section we have to define the coordinates of the nodes corresponding to Face A, and in the second part the coordinates of the nodes corresponding to Face B. Fortunately in case of the false skew arch the face A and B are planar surfaces, so all of the four nodes are in the same plane.

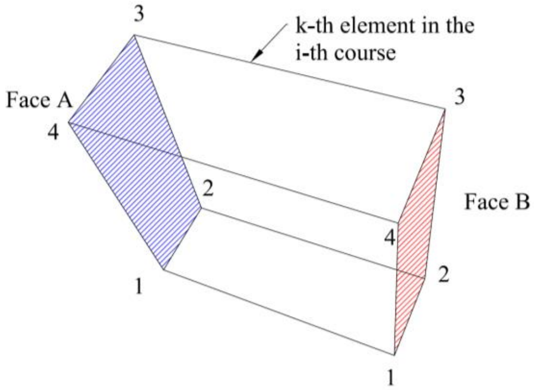

Figure 23 *– Numbering of the nodes.*

To arrange the blocks in brick bond pattern two adjacent elements were joined together. This gluing method should be defined with the $join\ contact\_on$ command.

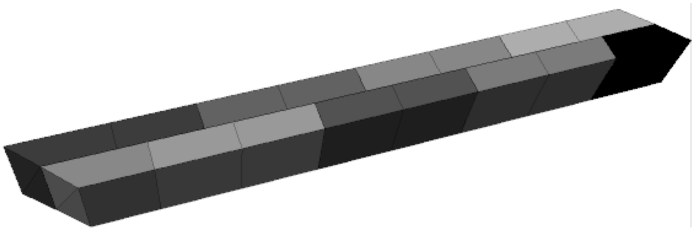

***Figure 24** – Brick bond pattern in two following courses*

False skew arches with different obliquities can be seen in ***Figure 25***:

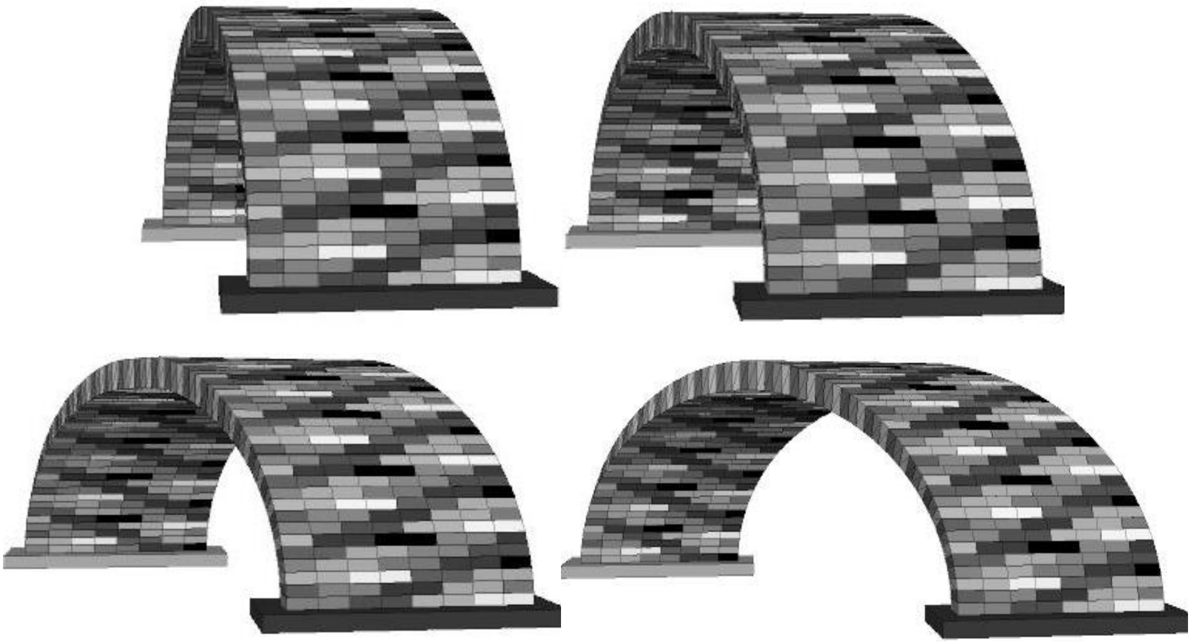

***Figure 25** – False skew arches with 70 course and 5 element/course*
Obliquities: 10°, 20°, 30°, 45°

4.1.2 Helicoidal method

In case of helicoidal methods the coursing joints are helix spirals. These spirals appear as straight lines on the developed surface. As it can be seen in **Figure 8** , on the developed extradosal and intradosal surfaces the coursing joints are not parallel with the coursing joints of the mid-surface. That is why β, β_{ext}, β_{int} have to be computed first.

$$\beta = \arctan\left(\frac{2 \cdot R_{mid} \cdot \tan(\Omega)}{R_{mid} \cdot \pi}\right)$$

With the help of β the length of x can be determined (see in **Figure 8**):

$$x = \frac{R_{mid}(1 + \pi/2)}{\tan(\beta)}$$

After this β_{ext}, β_{int} can be determined:

$$\beta_{int} = \arctan\left(\frac{R_{int}(1 + \pi/2)}{x}\right)$$

$$\beta_{ext} = \arctan\left(\frac{R_{ext}(1 + \pi/2)}{x}\right)$$

The number of the elements in one course and the shape of the element (length/width ratio) are not independent variables, all of them cannot be chosen arbitrary. Let's choose the number of the elements in one row in such a way that the stones run approximatively in stretcher bond[4]. The length to width ratio of the stones was approximatively 2:1.

After calculating these essential parameters, the coordinates of the stones on the developed intradosal and extradosal surfaces can be determined.

The arch which was built according to helicoidal method contains three main types of element:

- **Support elements**: these elements connect the abutments with the voussoirs.
- **Normal voussoirs:** most of the elements (each stone is exactly alike)

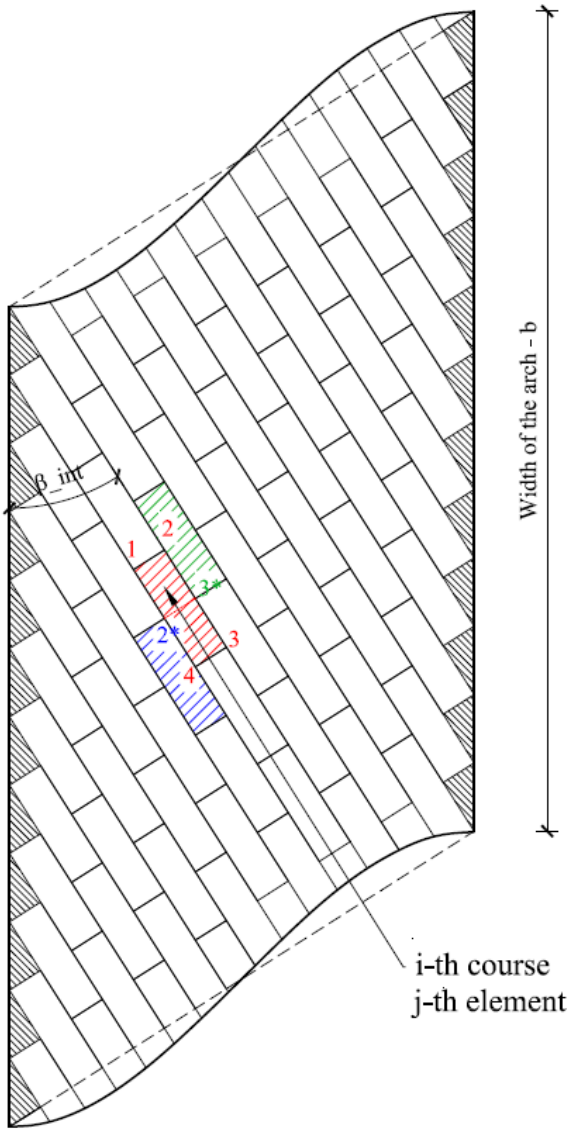

Figure 26 *– Development of the intradosal surface*

[4] In stretcher bond the stones in the above and below course have a half stone offset.

- **Quoins:** these special shaped elements connect the face of the arch with the normal elements.

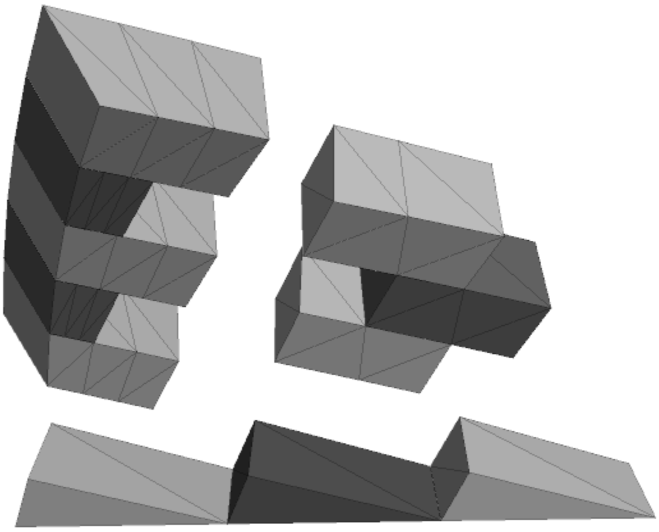

__Figure 27__ – Elements of the skew arch made according to the helicoidal method: quoins, normal voussoirs, support elements

The shape of the elements are bounded by helicoidal curves. It means that the edges of the stones are not straight and the faces are not planar. Unfortunately in 3DEC only polyhedral bodies can be defined, where the faces should be planar. Therefore the intradosal face of a stone is divided into four triangular shape part. This technique was repeated in case of extradosal surface, too. Triangular based prisms were created, and joined together. After this, two half voussoirs are joined again to create stretcher bond pattern.

Some geometrical arrangements, which were created with the developed code:

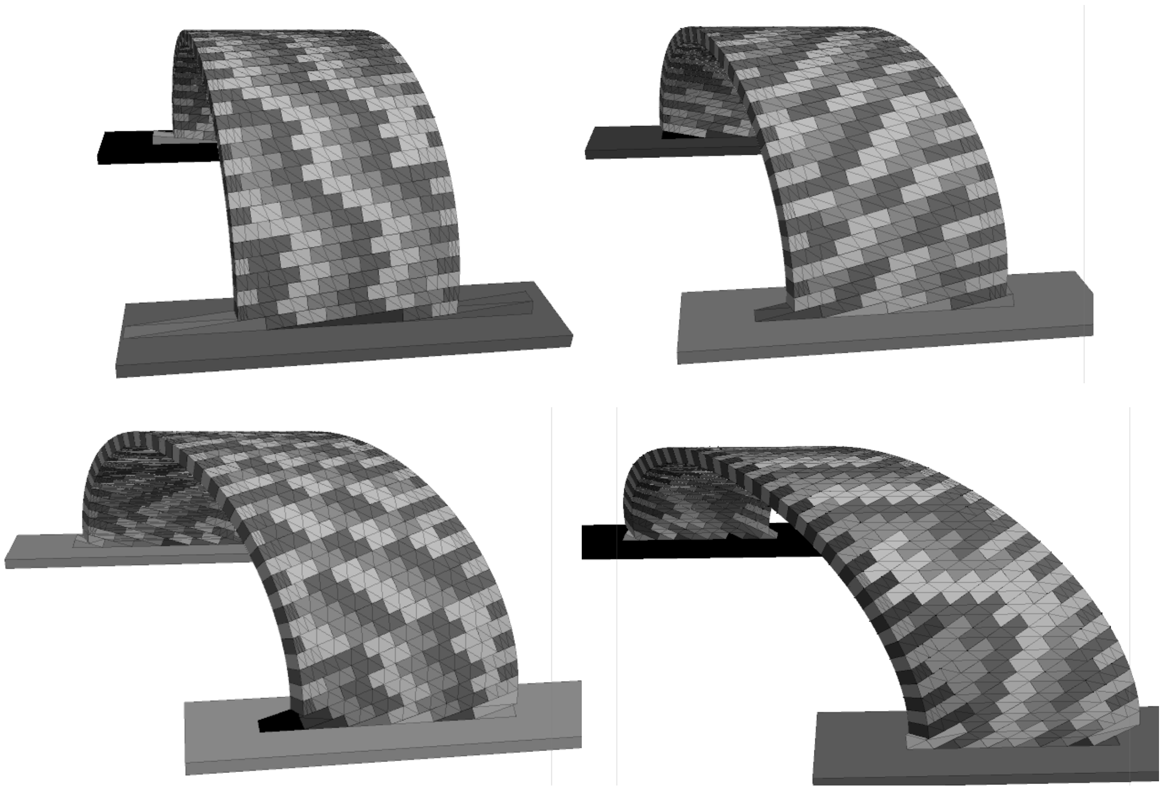

__Figure 28__ – Four skew arches created according to helicoidal method, obliquities: 10°, 20°, 30°, 45°

4.1.3 Logarithmic method

The calculation process of the nodes was the most complicated in case of the logarithmic method. This procedure was made on the development, which corresponds to the mid-surface.

The equation of the heading joints:

$$Y_{heading\_joint\_j} = R_{mid} \cdot \tan(\Omega) \cdot \sin\left(\frac{X}{R_{mid}}\right) + c_{2j} \qquad -\frac{b}{2} \leq c_{2j} \leq \frac{b}{2}$$

The c_{2j} constants should be equally spaced between the two face of the arch depending on how many elements we want to have in a course.

The equation of coursing joints is already known (see Chapter 2.3):

$$Y_{coursing\_joint\_i} = -\frac{R_{mid}}{\tan(\Omega)} \cdot \ln\left(sec\left(\frac{X}{R_{mid}}\right) + \tan\left(\frac{X}{R_{mid}}\right)\right) + c_{1i}$$

The c_{1i} constant in the equation of ith coursing joint should be determined in that way that the distance between the adjacent coursing joint should be the same at the centreline of the arch. To determine these c_{1i}constants the arc length of the centreline should be calculated. The curve of the centreline is equivalent with the curve of the heading joints, which is a sinusoidal curve in the development and a semi-ellipse in the 3D-space. To calculate the arch length of an arbitrary curve the following calculations should be done:

$$\Delta s = \sqrt{\Delta x^2 + \Delta y^2} = \sqrt{1 + \left(\frac{\Delta y}{\Delta \mathrm{x}}\right)^2} \cdot \Delta x$$

Let's take the limit of Δs as Δx approaches 0:

$$\lim_{\Delta x \to 0} \Delta s = \sqrt{1 + \left(\frac{dy}{\mathrm{dx}}\right)^2} \cdot dx$$

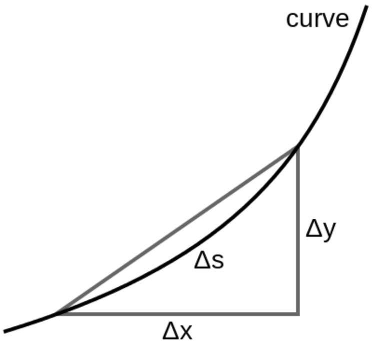

***Figure 29** – Arc length of an arbitrary curve*

Let's integrate the above function to obtain the length of the centreline of the arch:

$$\int_{\frac{-R\pi}{2}}^{\frac{R\pi}{2}} ds = \int_{\frac{-R\pi}{2}}^{\frac{-R\pi}{2}} \sqrt{1 + \left(\frac{dy}{\mathrm{dx}}\right)^2} \cdot dx$$

Unfortunately in case of the heading joint's curve this expression leads to a complete elliptic integral of the second kind:

$$s = \int_{\frac{-R\pi}{2}}^{\frac{R\pi}{2}} b_1 \sqrt{1 - b_2 (\sin(x))^2} \cdot dx$$

The result of this integral was calculated numerically. After it, the arc length was split into n equal part according to how many course we want.

To determine those x_i values which correspond to equal arc length to following non-linear equation was solved numerically:

$$f_i(x) = \int_{\frac{-R\pi}{2}}^{x_i} \sqrt{1 - \left(\frac{dy_{heading\_joint\_i}}{dx}\right)^2} \cdot dx - \frac{\int_{\frac{-R\pi}{2}}^{\frac{R\pi}{2}} \sqrt{1 - \left(\frac{dy_{heading\_joint\_i}}{dx}\right)^2} \cdot dx \cdot i}{n} = 0$$

Finally the c_{1i} constants can be obtained from:

$$c_{1i} = y_{heading\_joint\_i}(x = x_i) - y_{coursing\_joint\_i}(x = x_i)$$

In **Figure 30** the reader can see the functions of coursing and heading joints in case of 30 course and 5 element/course. The intersection points of these equations determine the coordinates of a vertex on the development.

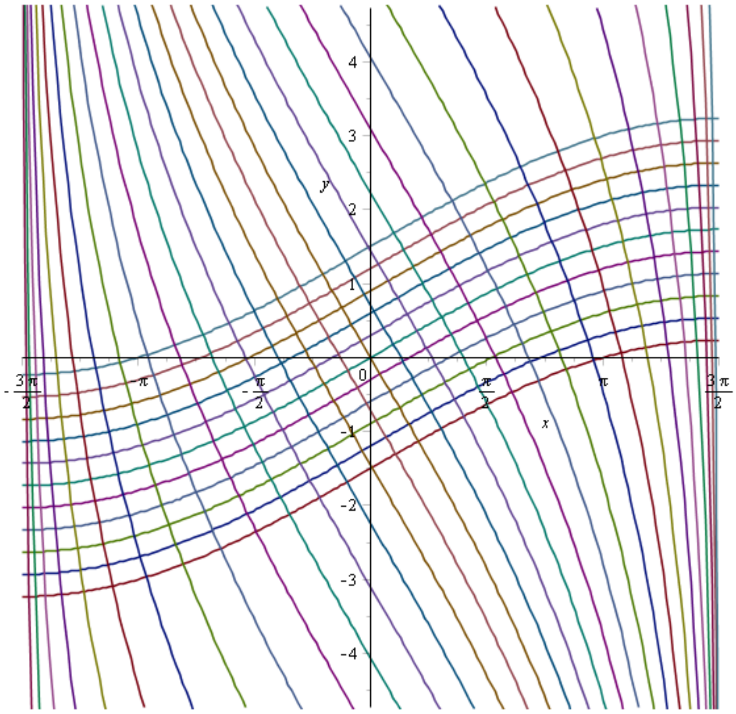

***Figure 30** – Equation of the coursing and heading joints*

To find these intersection points we have to solve the following non-linear equation:

$$h(X) = Y_{heading\ joint\ j}(X) - Y_{coursing\ joint\ i}(X) = 0$$

The built-in non-linear equation solver in Maple (based on the Newton-method) cannot solve those equations where the intersection point is very close to the boundary of the domain. So a bisection method-type solver was written, which is a closed-interval method to solve the nonlinear equation. Unfortunately the computational cost is higher than in the case of Newton-method, but I did not run into convergence problems as in the case of Newton-method. The main steps of the method are the following:

- We have to guess two point: a_1 and b_1. We know that the solution is placed between these values. In our case it is very easy, we know that the solution:
$$-\frac{R_{mid}\pi}{2} \leq X \leq \frac{R_{mid}\pi}{2}$$
- Let the first approximation be:
$$c_1 = \frac{a_1 + b_1}{2}$$
- Then we investigate whether $F(c_1) \cdot F(a_1) < 0$. If this requirement is fulfilled then $a_2 \coloneqq c_1$ else $b_2 \coloneqq c_1$. In each step we can divide into half the investigated interval.
- After we reach a necessary, prescribed precision the solver stops.

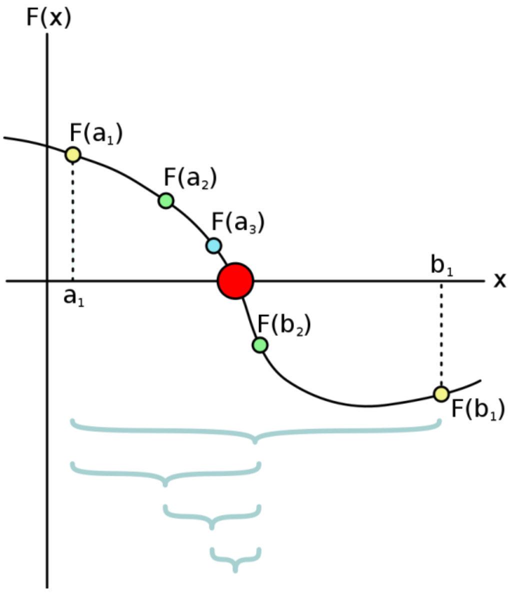

***Figure 31** – Bisection method*

After this procedure the planar coordinates were transform back to the intradosal and extradosal cylindrical surface by the following transformation:

$$x_{int} = \mathrm{R}_{int} \sin\left(\frac{X}{R_{mid}}\right) \qquad and \qquad x_{ext} = \mathrm{R}_{ext} \sin\left(\frac{X}{R_{mid}}\right)$$

$$y_{int} = Y \qquad and \qquad y_{ext} = Y$$

$$z_{int} = \mathrm{R}_{int} \cos\left(\frac{X}{R_{mid}}\right) \qquad and \qquad z_{ext} = \mathrm{R}_{ext} \cos\left(\frac{X}{R_{mid}}\right)$$

Finally the coordinates were rounded with given precision (determined with parameter α) in the following formula:

$$x_{rounded} = \frac{round(x \cdot 10^{\alpha})}{10^{\alpha}}$$

Unfortunately in case of logarithmic method none of the faces of a voussoir is planar theoretically. In reality the mortar layer between the voussoirs resolves the problem, but in 3DEC we can only define polyhedral bodies where the faces should be planar. That is way a half voussoirs is split into two halves. Triangular based prisms were created, and joined together. After this two half voussoir is joined again to create bond pattern.

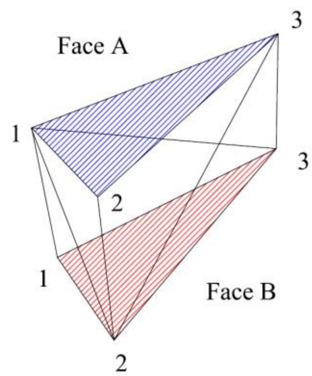

***Figure 32** – Triangular prism to create voussoir*

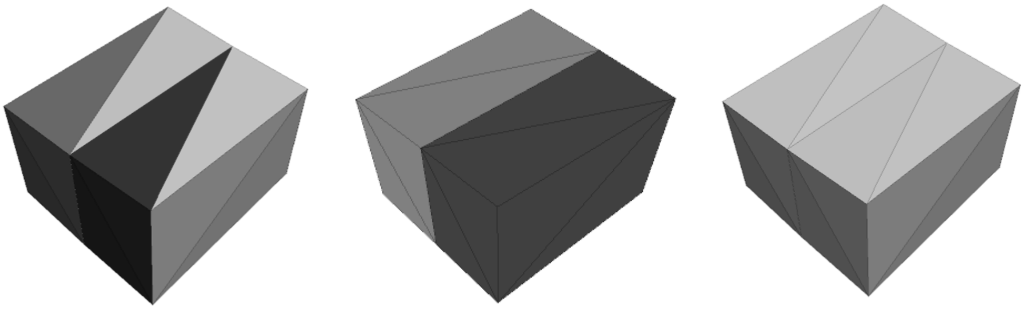

Figure 33 *– Steps of creating a voussoir in case of logarithmic method*

In **Figure 34** masonry arches with different obliquities constructed with logarithmic method can be seen. In the extreme case, when the obliquity is 0°, the regular arch is received back.

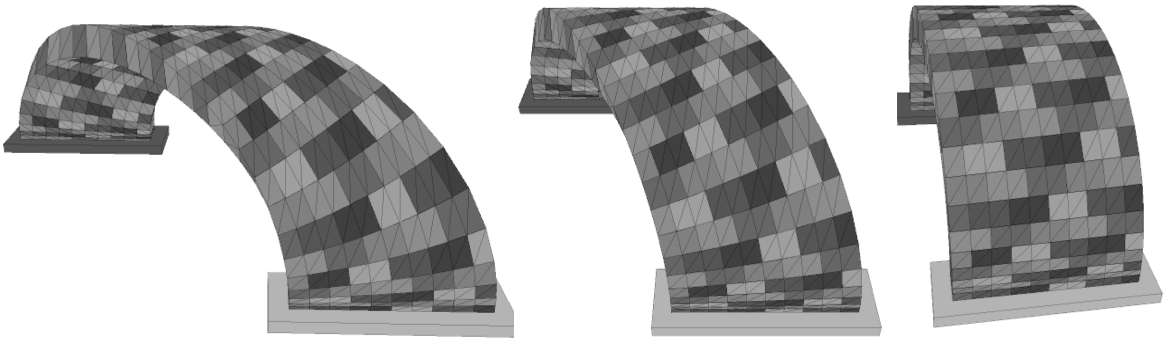

Figure 34 *– Oblique arches constructed with logarithmic method (Obliquities: 45°, 30°, 5°)*

4.2 Material properties, boundary conditions, loading

Material properties

As a fundamental principle the classical assumptions of Heyman were followed (see chapter 3.2). So in the developed three dimensional numerical models:

- **The elements are rigid. The stones have infinite compression strength and stiffness.**
  According to the experiments of Wang [2] the compressive failure of the elements (stones or bricks) is not typical. Especially in case of gravitational loading, the strains in the elements would be so low that they do not modify the failure mechanism.
  Furthermore, the computational time in case of rigid elements is much lower compared to the computational time in case of deformable elements.
- **Masonry has no tensile strength. Between the elements tensile stress cannot develop.**
  The strength parameters of the mortar in case of a 100 year old structure can be very unreliable. In spite of the fact that 3DEC could handle contact characteristics where tensile strength exists, I didn't use this option during the analysis. It can be considered as a conservative assumption.
- **Angle of friction.** During the analysis of regular arches Heyman excluded the possibility of sliding. He assumed that the internal angle of friction is high enough to avoid sliding type of failure. In case of oblique arches, on the other hand, the frictional resistance plays an important role in the load bearing capacity. So in case of the determination of critical barrel thickness the angle of friction was handled as a parameter. Later, in case of live loading a realistic value ($\varphi=40°$) was chosen.

In the numerical model, material properties and contact characteristic should be defined. The only necessary parameter concerning the blocks is their density. The density of the blocks were set up to 2700 kg/m^3, it is equivalent of the density of basalt or andesite.

The following contact parameters were obtained from the work of Jiang and Esaki [24]. They investigated the contact parameters at different weathering conditions. Because of the age of oblique arches, I used the parameters which belong to the most weathered stone:

- Joint normal stiffness: k_n: $7.64\cdot10^9$ N/m^3
- Joint shear stiffness: k_s: $1.79\cdot10^9$ N/m^3
- Joint friction: varying (during the determination of crit. thickness), $\varphi=40°$ (during the analysis of live loading)
- Joint tensile strength: 0 N/m^2
- Joint cohesive strength: 0 N/m^2
- Joint dilatation angle: 0°

Boundary conditions

The arches were supported from below with fixed support blocks. In contrast to the finite element models where supports can be defined with prescribed displacements at the nodes, in discrete element method the velocities are prescribed at the boundaries. The velocity of the nodes of the supporting blocks (**Figure 35Hiba! A hivatkozási forrás nem található.**) was set to 0 in the three orthogonal directions.

Oblique arches exhibit a 3D mechanical behaviour, so they cannot be investigated like regular arches, where for example a slice with unit length can be analysed, using the appropriate lateral boundary conditions. Because of the fact that the full width of the arch was analysed, artificial lateral supports are not necessary.

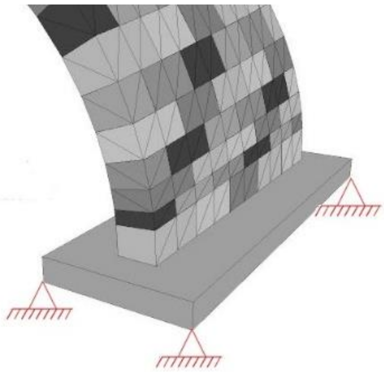

***Figure 35** – Support conditions at the springing*

Loading

Two loading situations were investigated:

- **Determination of the critical barrel thickness:** only gravitational forces were acting on the structure. The gravity was applied in a single step to the whole structure. It did not influence the results when the intensity of gravity was increased gradually, but the computational time was higher. Detailed simulation of the removing process of the formwork might perhaps have an influence on the results, but this question was not analysed during this work.
- **Effect of live loading:** the structures were equilibrated under self-weight in the same way as defined previously. Full width line load was applied with the help of a "loading element", whose density was increased incrementally until the ultimate load bearing capacity[5] was reached. The direction of the line load is described in more detail in Chapter 5.2.

The structure is considered to be in equilibrium if the unbalanced force of the system is below a certain prescribed limit. In case of collapse the stones begin to freefall, while unbalanced forces start to increase until becoming comparable to the weight of the structure.

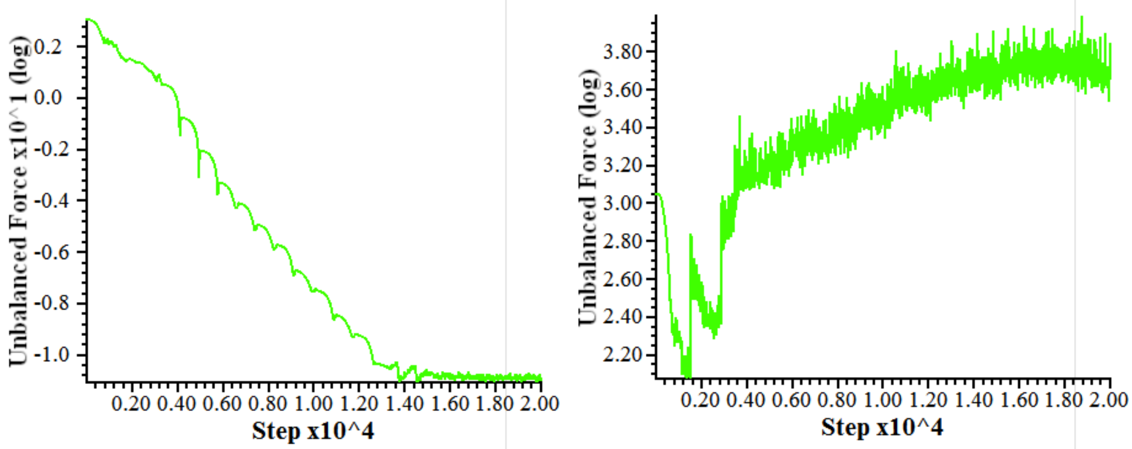

***Figure 36** – Unbalanced forces (log scale) in case of equilibrium (left) and in case of collapse (right)*

[5] Ultimate load bearing capacity: the maximum load, which can be resisted by the structure without failure. (Ultimate Limit State)

During the analysis of live load a force-displacement curve can be assembled in the following way:

- The type of the analysis is force-controlled, hence the descending part of the force-displacement curve cannot be tracked.
- After the gravitational load was applied on the structure, the arch reaches the equilibrium (after ~6000 step in this example). We can see that in equilibrium state the deflection-timestep curve has a constant value.
- A loading element is defined on the extrados of the arch. If the volume and the density of the loading element are known, then the live load can be calculated easily. In this example the density of the loading element was increased with 1000 kg/m^3 in every loading step. This means that the precision of the calculation is also defined. The starting point of a new load step can be found where the unbalanced force reaches a sufficiently small, pre-defined threshold value (i.e. the structure is in equilibrium).

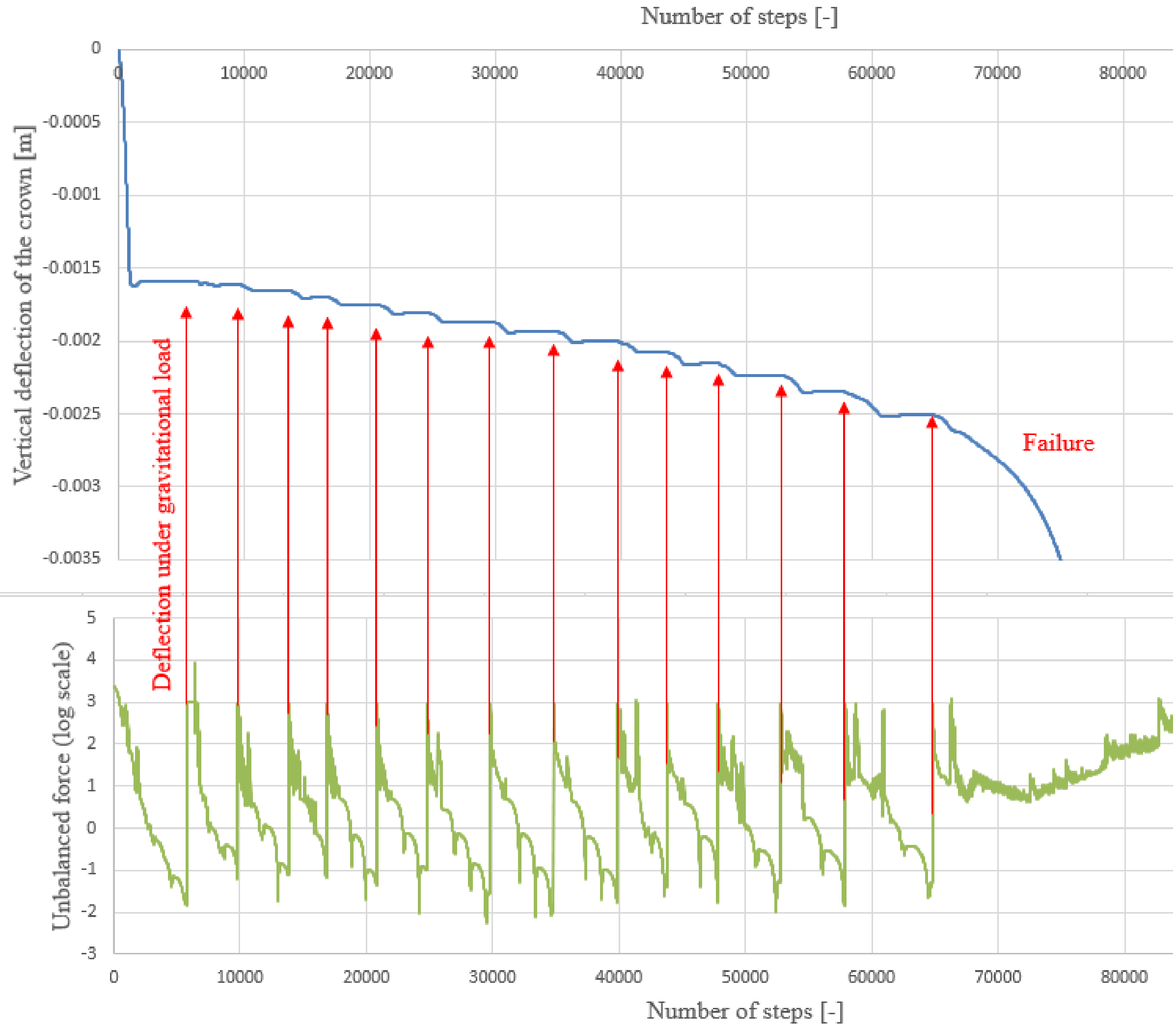

***Figure 37** – Determination of the load-deflection curve*

If the corresponding live load - deflection pairs are plotted, then the load-displacement curve can be assembled.

The curve is non-linear but it does not contain fractures or jumps. The reason of this smoothness is that the tensile strength between the elements was set to zero.

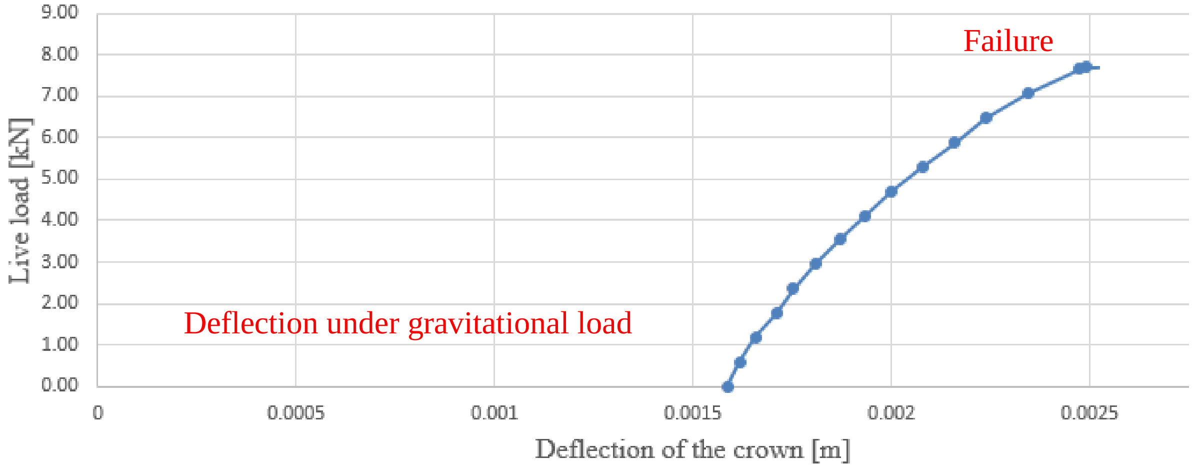

***Figure 38** – Live load – deflection curve*

Usually, cracks of 0.2mm and wider are visible to the naked eye. The load required to cause crack opening greater or equal to 0.2mm could be measured with the help of the 3DEC.

During a future work, when real circumstances are modelled (full bridge assemblies with tensile strength at the joints) the question of load at first crack plays a more important role because the stiffness of the structure decrease with the development of cracks

Without defining any tensile strength at the joints, the structure has around 0.2-0.4mm crack at the crown under self-weight if the barrel thickness is close to the critical barrel thickness. If the barrel thickness is around 0.200R, then all of the joints are closed.

4.3 Verification

Before using a numerical model it is necessary to compare and validate its predictions with theoretical and/or experimental results.

Compared to skew arches where the mechanical behaviour is mostly unknown, the mechanical behaviour of a direct arch is well-known, so the verification was made with the help of a direct arch. The classical issue of finding the minimum thickness required for equilibrium of a continuous circular masonry arch, with 90°half-angle of embrace, subjected only to its own weight has been investigated by several engineers. The issue is practically settled for today: the (purely-rotational) collapse mechanism that develops when the thickness of the arch is critically small is known and displays as a symmetric five-hinge mechanism with a hinge at the extrados at the keystone, two hinges at the extrados at the shoulders and two hinges at the intrados at the haunches.

As a starting point, Couplet, in 1730, assumes for the full semi-circular arch that the angular position of the haunches' hinges (β_{cr}) (measured from the vertical axis) is at 45° and to obtain that t_{min} = 0.101*R, where R is the radius of the mid-surface.

Heyman [16] reports analytical formulas that can be used to determine β_{cr} and t_{min}. As a reference instance, for a complete semi-circular arch the solution of Heyman's formulas renders the following usually-referenced values:

$$\boldsymbol{Heyman}: \beta_{cr} = 58.82° \quad and \;\; t_{min} = 0.105965R$$

Unfortunately Heyman's work is based on a few incorrect assumptions (incorrect tangency condition of the contact forces at the haunches, incorrect location of the centre of gravity of the elements) [25].

But a Serbian researcher, Milankovitch developed a quite general analysis [26] which handled the above problems correctly already in 1904 (though his work was forgotten, and re-discovered around the end of the XXth century only). His result:

$$\boldsymbol{Milankovitch}: \beta_{cr} = 54.48° \quad and \;\; t_{min} = 0.107478R$$

The numerical results obtained from my model (see **Figure 39**) were very close to the theoretically proper solution of Milankovitch. The precision of my model is ±1.5° and ±0.0005R.

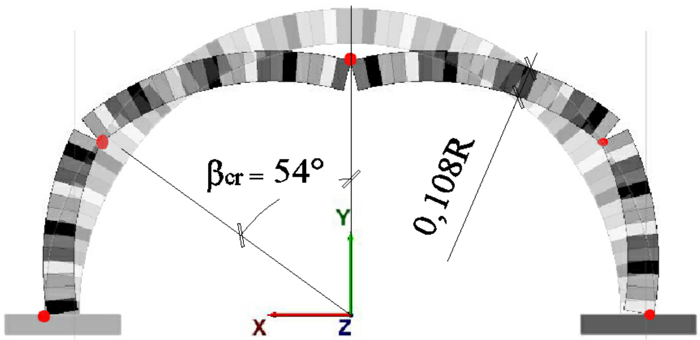

Figure 39 – Angular position of the haunches' hinges β_{cr}, and critical barrel thickness obtained from my numerical model

Another verification can be made by investigating the sliding type of failure. This failure occurs when the compression force reaches the boundary of the cone of friction (α=φ).

If we could calculate the angle of deviation between the line of thrust and the contact normal, then the minimal necessary friction to avoid the sliding type of failure in case of the self-weight can be determined.

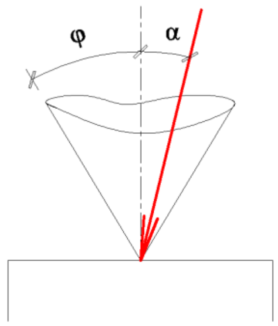

Figure 40 *– Cone of friction*

After Cocchetti et al. [25] the equation of line of thrust can be written in the following form:

$$r(\beta) = \frac{2\beta\sin(\beta) - 2(1-\cos(\beta)) - h(2+\eta-2\cos(\beta)}{\eta(\beta\sin(\beta) + hcos(\beta)}\cdot\frac{\eta}{2}\cdot R + R$$

where β is the inclination angle measured from the vertical axis of symmetry.

η is the thickness/radius ratio, in case of critical barrel thickness 0.107478

R is the radius of the arch.

h is the non-dimensional horizontal thrust, in case of crit. thickness. 0.621772

The derivative of a polar function can be calculated as:

$$\frac{dy}{dx} = \frac{\frac{dr(\beta)}{d\beta}\cdot\sin(\beta) + r(\beta)\cdot\cos(\beta)}{\frac{dr(\beta)}{d\beta}\cdot\cos(\beta) - r(\beta)\cdot\sin(\beta)}$$

If we make the distinction between the derivative of contact normal and between the tangent of the line of thrust, we obtain the necessary angle of friction:

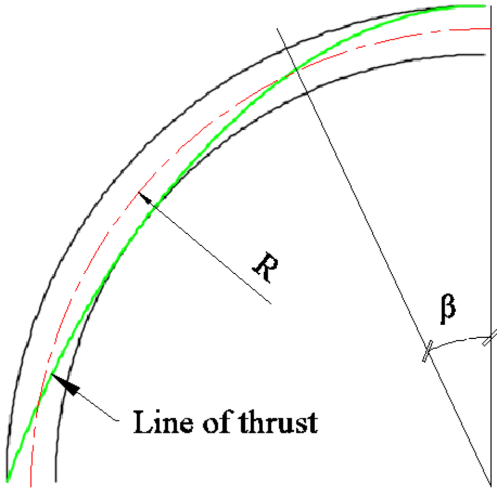

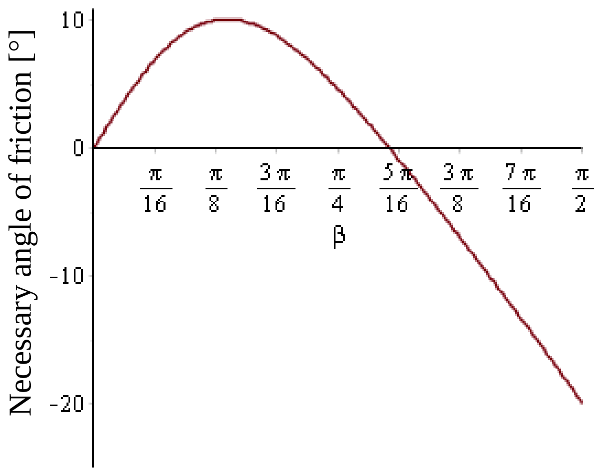

Figure 41*: The necessary angle of friction to resist the self-weight in case of semi-circular arch and minimum barrel thickness*

As seen in **Figure 41**, the maximal frictional resistance is needed at the springing line of the arch, where β=π/2. The minimum necessary angle of friction according this calculation is 19.97°.

My numerical model suffered sliding type mechanism in case of 20° of friction, while at 21° it remained stable. The obtained failure mechanisms in case of a direct arch can be seen in **Figure 42**. The results of the numerical model are in good agreement with the analytical derivations.

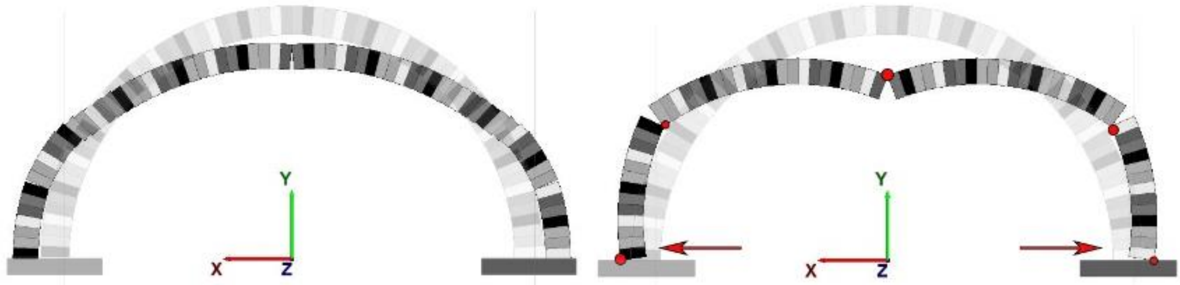

Figure 42 *– Failure modes, when the angle of friction is 5° (left) and 20° (right)*

The last comparison was made with the help of LimitState:RING 3.0f. This program uses the theory of limit analysis, with a linear programming technique to determine the maximum value of live load at a given position.[6]. A regular arch was analysed in respect of load bearing capacity. As the reader can see in ***Figure 43*** there is a good agreement between the two different numerical techniques.

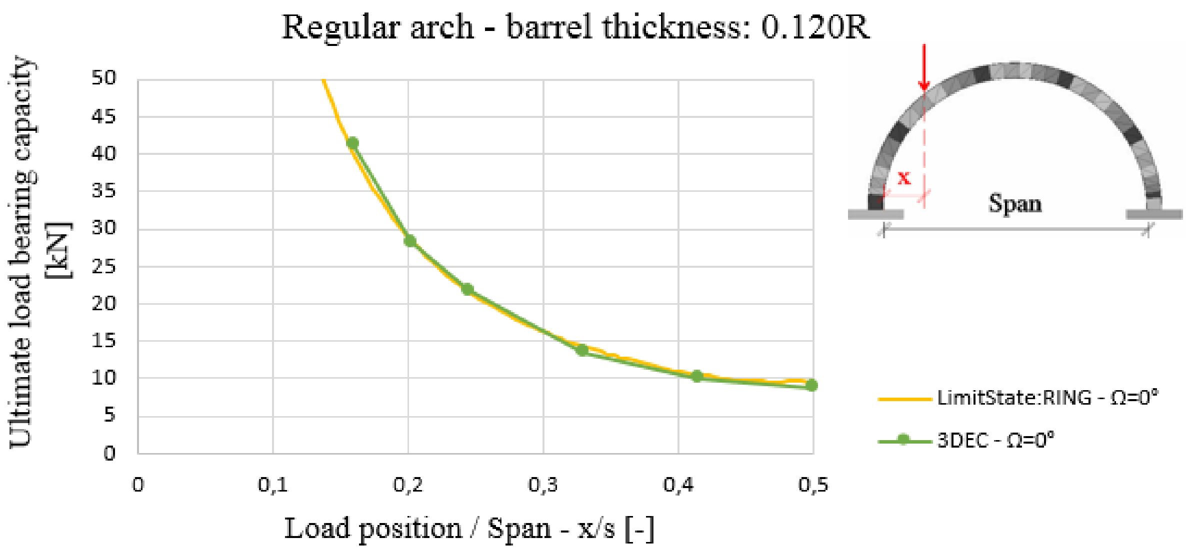

Figure 43 *– Load bearing capacity calculated with 3DEC model and LimitState:RING*

5 Results and discussion

During the diploma work two main types of analysis were carried out:

[6] The details of LimitState:RING were described in Chapter 3.2.1.

- **Determination of the critical barrel thickness:** Only gravitational loading acted on the arch. In this situation the barrel thickness of the arch was decreased until the critical barrel thickness was found. The structure collapses when the barrel was so narrow that the line of pressure could not fit inside the boundaries of intrados and extrados surfaces.
- **Effect of full width external line load:** after the structure reached the equilibrium state under its self-weight, a full-width external load was applied to the extrados of the arch. As a consequence of the increasing load the shape of the line of pressure changed. Finally, this altering line of pressure exceeded the boundaries of the arch, and the structure reached the state of failure.

Unfortunately, there is a wide set of parameters which can influence the behaviour of the skew arch. These parameters are summarized in the following.

- **Obliquity of the arch**

  The effect of obliquity was investigated in the range of 0° to 45°. Higher obliquity angles would be unrealistic as they do not appear in the practice.

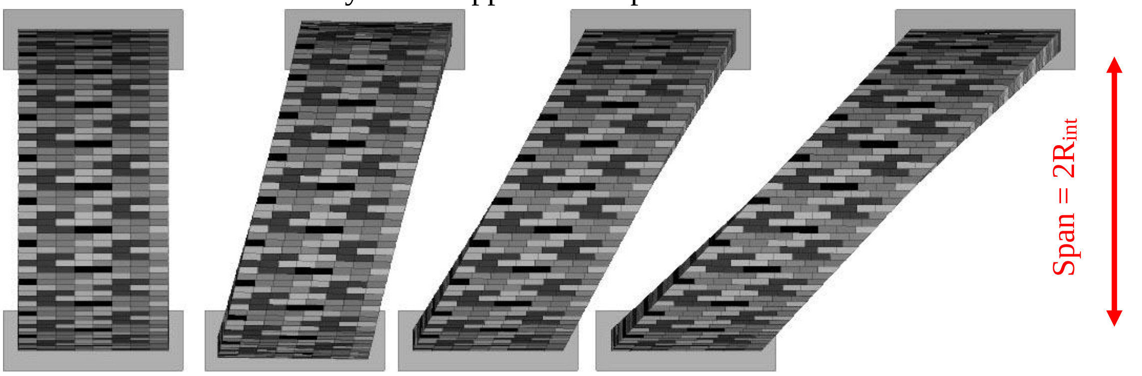

Figure 44 *– Different obliquities: 0°, 15°, 30°, 45°*

- **Width of the arch**

  The oblique arch expresses a 3D mechanical behaviour, so the width of the arch might have an influence on the critical barrel thickness, which should be investigated.

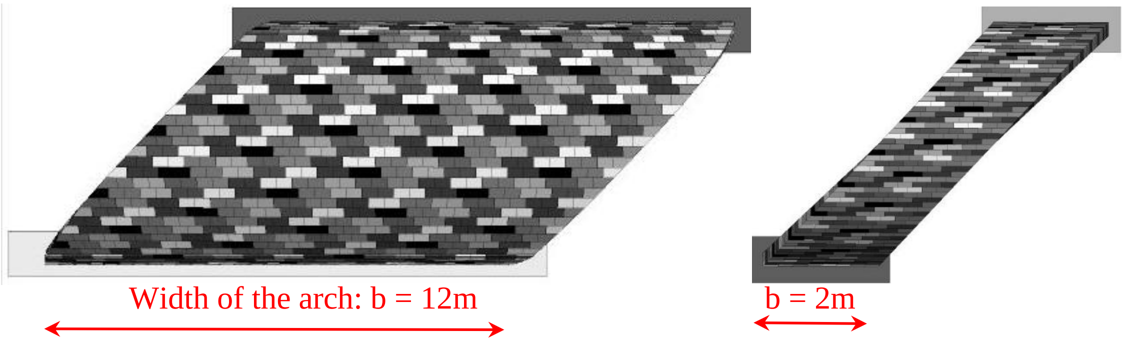

Figure 45 *– A wide (12m) and a narrow (2m) arch*

- **Method of construction**

  All the three previously introduced methods of construction were analysed. These methods were the false skew arch, the helicoidal method and the logarithmic method.

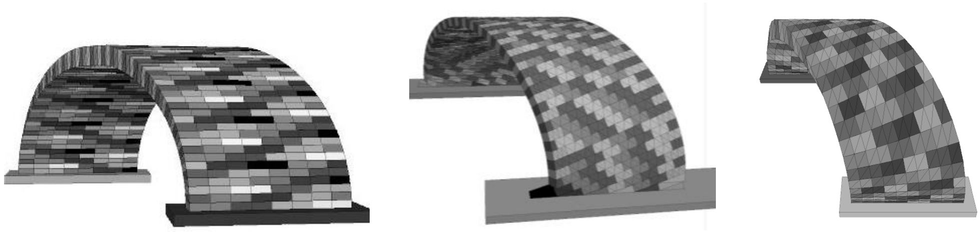

Figure 46 *– Different methods of construction: false skew arch, helicoidal method, logarithmic method*

- **Embrace of the arch**

  In the framework of this project only semi-circular arches were investigated, so the half-angle of embrace was 90°. Later, shallow arches, where the angle of embrace is less than 90° (i.e., span/rise ratio is higher than 2) can be investigated.

- **Size of the elements**

  The shape and size of the elements could also affect the mechanical behaviour. During my investigations I assumed that the arch was made of a single-ring of stone, hence the height of the elements can be considered as a given data. The shape and size of the elements were chosen in the realistic range. As a side-line of the diploma work the ratio between the length and the width of the elements was also investigated.

- **Frictional resistance between the stones**

  Heyman assumed during the analysis of regular arches that the angle of friction is high enough to avoid sliding type of failure. In case of regular arches this assumption might be proper. In Chapter 4.3, it was demonstrated with numerical and theoretical examples that for direct arches, the minimally necessary angle of friction to resist the self-weight is around 20-21°. In case of real circumstances the angle of friction is between 30°-45°. As we will see in case of oblique arches the frictional resistance plays a very important role in the load bearing capacity. The effect of angle of friction on the mechanical behaviour is investigated during the determination of critical barrel thickness.

5.1 Determination of the critical barrel thickness

The minimal barrel thickness which can resist the self-weight of an oblique arch is unknown in the literature.

The flowchart of the determination of critical barrel thickness[7] can be seen on the following figure. After the geometry was created with the given width, radius, obliquity and method of construction, an unrealistically thin barrel thickness was defined, with infinite frictional resistance. This structure collapsed with high probability. In this case the barrel thickness was increased, until a stable structure was reached. After this point the frictional resistance was decreased between the elements, until the structure collapsed again. In this way we can decide what is the critical barrel thickness for infinite friction, and whether a given barrel thickness and angle of friction pair is stable or not.

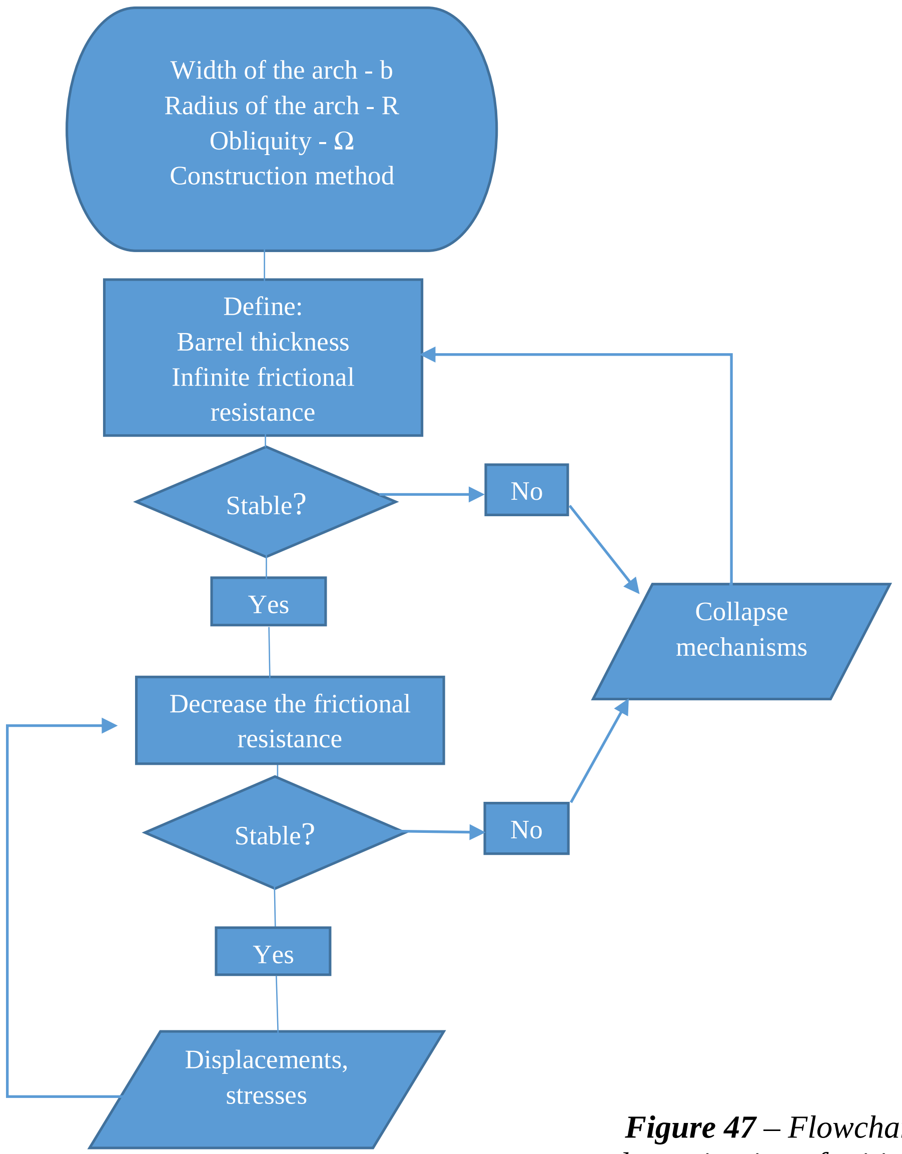

Figure 47 *– Flowchart of the determination of critical barrel thickness*

[7] The critical barrel thickness is determined usually with a non-dimensional parameter, as a thickness/radius ratio. $\eta = t/R$ [-].

5.1.1 Displacements

During the analysis rigid elements were used. Hence, with a given geometry (span, width, barrel thickness, obliquity and construction method) the magnitude of the displacements depends only on the contact parameters and the number of elements. If the normal and shear contact stiffness would be increased then the magnitude of the displacements would decrease. Similarly, if smaller elements would be used then the number of contacts would increase, so the magnitude of displacements would increase.

In the framework of this diploma work only the distribution of the displacements along the arch will be presented and discussed. The common parameters of the arches were the radius, the width, the obliquity and the barrel thickness, while the methods of construction differed.

Vertical displacements

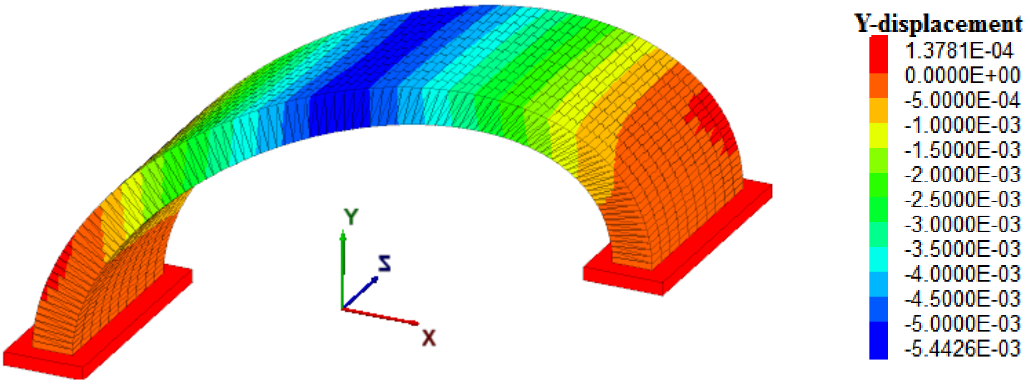

Figure 48 *– Vertical displacements of the* ***false skew arch***

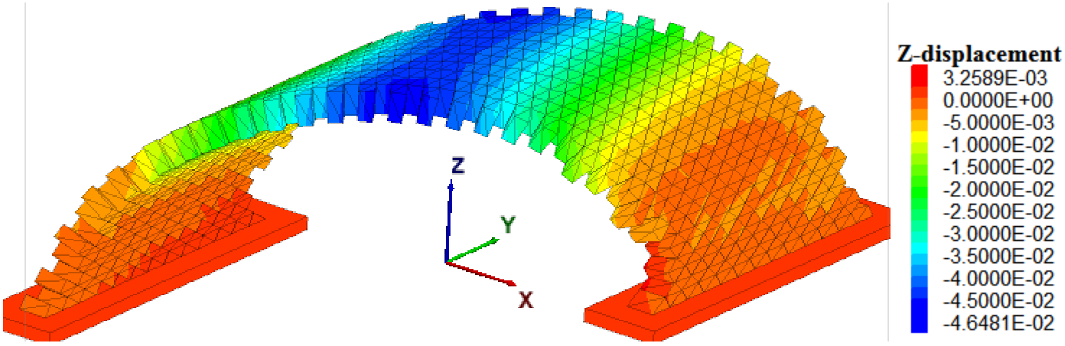

Figure 49 *– Vertical displacements of the* ***helicoidal method***

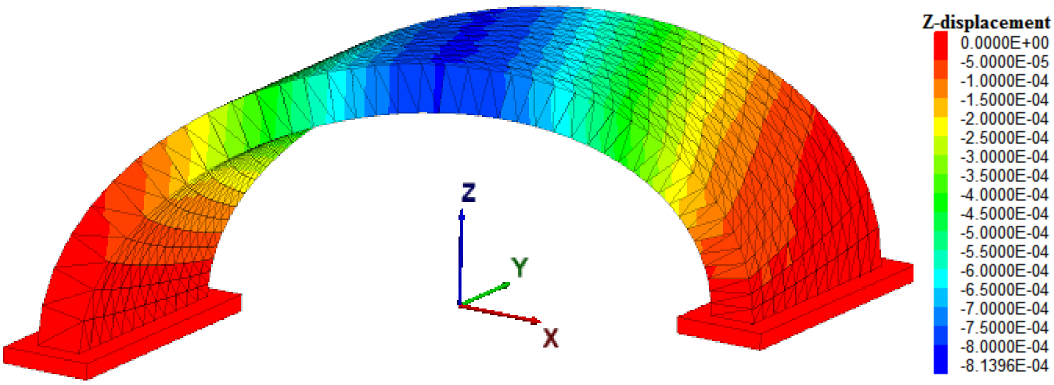

Figure 50 *– Vertical displacements in case of* ***logarithmic method***

The maximum vertical displacements can be found at the crown. While in case of the false skew arch the iso-levels of the displacements are parallel with the longitudinal axis of the arch in case of logarithmic method the iso-levels are rather perpendicular to the face of the arch. This phenomena is connected to the barrel thickness. If the applied barrel thickness is significantly thicker than the critical barrel thickness, then cracks don't develop at any cross section, the iso-levels are perpendicular to the face. Decreasing the barrel thickness, cracks develop in line with the longitudinal axis of the arch: first at the crown, then at the abutments, finally at the haunches until the structure turns into a mechanism.

Crosswise displacements (in X-direction)

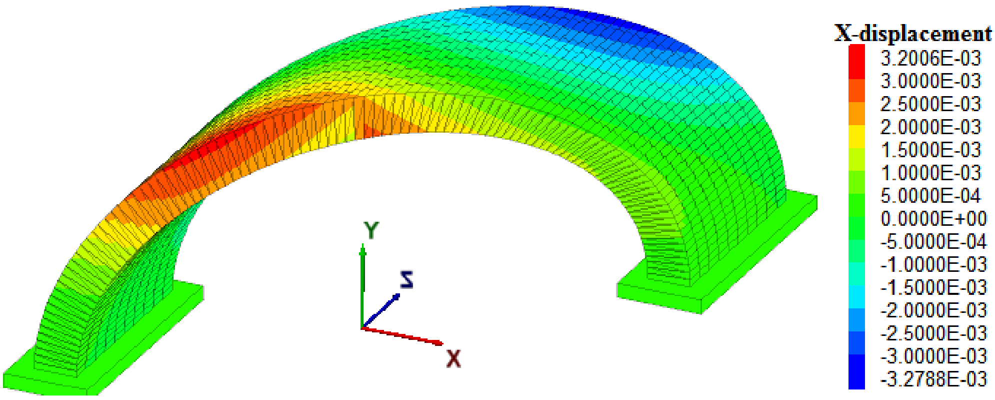

Figure 51 *– Crosswise-displacements in case of the* ***false skew arch***

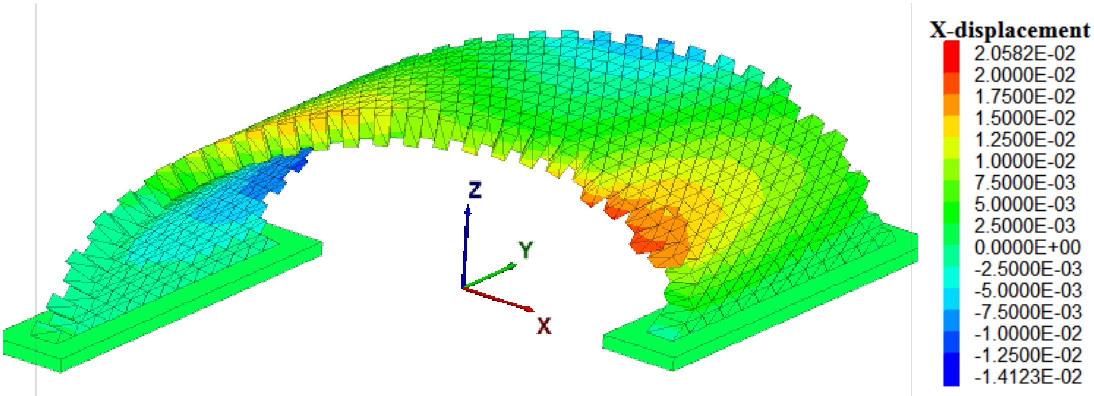

Figure 52 *– Crosswise-displacements of the* ***helicoidal method***

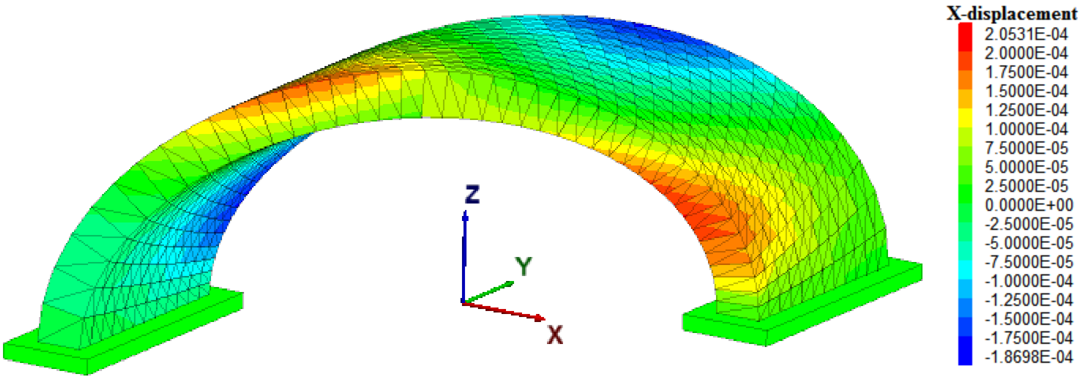

Figure 53 *– Crosswise displacements in case of* ***logarithmic method***

In case of the false skew arch “the unsupported” parts of the arch at the obtuse angles have significant displacements in the X-direction. The distribution of the displacements is a bit different in case of the logarithmic and helicoidal method compared to the false skew arch.

The silhouette of the structures is point symmetric but the joints are not definitely not located symmetriccally, hence the displacements of two corresponding point are not perfectly equal.

Horizontal displacements in the longitudinal direction

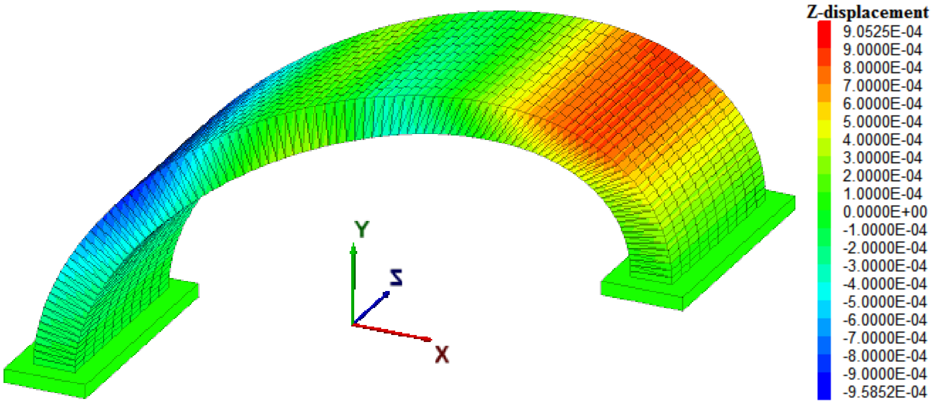

Figure 54** - Longitudinal displacements in case of the **false skew arch

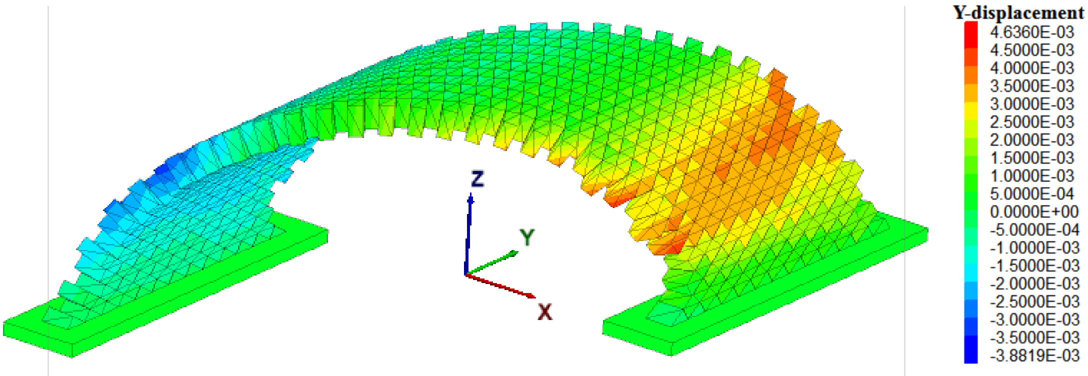

Figure 55** - Longitudinal displacements in case of **helicoidal method

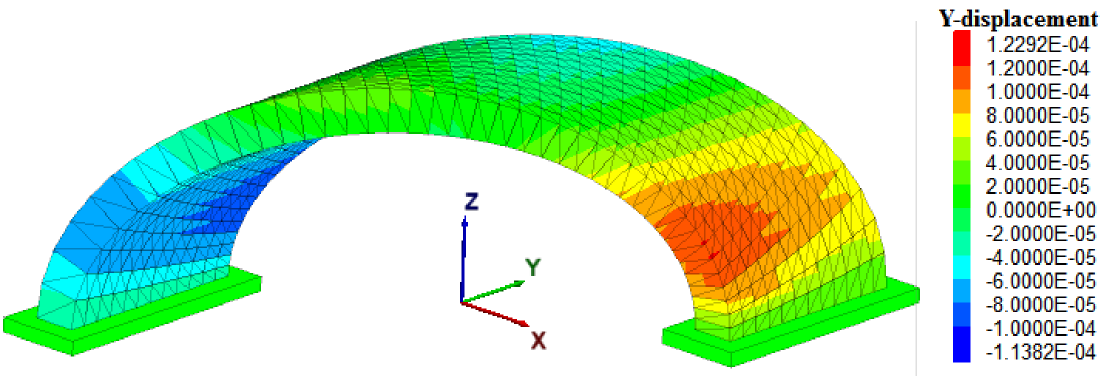

Figure 56** – Longitudinal displacements in case of **logarithmic method

The distribution of the longitudinal displacements is very similar in all case.

5.1.2 Joint normal and shear stress distributions

During the discussion of joint stress distributions the results of the false skew arch, the helicoidal method and the logarithmic method will be compared. The vertices and the edges of the adjacent elements should connect perfectly if we want to plot the properties of the joints.

The arches in this comparison has the following parameters:

Common parameters		Differing properties
Radius:	3m	Method of construction
Width of the arch:	5m	
Barrel thickness:	0.12·R = 0.36m	
Avg. element length	0.5m	
Number of courses:	40	
Angle of friction:	40	

Table 1 *- Parameters of the investigated arches*

Shear stress distributions

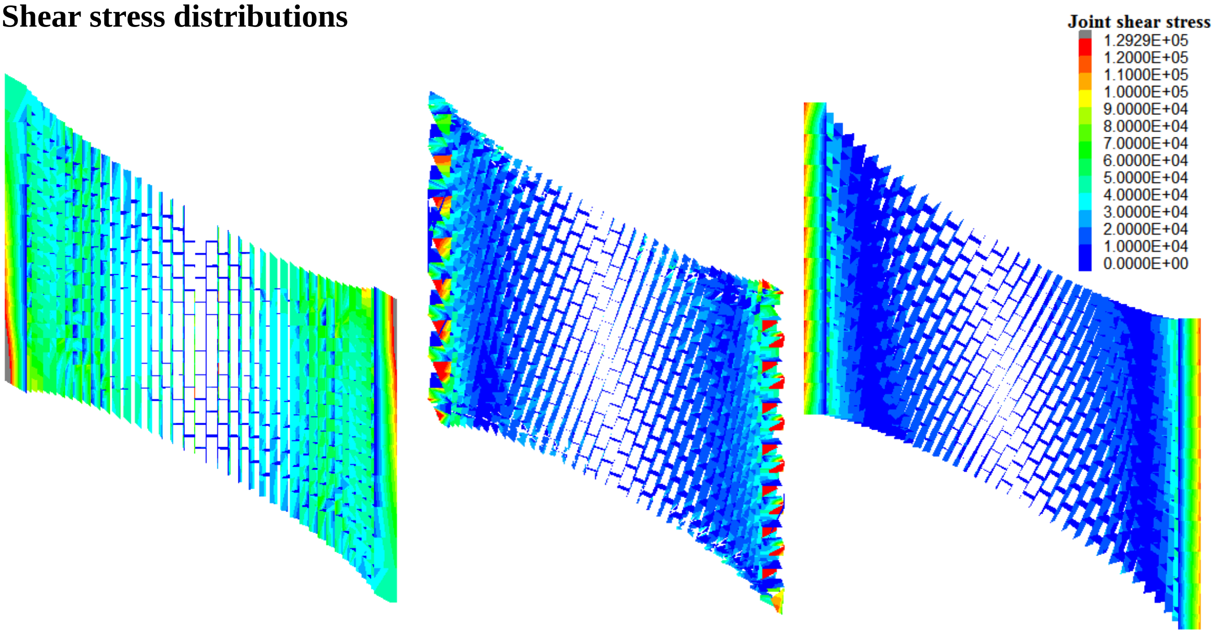

False skew arch **Helicoidal method** **Logarithmic method**

Figure 57 *– Joint shear stresses (bottom view)*

The maximum shear stress arises at the abutments in every case. At this contact surface the distribution of the shear stresses is not uniform in case of false skew arch: the acute angle of the arch is more overloaded, the shear stresses are concentrated here. Interestingly, the distribution of the shear stresses is almost uniform in case of the logarithmic method at the springings. The shear stresses at the higher level coursing joints in case of advanced methods (logarithmic and helicoidal) are much smaller compared to the false skew arch. This was indeed the original aim of the inventors of this method in the 19th century.

In contrast with the regular arch, shear stresses arise at the heading joints too. The magnitudes of these shear stresses are smaller with one order of magnitude compared to the shear stresses on the coursing joints. The highest shear stresses arise in case of helicoidal method around the abutments, hence here is the biggest deviation between the optimal and the applied coursing joints direction.

The shear stresses of heading joints are concentrated to the haunches of the arch in case of logarithmic method.

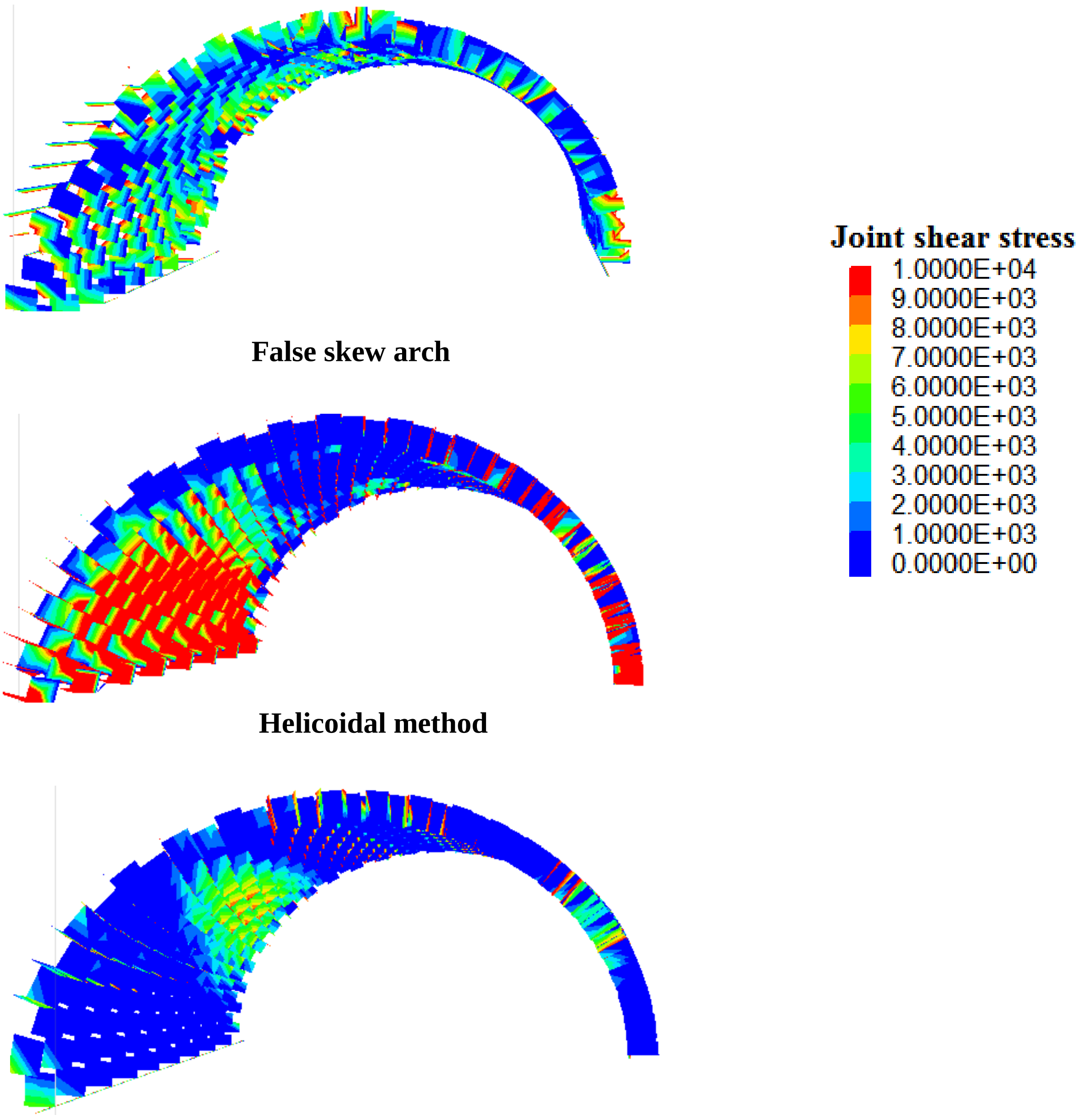

***Figure 58** – Shear stress distributions of the heading joints*

Normal stress distributions

The normal stress distribution of the false skew arch and the helicoidal method is non-uniform. The coursing joints at the acute angles are more overloaded compared to coursing joints at the obtuse angle of the arch (**Figure 59**).

In case of the logarithmic arch the stress distribution is smoother compared to the false skew arch. The stress distribution at the abutments is more uniformly distributed along the width of the arch.

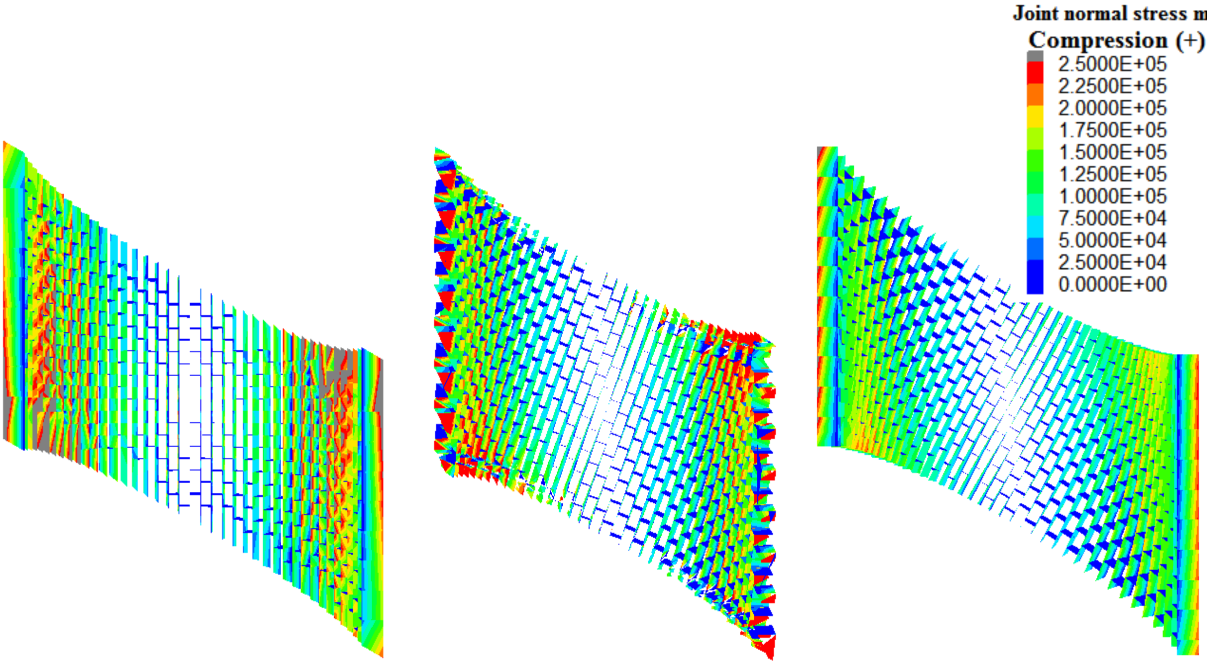

False skew arch **Helicoidal method** **Logarithmic method**

Figure 59 – Normal stress distribution (bottom view)

In **Figure 60** the normal stresses of the heading joints can be seen. The normal stresses are smaller with one order of magnitude compared to the normal stresses of the coursing joints. The highest stresses arise in case of helicoidal method around the abutment. The distribution of the normal stresses on the heading joints in case of logarithmic method is smoother compared to the other methods and nevertheless the values are the smallest in this advanced method.

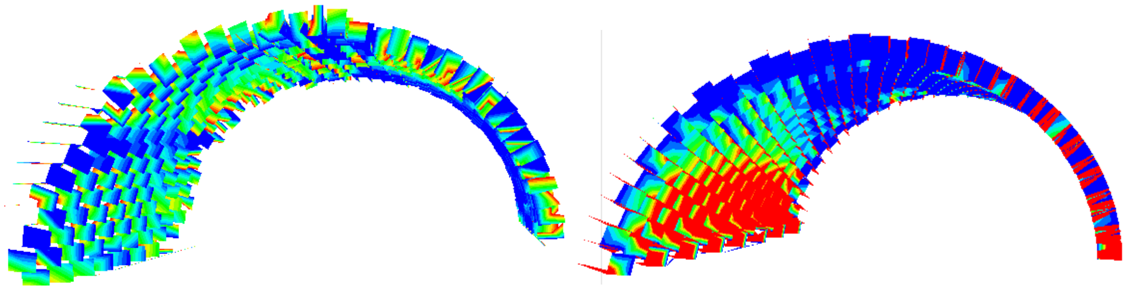

False skew arch **Helicoidal method**

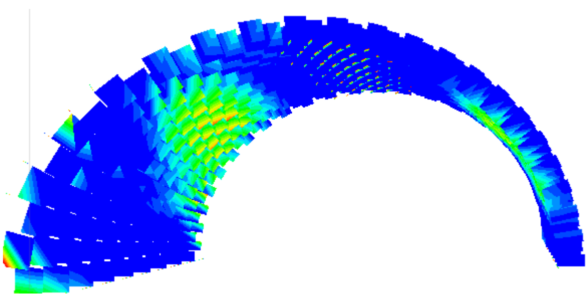

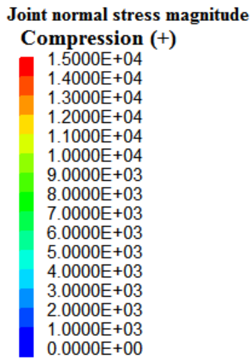

Logarithmic method

Figure 60 – Normal stress distributions at the heading joints

5.1.3 Collapse mechanisms

A regular arch shows a classic 5-hinge type rotational collapse mechanism under gravitational load if the angle of friction is in the realistic range. Because of the symmetry of the structure, the collapse mechanism is also symmetric: a hinge develops at the crown, two others at the abutments, and finally two hinges develop at the haunches of the arch.

During the investigation of skew arches a similar 5-hinge type rotational collapse mechanism can be recognised. The hinge-rows are parallel to the abutments at all methods of construction and at arbitrary obliquity. (Assuming realistic angle of friction and realistic element shapes.)

The hinge rows can develop along a straight line because the coursing joints are parallel to the hinge-rows. Compared to this, the hinge rows can develop only in zigzag pattern in case of the helicoidal and the logarithmic method.

Comparing the rotational collapse mechanisms of the three investigated methods of construction, we can observe that in the case of the helicoidal and logarithmic method the blocks in a given hinge-row not just tilt on each other (as in the case of false skew arch), but they also have to slide upon each other at the same time. This additional resistance, caused by the friction between the elements, contributes to the overall resistance of the arch. With this phenomenon the smaller critical barrel thickness of the helicoidal and logarithmic methods can be understood.

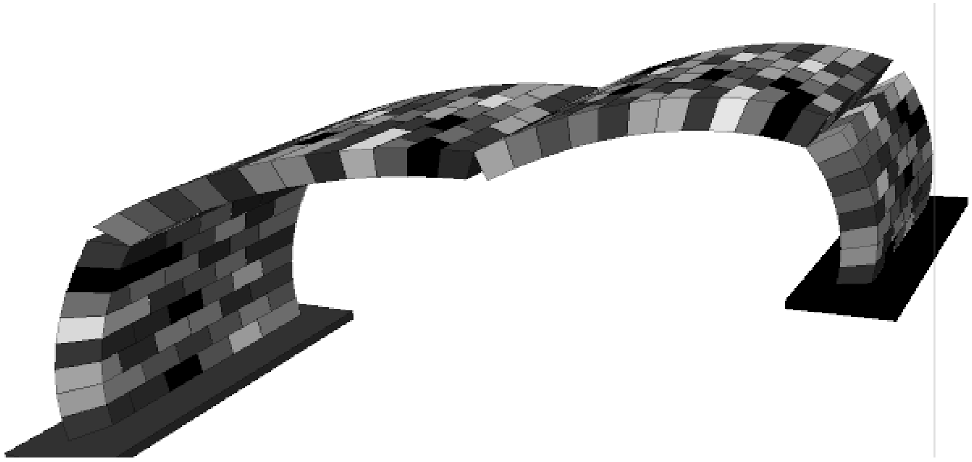

Figure 61 *– Rotational collapse mechanism of the false skew arch*

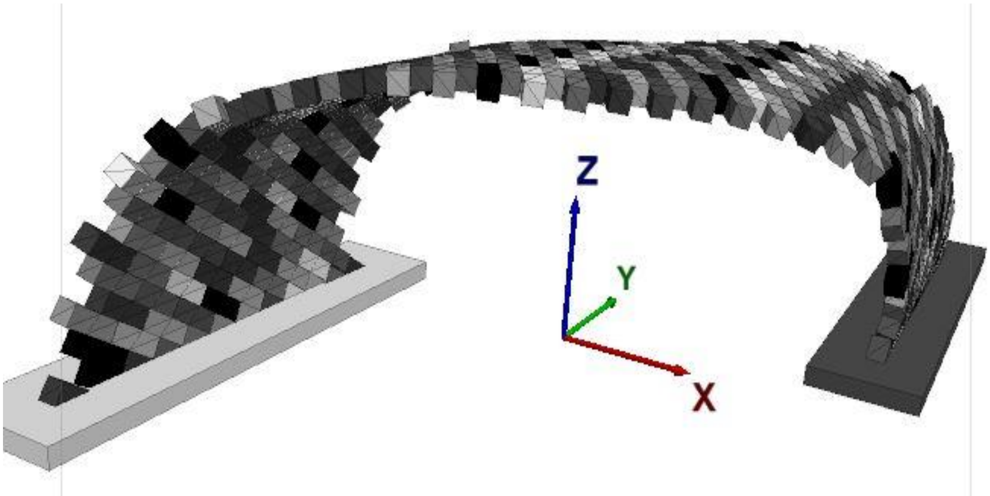

Figure 62 *– Rotational collapse mechanism of helicoidal method*

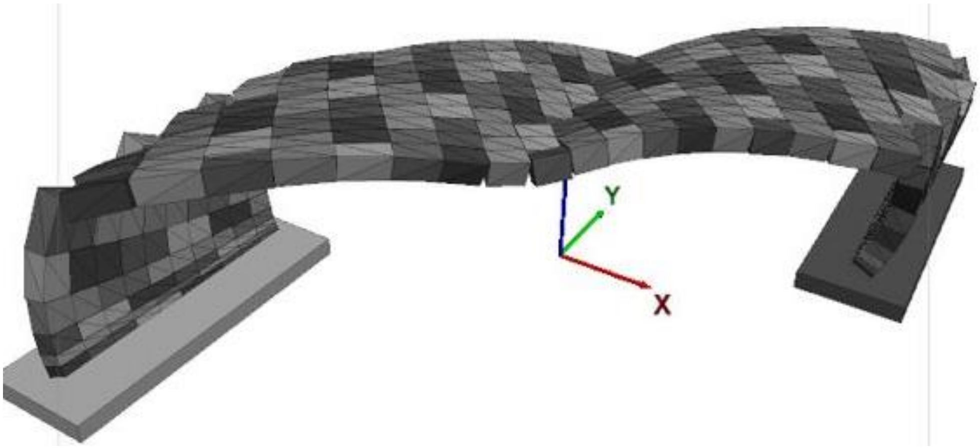

Figure 63 *– Rotational collapse mechanism of logarithmic method*

The failure modes are influenced furthermore by the angle of friction. The effect of angle of friction is demonstrated with the help of structures built by the logarithmic method. **Figure 64** shows a chart where on the horizontal axis the applied angle of friction can be seen, while on the vertical axis the applied barrel thickness is shown. The plotted points mean those pairs of the angle of friction – barrel thickness values where the structure just remains stable. Above those points the structure is in equilibrium, but below those points the structure would collapse. In this way the collapse mechanisms can be categorized. The precision of the critical barrel thickness is ±0.001R, while the precision of the angle of friction is ±1°.

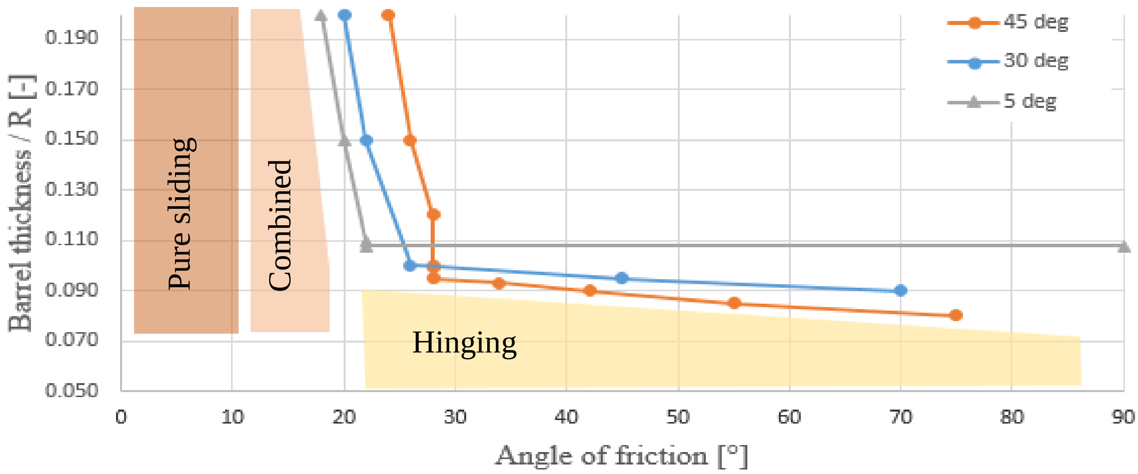

Figure 64 *– Characterizing the failure modes in case of logarithmic method*

- If the applied angle of friction is very low (i.e. less than 10°), almost pure sliding type mechanism occurs. In this case every course starts to slide upon each other. Usually this failure mode doesn't occur in reality, because the realistic angle of friction between the stones is much larger, around 25-45°.

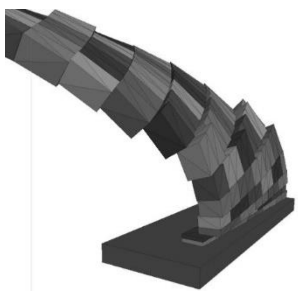

Figure 65 *- Pure sliding mechanism*

- If the applied barrel thickness is very small, a purely rotational collapse mechanism occurs, which is nearly independent from the applied angle of friction. The direction of the developing five hinge-rows is parallel to the axis of the arch (y-axis).

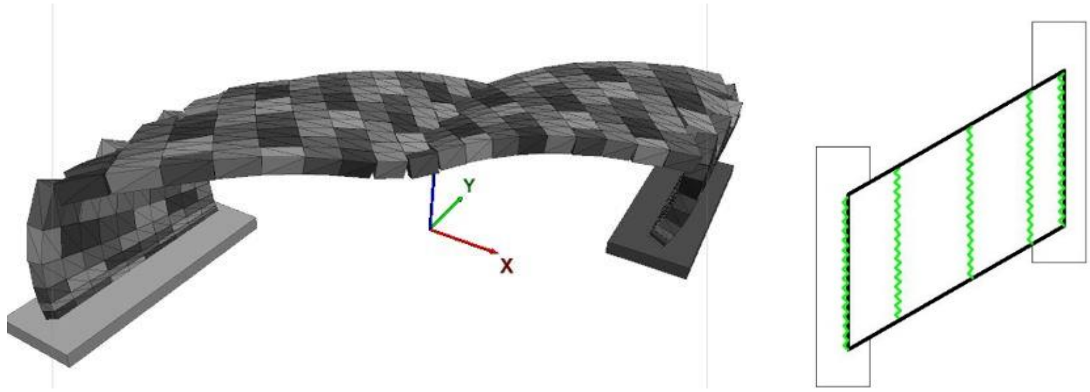

Figure 66 *– Purely rotational collapse mechanism*

- There is no sharp boundary between the above mentioned two failure modes. In the intermediate region, where the angle of friction is around 10-25°, a mixed type of failure occurs. During the failure the arch begins to slide at the springings around the acute angle, then hinge-rows develop. But these hinge-rows are not parallel to the original position of the abutments, rather perpendicular to the faces of the arch.

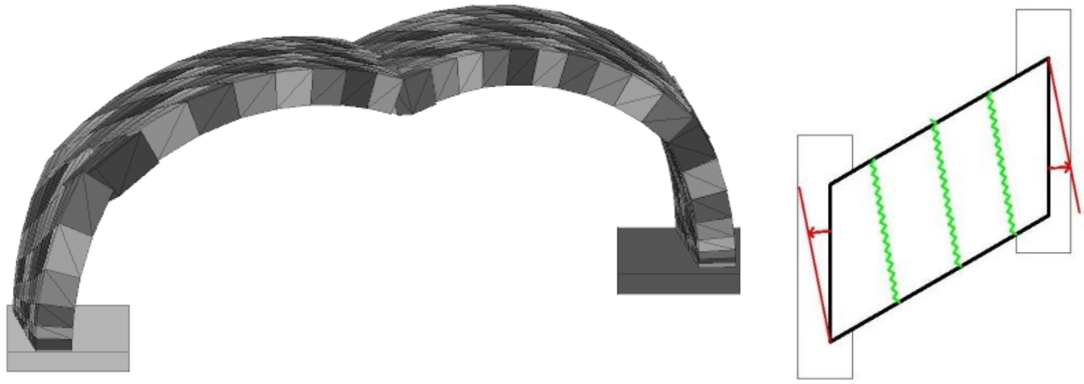

Figure 67 *– Combined failure mode of an oblique arch*

According to **Figure 64** it can be observed that if the angle of friction is smaller than ~20° then the structure will collapse, no matter how thick is the barrel. Similarly, if the barrel thickness is small enough then no matter how big is the angle of friction.

The results related to the critical barrel thickness are summarized in **Figure 68**. The continuous lines mean those (unrealistic) models where the frictional resistance is infinite (i.e. sliding cannot occur between the elements).

The arches in this comparison has the following parameters:

Common parameters		Differing properties
Radius:	3m	
Width of the arch:	3m	Method of construction
Barrel thickness:	0.12·R = 0.36m	
Avg. element length	0.5m	
Number of courses:	40	Obliquity
Angle of friction:	40° / 90°	

Table 2 *- Parameters of the investigated arches*

The dotted lines in **Figure 68** were calculated on models with a realistic angle of friction (φ=40°). The following conclusions can be made:

- If the angle of skew is set to 0° (the case of a regular arch), each construction method gives back the well-known critical barrel thickness of regular arch (~0.108R).
- In case of the false skew arch, as the angle of obliquity increases, higher and higher barrel thickness has to be applied to maintain equilibrium. The relation between the critical barrel thickness and the obliquity is almost linear.
- Surprisingly, in case of logarithmic and helicoidal method, as the angle of obliquity increases, the critical barrel thickness decreases. It means that these two methods require smaller barrel thickness than the regular arch with the same span. The reason of this phenomenon was described at the introduction of the collapse mechanisms in Chapter 5.1.3.

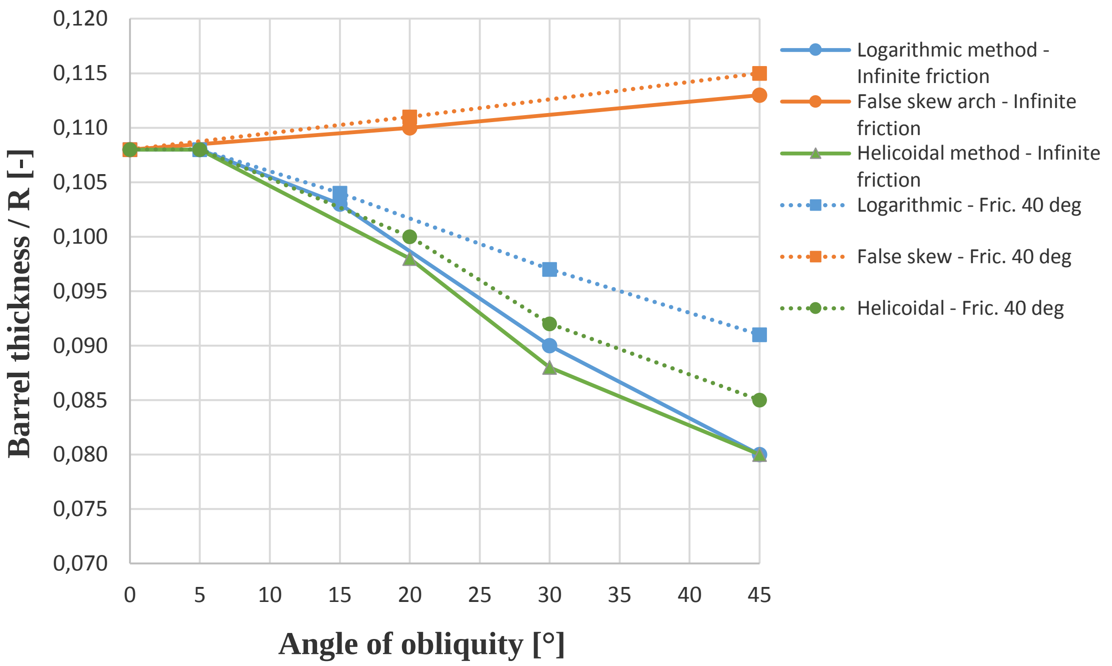

Figure 68 *– Critical barrel thickness in case of different methods of construction*

5.2 Effect of live load

Before going into the details, questions regarding the position and the direction of live loading have to be addressed.

Where is the critical position of the live load?

The exact and unique answer is not known even in the case of a direct arch. Most of the researchers apply line load at quarter span, some of them apply it at third span. With the help of the commercial software, LimitState:RING, described in Chapter 3.2.1. I analysed regular arches with the same span, but various thicknesses. The results of this investigation are summarized in **Figure 69**.

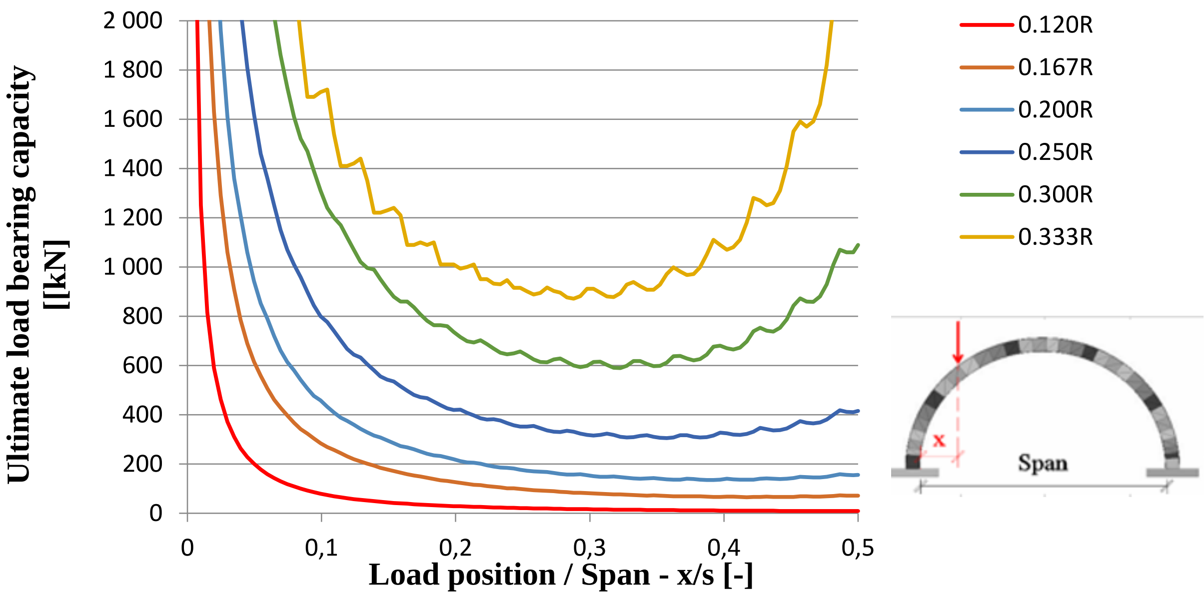

Figure 69 *– Critical positions in case of different barrel thicknesses (regular arch) using LimitState:RING 3.0f*

During the investigation, a regular, semi-circular (span : rise 2:1) arch was analysed with 3m width. The span was set to 5.64m. The angle of friction was set to 40°. Effects of backfill and horizontal earth pressures were not taken into account.

The critical position is located where the corresponding ultimate load bearing capacity is minimal. As shown by the diagrams in Figure 39, if we are very close to the critical barrel thickness, then the critical position for the live load is at the mid-span. By increasing the barrel thickness the critical position for live load gets shifted towards to third then to quarter span.

What should be the direction of the applied live load (see definition in Figure 70)?

In case of regular arches the answer is simple. The line load should be parallel with the springing and perpendicular to the face. These two conditions can be fulfilled together. Unfortunately the situation is complicated in the case of oblique arches. Most of the authors [27] [3] defined line load parallel to the abutments (Type I). Considering the real direction of the vehicles, the loading type which is perpendicular to the face (Type II) would be more realistic. In case of real circumstances, where full bridge with backfill is present, the thickness of the backfill layer between the Type II loading and the arch varies so the load dispersion effect of backfill can cause complex loading situations.

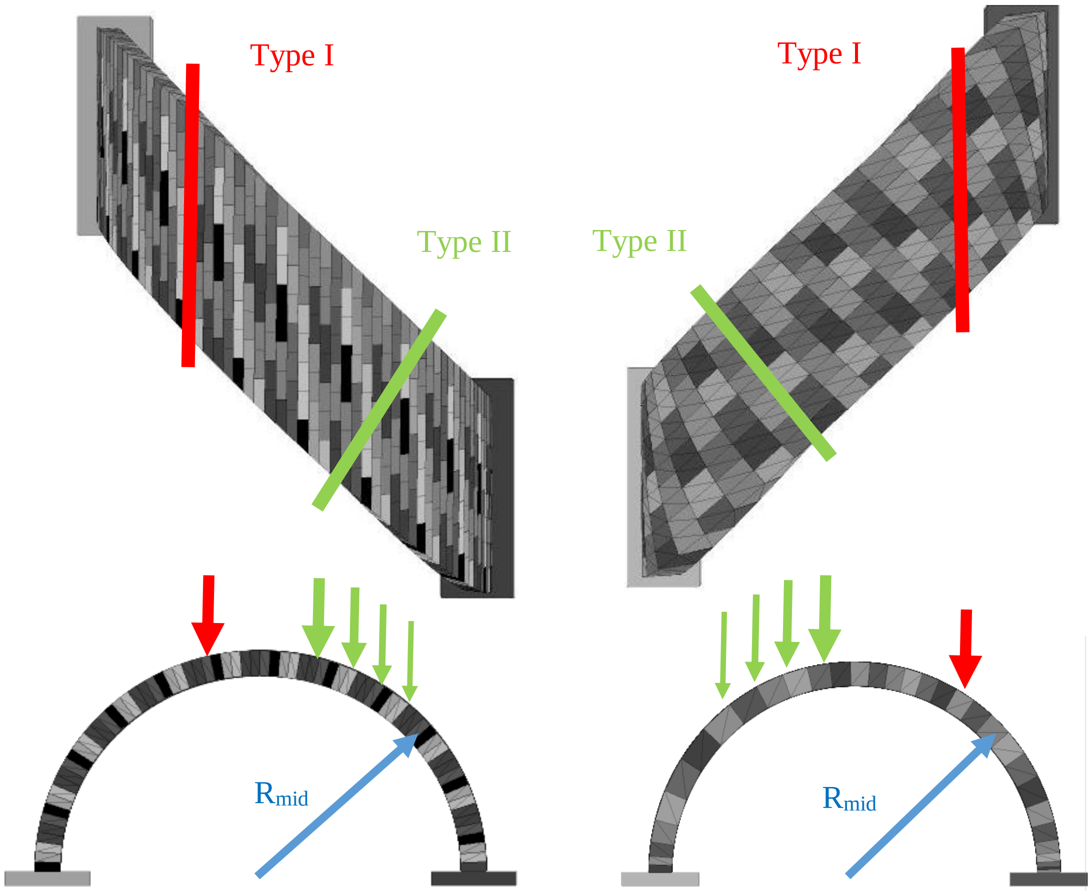

***Figure 70** – Two possible directions of line loading presented in case of false skew arch and in case of logarithmic method. Red: line load parallel to the springing, green: line load perpendicular to the face.*

In order to have a possibly clear insight into the mechanics of the skew arches without simulating the backfill and other structural components of a whole bridge, in the framework of this Diploma Work Type I loading was applied only. Later on, the differences between the Type I and Type II loading can be analysed in more detail in the future.

5.2.1 Critical position of the live load

To compare the methods of construction in case of live loading, the following parameters were chosen commonly:

- Geometry:
    - Radius of the mid-surface (R_{mid}): 3.00m
    - Width of the arch (b): 3.00m
    - Barrel thickness (t): 0.120*R= 0.36m
- Material properties:
    - Density of the blocks (ρ): 2700 kg/m^3
    - Internal angle of friction (φ): 40°

Three construction method (false skew arch, helicoidal method, logarithmic method) and four obliquities (0°, 15°, 30°, 45°) were compared.

In **Figure 71** the load bearing capacity of different methods of construction can be seen in case of different obliquities.

Theoretically all of the investigated methods of construction gives back the regular arch, if the angle of obliquity is set to 0°.

The ultimate load bearing capacity of false skew arch with a given non-zero obliquity is always less than the load bearing capacity of the regular arch.

However, the load bearing capacity of arches constructed with helicoidal or logarithmic method is always higher than the load bearing capacity of the regular arch. The strongest oblique arch can be constructed with logarithmic method, followed by the helicoidal method.

The applied barrel thickness (0.120*R) is rather close to the critical barrel thickness in case of false skew arch. The critical position of live loading is at the crown in this case. In case of helicoidal and logarithmic method, the applied barrel thickness is far above from the critical barrel thickness, so the critical position of the live load gets shifted to the direction of the abutments.

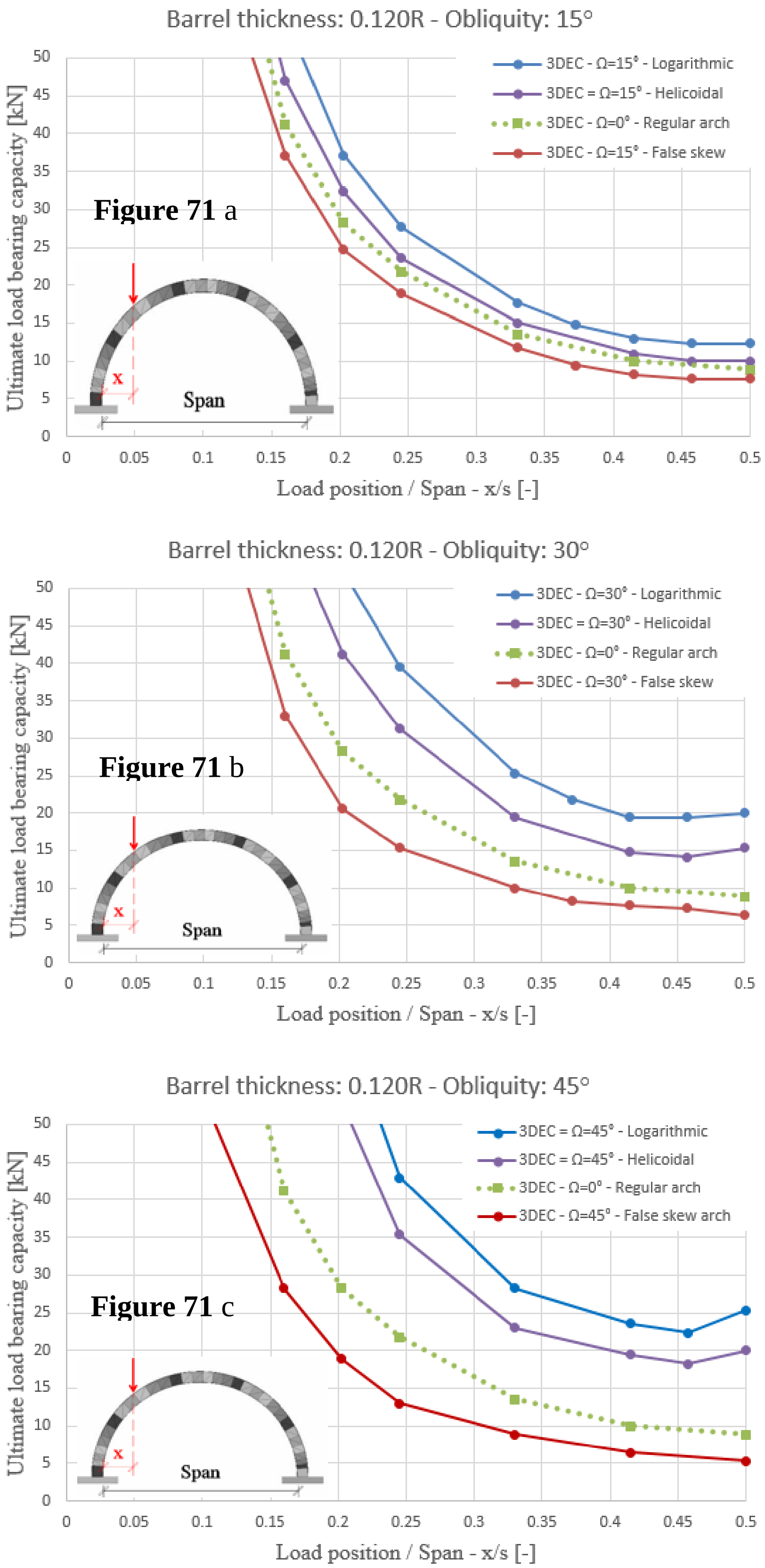

Figure 71 *– Load bearing capacity of different methods of construction in case of different obliquities*

As the obliquity is increasing the difference between the load bearing capacity of the regular arch and the oblique arches is higher and higher.

In **Figure 72** the result are categorized according to construction methods.

The obliquity of the investigated arches was: 0°, 15°, 30°, 45°.

Although the angle of obliquity is increasing linearly, the load bearing capacity of the arches is changing non-linearly in case of helicoidal and logarithmic method.

In the case of false skew arch the load bearing capacity is decreasing as the angle of obliquity increasing, while the load bearing capacity of advanced methods of construction (helicoidal, logarithmic) is increasing as the angle of obliquity increasing.

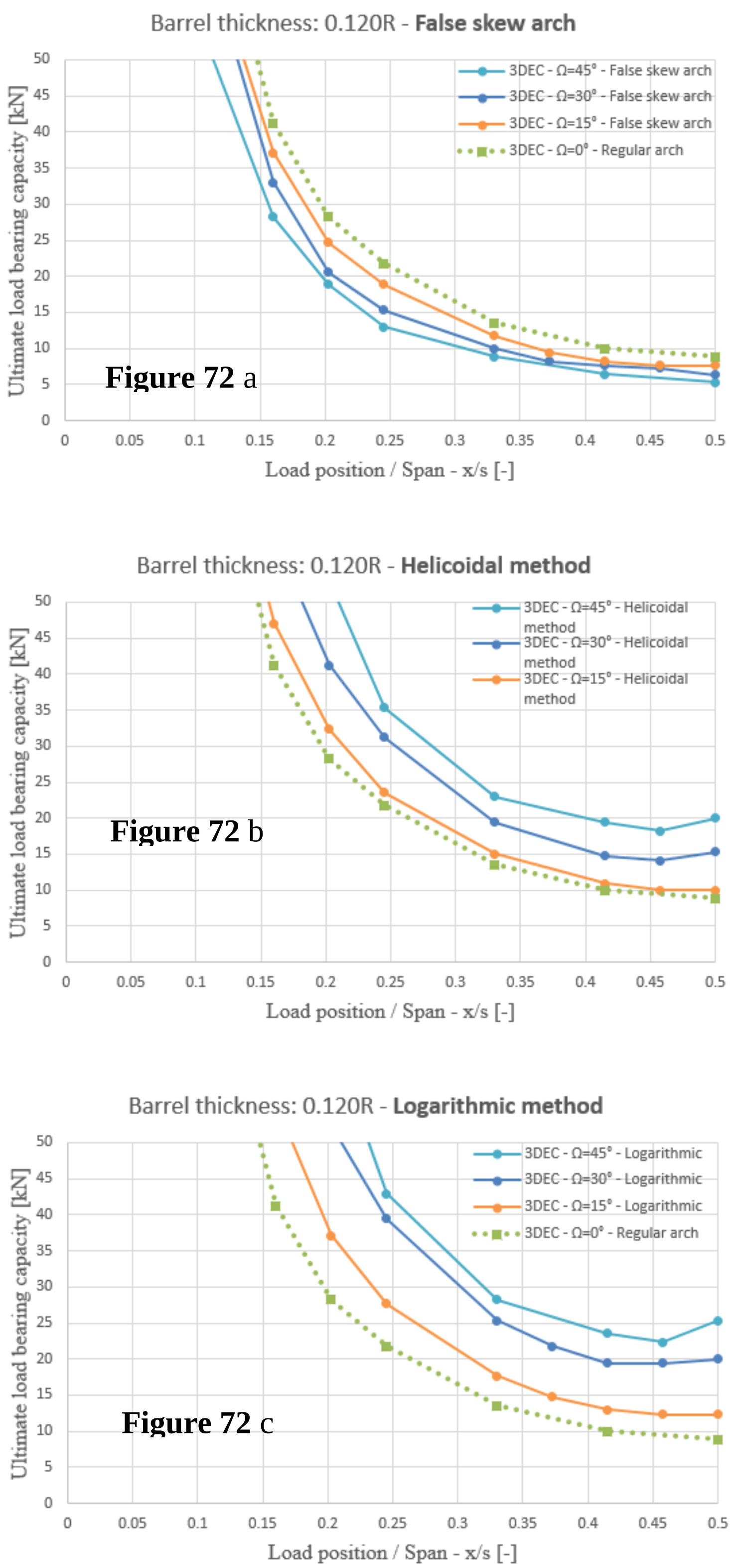

***Figure 72** – Load bearing capacity of a given construction method with different obliquities*

In **Figure 73**, the minimum of the load bearing capacity (which corresponds to the critical position of the live load) is compared to the load bearing capacity of the regular arch.

The load bearing capacity of the false skew arch is almost linearly decreasing as the angle of obliquity increasing. In case of high obliquities (e.g. 45°) the load bearing capacity is only 50% of the load bearing capacity of the regular arch.

The load bearing capacity of skew arches constructed with the helicoidal or the logarithmic method is always higher than the load bearing capacity of the regular arch of the same span, but the relation between the obliquity and the load bearing capacity is a nonlinear function. The load bearing capacity of the oblique arch (45°) constructed according to the logarithmic method can be two and a half times higher than the load bearing capacity of the regular arch with the same span.

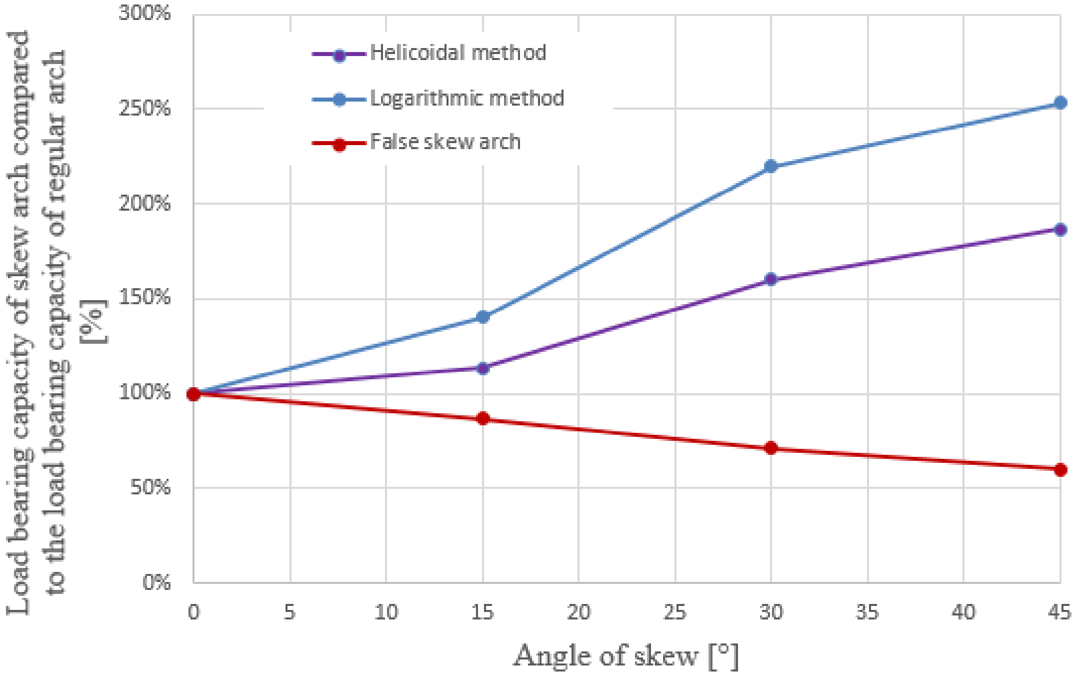

Figure 73 – Load bearing capacity of skew arch compared to the equivalent regular arch.

In **Figure 74** the shear stress distributions can be seen in case of an oblique arch where the obliquity 30° and the arch constructed according to the helicoidal method. During the loading process a full width line load acts at the crown.

The pictures in **Figure 74** visualize the process of failure: the upper left picture (**Figure 74** a) shows the state when only gravity acts on the structure. As the live load begins to increase, shear stresses begin to increase at the vicinity of the developing hinge-rows. The first hinge appears at the crown (**Figure 74** b). After it, two hinges appear simultaneously at the haunches, and two other hinges at the springings (**Figure 74** c,d).

It can be clearly seen that the obtuse angles of the oblique arch are highly overloaded, compared to the acute angles. The deep blue colour means those contact surfaces where shear stresses don’t develop, while the red means those contact surfaces where the highest shear stresses arise.

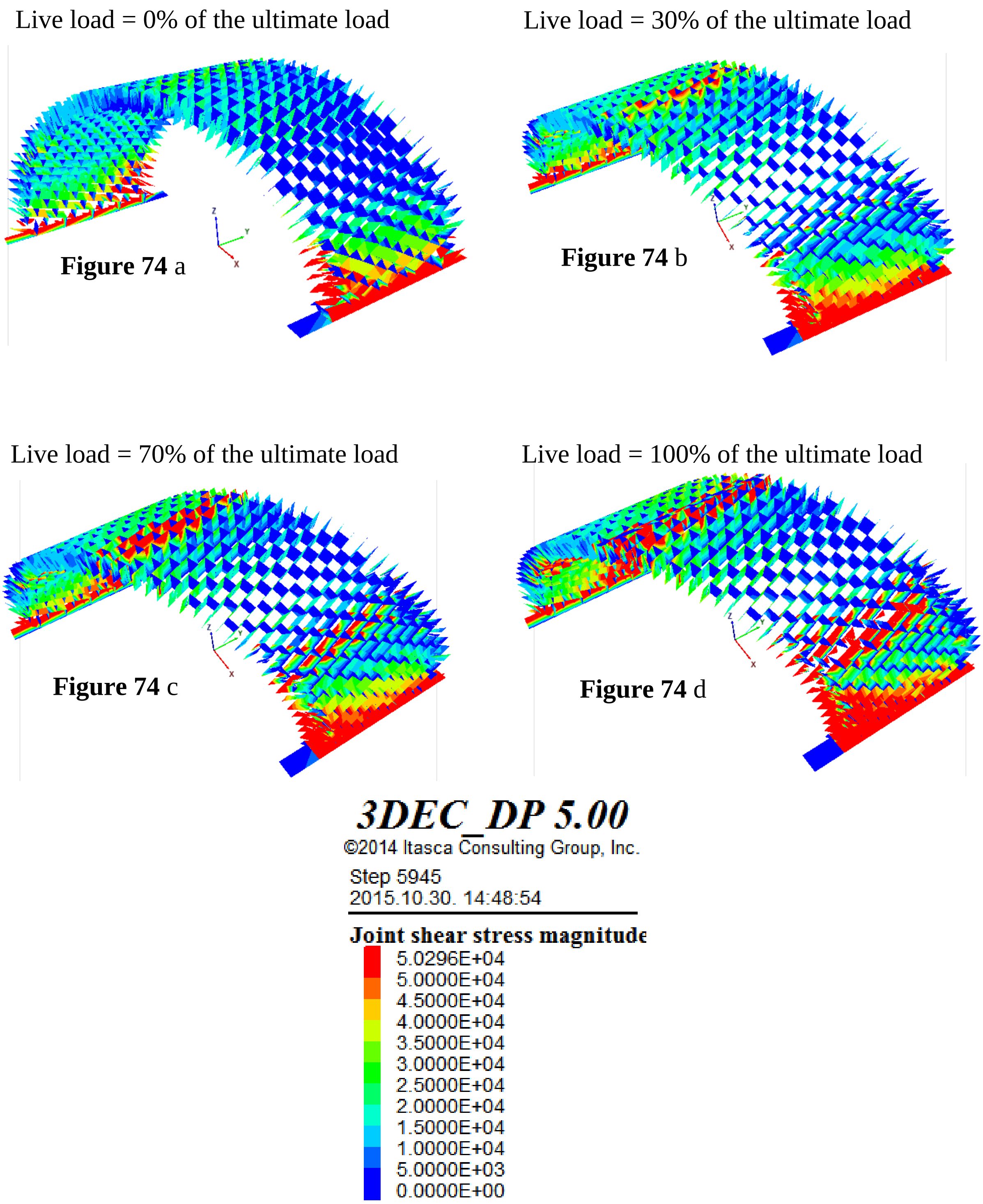

Figure 74 *- Shear stress distribution as the structure reaches the state of failure*

5.2.2 Effect of the width of the arch

As it was mentioned before, the behaviour of the skew arch is three-dimensional, hence the ratio between the width of the arch and the radius of the arch should be investigated. During this investigation the false skew arch was compared to the logarithmic method. According to my expectations the results of helicoidal method would be very close to the results of logarithmic method.

The arches in this comparison has the following parameters:

Common parameters		**Differing properties**
Radius:	3m	Method of construction
Width of the arch:	3m	
Barrel thickness:	0.12·R = 0.36m	Obliquity
Avg. element length	0.5m	
Number of courses:	40	Width of the arch
Angle of friction:	40°	

Table 3 *– Parameters of the investigated arches*

The length of the element was kept constant during the investigation. It means that the wider arches contain more discontinuities, more heading joints. The loading element is one rigid block parallel to the abutments, hence the vertical deflections under the loading element are the same along the length of the arch. The position of the loading element was determined according to the critical position calculated in Chapter 5.2.1.

The results are summarized in **Figure 75**. The vertical axis means the average load bearing capacity that corresponds to unit length, so the total load bearing capacity of a 10m wide arch is ten times higher. It can be seen that the arches are not so sensitive to the change of width (except some unrealisticly narrow arches).

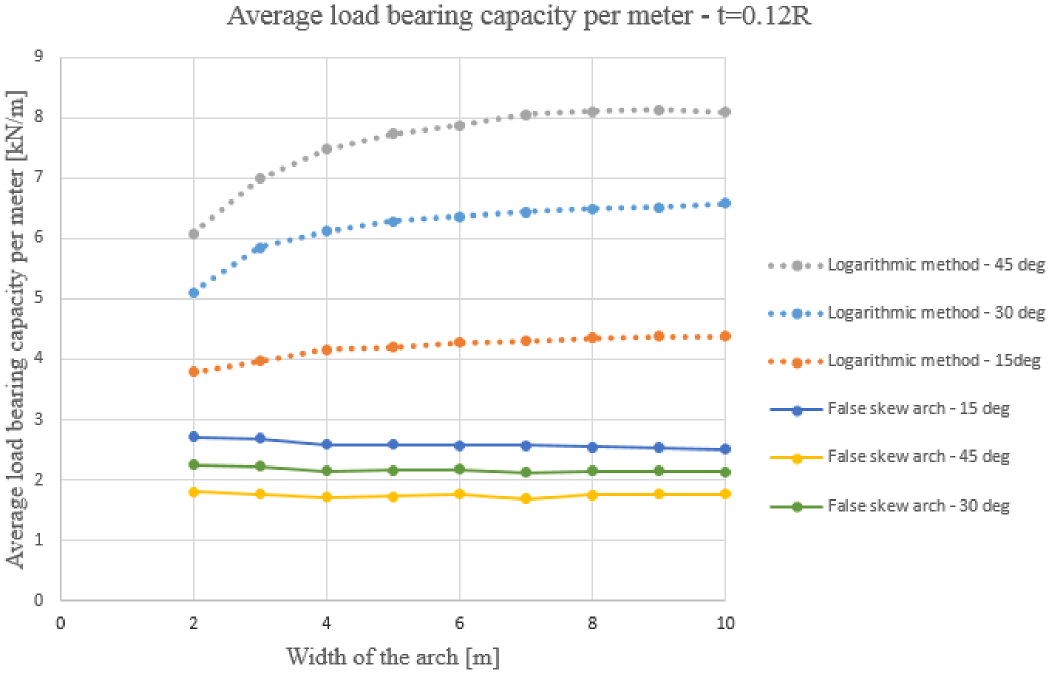

Figure 75 *– Relation between the width of the arch and the ultimate load bearing capacity*

In case of the logarithmic method the average load bearing capacity is increasing with the increasing width of the arch.

The reason of the higher load bearing capacity can be the following: in this method with the increasing width wider and wider elements are created at acute angle of the arch. These bigger elements strongly divert the cracks from the straight line.

The location of the imminent hinges doesn’t change with the alteration of the arch’s width.

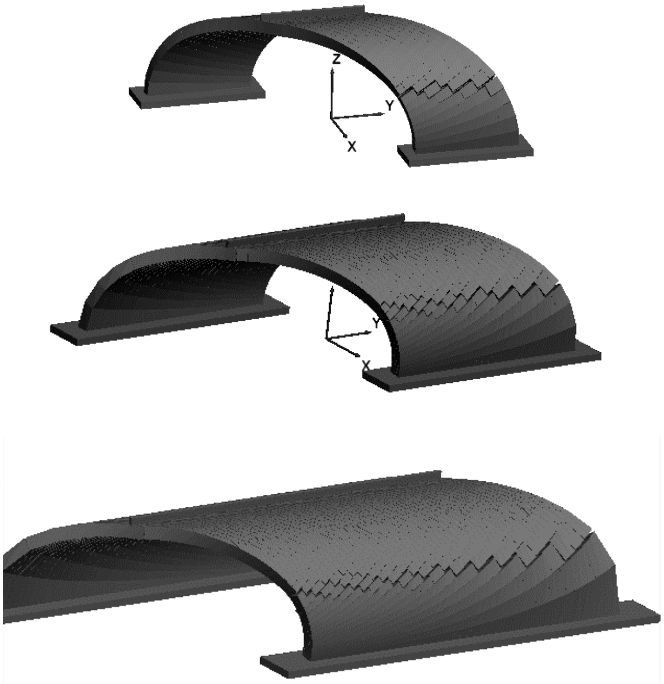

Figure 76 *– Crack pattern of the logarithmic method in case of different widths*

The false skew arch shows a different tendency. One can expect that as the width increases the average load bearing capacity should converge to the load bearing capacity of the regular arch. In spite of this as the width of the arch increases the average load bearing capacity is constant or lightly decreasing in ***Figure 75***.

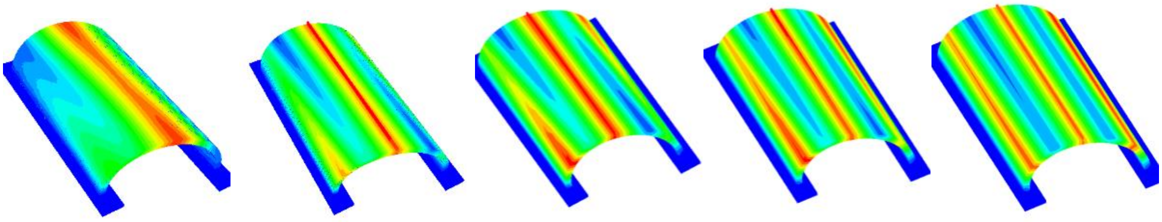

Figure 77 *– Mechanism of the failure in case of false skew arch (from left to right: the intensity of the loading is increasing until the 5-hinge collapse mechanism is reached)*

The reason of it can be the following: the failure mechanism is strongly progressive. The acute angle of the arch is overloaded, the imminent hinge develops and this part reaches its ultimate load bearing capacity. This part of the structure cannot take more loads, so the blocks start to load the nearest adjacent elements. In this way the hinge-row starts to develop towards to the direction of the obtuse angle. The result of this progressive mode of failure is that the ultimate load bearing capacity of the false skew arch doesn’t converge to the ultimate load bearing capacity of the direct arch.

5.2.3 Effect of heading joints

The analysis of the width of the arch inspired another investigation in case of false skew arch. Let's investigate the effect of the number of heading joints or, in other words, the effect of the shape of the element. The analysed range: from 0 heading joint (i.e. one element per course) to 20 element per course.

The project description of the diploma work did not prescribe this investigation. The motivation was the slightly decreasing tendency in load bearing capacity of the false skew arch in **Figure 75**.

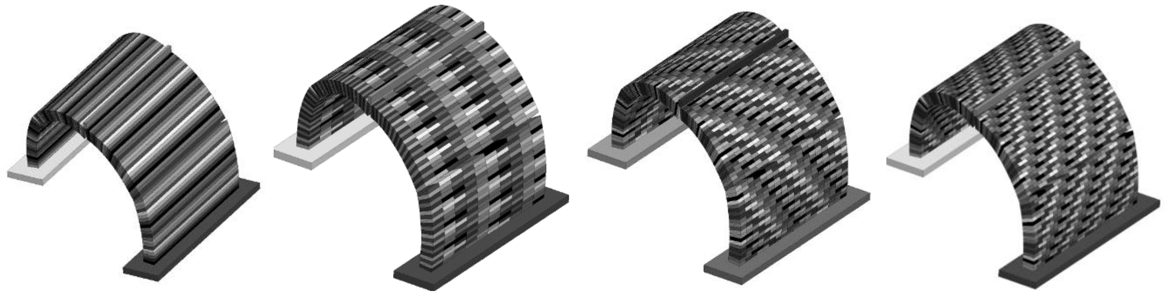

Figure 78 *– Different element width to length ratios*

In case of full width vertical line load the number of applied heading joint does not modify the ultimate load bearing capacity of the regular arch. Interestingly, if a course contains only one element, then the load bearing capacity of the skew arch is almost equal with the load bearing capacity of the regular arch. With the increasing number of heading joints the load bearing capacity decreases. In the range of the realistic element shape the ultimate load bearing capacity tends to be almost constant.

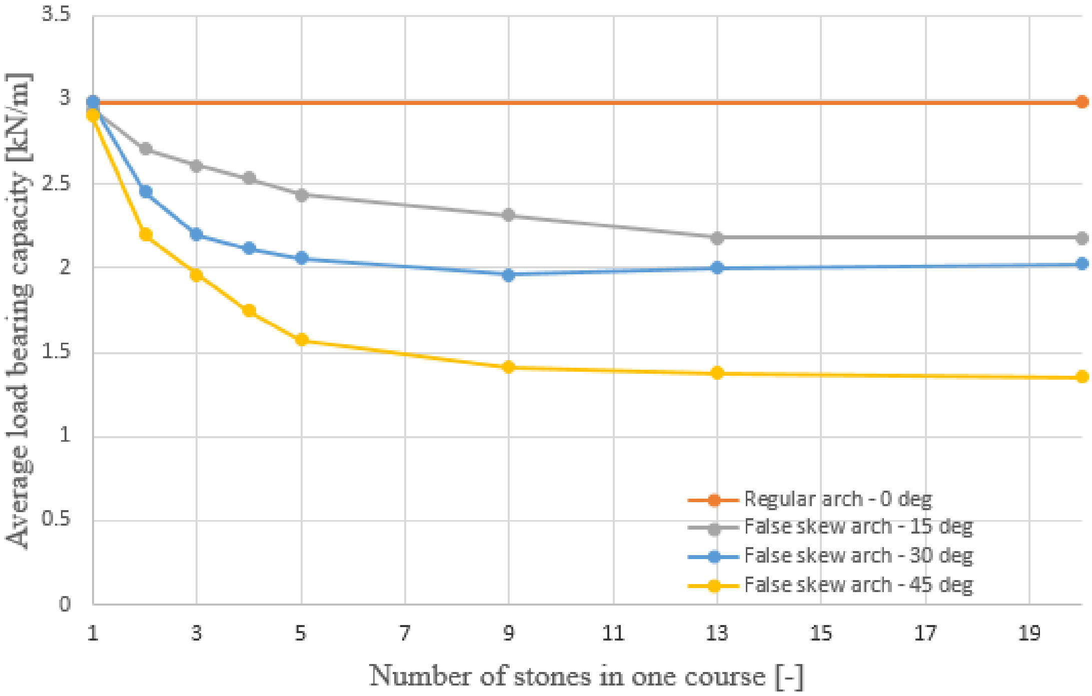

Figure 79 *– Effect of the number of heading joints*

6 Conclusions and recommendations for further research

In the framework of this diploma work the different methods of construction of skewed masonry arches were introduced on the basis of literature from the beginning of the 19th century. The old geometric construction methods were also presented.

During the project the discrete element method was applied to understand the mechanical behaviour of skew arches. Three-dimensional parametric model of the geometry was created in MAPLE 17, so that the geometry of the arch can be easily modified later on.

The verification of the model was extensive: the numerical model was verified against analytical solutions of similar problems, and was validated against the results provided by another commercial software, LimitState:RING.

The critical barrel thickness of skew arches was unknown up to the present day. With the help of my model, the critical barrel thickness was determined numerically to the three main types of construction using 3DEC.

Astonishingly, with a suitably chosen method of construction (logarithmic and helicoidal method) the critical barrel thickness can be lower than the critical thickness which corresponds to the regular masonry arch.

During the investigation of live loading, full width line load acting parallel to the springing was analysed. In a very good accordance with the analysis of the critical barrel thickness it can be stated that the highest load bearing capacity is ensured by the logarithmic method, followed by the helicoidal method. These two methods ensure higher load bearing capacity compared to the regular arch. The false skew arch was proven to be the weakest structure. The load bearing capacity of the false skew arch is always less than the load bearing capacity of regular arch of the same span and thickness.

The application of the 3DEC discrete element software as the everyday tool of an engineer would be inconvenient at the time of the project.The evaluation of the results is troublesome, the computational time on a PC is excessive. With 1-2000 discrete elements the determination of a load bearing capacity can endure up to 5-6 hours. So there is a demand to create such formulas where the engineers specify the parameters of the oblique arch and the load bearing capacity of the equivalent regular arch which can be calculated in an easy and fast way for example with LimitState:RING. These input data can be substituted to the formulas, which would provide the load bearing capacity of the oblique arch:

$$R_{oblique} = \alpha_{construction\ method} \cdot \alpha_{obliquity}(\Omega) \cdot \alpha_{width}(b/R) \cdot R_{regular}$$

This will be the next step to continue to the analysis presented in this report.

References

[1] Z. Orbán, Számítási modellek és diagnosztikai eljárások fejlesztése műemlék jellegű, falazott hídszerkezetek teherbírásának megállapítására és használhatósági követelményeinek ellenőrzésére, Pécs: OTKA zárójelentés, 2009.

[2] J. Wang, The three dimensional behaviour of masonry arches. PhD Thesis, UK, University of Salford, 2004.

[3] J. Hodgson, The behaviour of skewed masonry arches, UK, University of Salford, 1996.

[4] V. Sarhosis, D. Oliveira, J. Lemos, Sheng, P.B. and Lourenco, "The behaviour of single span stone masonry skew arches," in *7th International Conference on Arch Bridges,* Croatia, 2013.

[5] C. Melbourne and J. Hodgson, "The behaviour of skewed brickwork arch bridges," in *In Arch Bridges: Proceedings of the First International Conference of Arch Bridges*, London, 1995.

[6] "Wikipedia - Skew Arches," [Online]. Available: https://en.wikipedia.org/wiki/Skew_arch. [Accessed 20. October 2015.].

[7] P. Nicholson, The Guide to Railway Masonry, London: John Weale, 1839.

[8] C. Fox, "On the Construction of Skew Arches," *Architectural Magazine,* vol. III., pp. 251-260, 1836.

[9] F. Bashfort, Oblique Bridges with Spiral and with Equilibrated Courses, London: E.&F.N Spon, 1855.

[10] E. Sang, "An Essay on the Construction of Oblique Arches," *The Civil Engineer and Architectural Journal,* pp. 232-235, 1840.

[11] E. Hyde, Skew Arches - Advantages and Disadvantages of Different Methods of Construction, New York: D. Van Nostrand Company, 1899.

[12] A. Pippard, E. Tranter and L. Chitty, "The mechanics of the voussoir arch," *Journal Inst. Civil Engineering,* 1836.

[13] J. Wang, J. Haynes and C. Melbourne, "A comparison between the MEXE and Pippard's methods of assessing the load carrying capacity of masonry arch bridges," in *7th International Conference on Arch Bridges,* Trogir-Split, Croatia, 2013.

[14] "The Assessment of Highway Bridges and Structures - BA16/97," in *Scottish Executive Development Department*, 2001.

[15] J. Heyman, The Masonry Arch, Chichester, UK: Ellis Horwood, 1982.

[16] J. Heyman, Equilibrium of Shell Structures, Oxford, UK: Oxford University Press, 1977.

[17] J. Heyman, “The Stone Skeleton,” *International Journal of Solids and Structures,* vol. Vol. 2., pp. 249-279, 1966.

[18] A. Kooharian, “Limit analysis of voussoir (segmental) and concrete arches,” *Journal of the American Concrete Institute,* vol. Vol. 24. No. 4., pp. 317-328, 1952.

[19] S. Kaliszky, K. Kurutzné and G. Szilágyi, Szilárdságtan, Budapest: Nemzeti Tankönyvkiadó, 2006.

[20] LimitState:RING User's Manual, LimitState Ltd., 2014.

[21] C. Martinez, “Application of non-linear finite element analysis to a seven span masonry arch bridge.,” *Master Thesis UPV,* 2012.

[22] P. Cundall and D. Hart, “Numerical modelling of discontinua.,” *Journal of Engineering Computations,* vol. Vol. 9., pp. 101-113, 1992.

[23] ITASCA, 3DEC - Universal Distinct Element Code Manual. Theory and Background, Miniapolis: Itasca Consulting Group, 2004.

[24] K. Jiang and T. Esaki, “Qualitative evaluation of stability changes in historical stone bridges in Kagoshima, Japan, by weathering,” *Eng. Geol.,* vol. 63, pp. 83-91, 2002.

[25] G. Cocchetti, G. Colasante and E. Rizzi, “On the Analysis of Minimum Thickness in Circular Masonry Arches,” *Applied Mechanics Review,* vol. Vol. 64, 2011.

[26] M. Milankovitch, Beitrag zur Theorie der Druckkurven. PhD Thesis, Vienna, Austria: K.K. Technische Hochschule, 1907.

[27] V. Sarhosis, D. Oliveira, J. Lemos and P. Lourenco, “The effect of skew angle on the mechanical behaviour of masonry arches,” *Mechanics Research Communications,* vol. 61, pp. 53-59, 2014.

Appendix A - Terminologies

The following appendix helps to understand the basic terminologies concerning arch bridges.

Fundamental notations

The inferior and superior surfaces of an arch are called respectively the **intrados (or soffit)**, and the **extrados**.

The continuous surfaces, generally covered with mortar or cement, which divide successive courses of arch stones, are the **beds** of the arch stones. The curved lines in which these beds meet the extrados and intrados are called respectively the **extradosal and intradosal coursing joints.** The other short discontinuous joints are the **heading joints.**

The vertical planes which limit the length of the arch are called **the faces of the arch**, and those stones, which are cut by these planes, are the **quoins** of the arch.

The abutments are the upright walls which bound the width of the road under, and support the arch for carrying the road over the bridge.

The section of the arch made by a plane at right angles to the axis of the intrados is a **right section**, commonly called “section on the square”.

Cylindrical surfaces are developable, that is if we suppose a thin, flexible and inextensible sheet to coincide with the surface of a cylinder, this sheet admits of being extended on a plane without being rumpled and torn.

The obliquity of the arch: in an oblique arch the axis of the barrel is not perpendicular to the face, the deviation from perpendicularity being known as the obliquity of the arch. (see in **Figure 1**)

Terminologies related to arch bridges

Masonry arch bridges are very different to the steel and concrete bridges which are instead constructed in their place nowadays. As the terminology used to describe different parts of masonry arch bridges can appear obscure to the non-specialist, common terms are given in **Figure 80**.

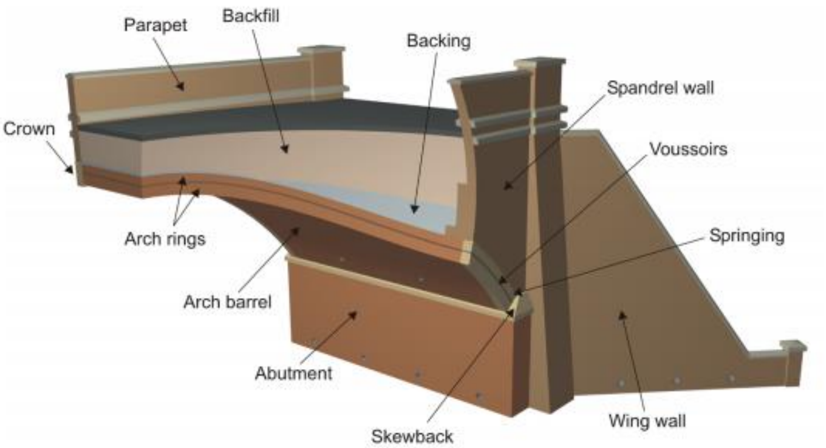

Figure 80 – Masonry arch terminology [20]

Relation between the cylindrical surface and the development

During the calculation of the geometry, the arrangement of the courses is determined on the developed cylindrical surface.

After I determined the coordinates of the stones on the development I transformed back these 2D coordinates into the 3D cylindrical surface.

If I denote the coordinates of P on the 3D surface with (x,y,z) and on the 2D development with (X,Y), then the connection between them is:

$$x = \mathrm{R}\sin\left(\frac{X}{R}\right)$$

$$y = Y$$

$$z = \mathrm{R}\cos\left(\frac{X}{R}\right)$$

We can notice that X/R is equal to α.

The boundaries of the coordinates:

$$-R \leq x \leq R$$

$$-R\tan(\Omega) - \frac{b}{2} \leq y \leq R\tan(\Omega) + \frac{b}{2}$$

$$0 \leq z \leq R$$

The equation of the face on the cylindrical surface:

$$y = x \cdot \tan(\Omega) \pm \frac{b}{2}$$

If we substitute the relation between x-X and y-Y we get the equation of the face on the development:

$$Y = R \cdot \tan(\Omega) \cdot \sin\left(\frac{X}{R}\right) \pm \frac{b}{2}$$

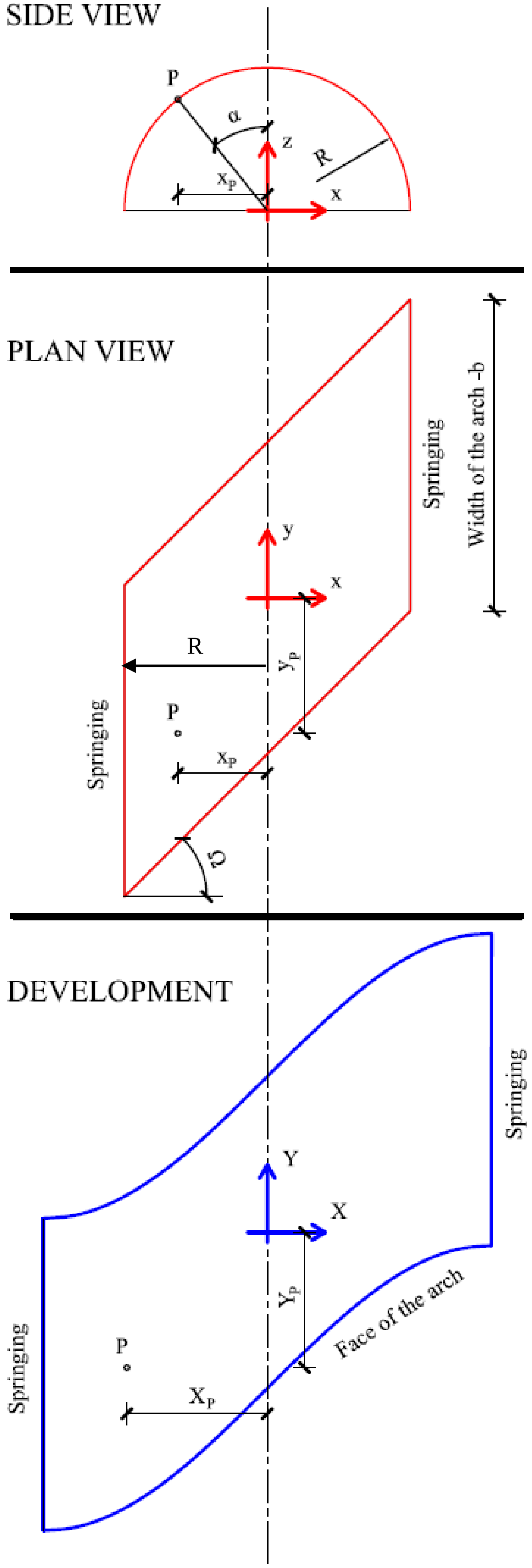

Appendix B – 3DEC Input file

```
new;

; Here comes the coordinates of the elements with the following order:
polyhedron prism a x1 y1 z1 x2 y2 z2 x3 y3 z3 x4 y4 z4 b x1 y1 z1 x2 y2 z2 x3 y3 z3 x4 y4 z4

; Setting up variables to the definition of support-blocks and loading element
def adatok
b
r_mid
beta
tfal
end
set @b = 5
set @r_mid = 3
set @beta = 0.523598776
set @tfal = 0.12

; Definition of the support-blocks
def tamasz
bx1= -r_mid*1.2
bx2= -r_mid*0.8
by1= -0.1
by2= 0
bz1= -0.7*b-r_mid*tan(beta)
bz2= 0.7*b-r_mid*tan(beta)
jx1= 0.8*r_mid
jx2= 1.2*r_mid
jy1=-0.1
jy2=0
jz1=-0.7*b+r_mid*tan(beta)
jz2=0.7*b+r_mid*tan(beta)
end

@tamasz
hide;
poly brick @bx1 @bx2 @by1 @by2 @bz1 @bz2
poly brick @jx1 @jx2 @jy1 @jy2 @jz1 @jz2
fix;      ; It fixies the visible elements → two support-blocks
seek;     ; This command makes visible all of the previously defined elements
mark reg 2000;          ; We reference the visible elements as region 2000.

; Material properties
prop mat=1 dens=2700          ; Element properties
change mat 1 cons 1 range reg 2000
change mat=1 range reg 2000

prop jmat=1 jkn 7.64e9 jks 1.79e9 jfri 40;      ; Contact properties
```

```
gravity 0, -9.81 , 0        ; Loading

damping auto 0.1            ; Sets the fraction of global adaptive damping to 0.1

hist unbal id=1;
hist ydisp (0,3.0,0.0) id=2

solve rat 1e-7              ; Solves the above problem under gravitational load

; Definition of the loading element:
def szog
loadposition=0.0001
alfa=acos(loadposition/((1+tfal/2)*r_mid))
end
@szog ; Define the angular position of the loading element from the horizontal axis

def loadingelement
xa1= -((1+tfal/2)*r_mid)*cos(alfa)-0.5*0.1
xa2= -((1+tfal/2)*r_mid)*cos(alfa)+0.5*0.1
xa3= -((1+tfal/2)*r_mid)*cos(alfa)+0.5*0.1
xa4= -((1+tfal/2)*r_mid)*cos(alfa)-0.5*0.1
ya1= ((1+tfal/2)*r_mid)*sin(alfa)-0.05/tan(alfa)
ya2= ((1+tfal/2)*r_mid)*sin(alfa)+0.05/tan(alfa)
ya3= ((1+tfal/2)*r_mid)*sin(alfa)+0.2
ya4= ((1+tfal/2)*r_mid)*sin(alfa)+0.2
za1= -((1+tfal/2)*r_mid*cos(alfa))*tan(beta)-0.5*b
za2= -((1+tfal/2)*r_mid*cos(alfa))*tan(beta)-0.5*b
za3= -((1+tfal/2)*r_mid*cos(alfa))*tan(beta)-0.5*b
za4= -((1+tfal/2)*r_mid*cos(alfa))*tan(beta)-0.5*b
xb1= -((1+tfal/2)*r_mid)*cos(alfa)-0.5*0.1
xb2= -((1+tfal/2)*r_mid)*cos(alfa)+0.5*0.1
xb3= -((1+tfal/2)*r_mid)*cos(alfa)+0.5*0.1
xb4= -((1+tfal/2)*r_mid)*cos(alfa)-0.5*0.1
yb1= ((1+tfal/2)*r_mid)*sin(alfa)-0.05/tan(alfa)
yb2= ((1+tfal/2)*r_mid)*sin(alfa)+0.05/tan(alfa)
yb3= ((1+tfal/2)*r_mid)*sin(alfa)+0.2
yb4= ((1+tfal/2)*r_mid)*sin(alfa)+0.2
zb1= -((1+tfal/2)*r_mid*cos(alfa))*tan(beta)+0.5*b
zb2= -((1+tfal/2)*r_mid*cos(alfa))*tan(beta)+0.5*b
zb3= -((1+tfal/2)*r_mid*cos(alfa))*tan(beta)+0.5*b
zb4= -((1+tfal/2)*r_mid*cos(alfa))*tan(beta)+0.5*b
end
@loadingelement

hide;
polyhedron prism a @xa1 @ya1 @za1 @xa2 @ya2 @za2 @xa3 @ya3 @za3 @xa4 @ya4
@za4 b @xb1 @yb1 @zb1 @xb2 @yb2 @zb2 @xb3 @yb3 @zb3 @xb4 @yb4 @zb4
mark reg 1000;
seek;
def adatok
```

```
        i
end
set @i = 1

def LIVE                ; It sets up the density of the loading element
        density=i*1000+0000
        command
                prop mat=2 dens=@density
                change mat 2 cons 1 range reg 1000
                change mat=2 range reg 1000
                cycle 1000
        end_command
end

def CONTROLL
        indicator=1
        i=1.00
        loop while indicator#0          ; Meaning: Continue while indicator is not equal to 0
        LIVE
        nevt='live_parallel_beta30_b'+string(b)+'_rmid'+string(r_mid)+'_loadposition'+string(
        loadposition)+'_0plus100_'+ string(i)+'.3dsav'
        maxy=0
        blocknum=block_head
                loop while blocknum#0          ; Meaning: Go through all of the elements
                        gpnum=b_gp(blocknum)
                        loop while gpnum#0
                                if abs(gp_ydis(gpnum))>maxy
                                maxy= abs(gp_ydis(gpnum))
                                endif
                        gpnum=gp_next(gpnum)
                        end_loop
        blocknum=b_next(blocknum)
        end_loop
if unbal > 0.1  ; If the unbalanced force is bigger than 0.1 → structure is not in equilibrium.
        i=i     ; The density of the loading element is unchanged.
else
        i=i+1   ; The density of the loading element is increased
endif

if maxy>0.2 ;If the max. vert. disp. is bigger than 0.2m → structure is collapsed
        indicator=0     ; The calculation process is continued
else
        indicator=1     ; The calculation process is stopped
endif
end_loop
command
save @nevt      ; After solution the results are saved
end_command
end
@CONTROLL
```